

**CERESiS: ContaminatEd land  
Remediation through Energy crops for  
Soil improvement to liquid biofuel  
Strategies**



**D3.1: Process specifications for SCWG  
and FP and decontamination  
technologies integration**

**H2020-LC-SC3-2018-2019-2020**

**Contract No: 101006717**

**JULY 2021**



The project has received funding from the European Union's Horizon 2020 research and innovation programme under grant agreement No 101006717

## Document control sheet

Project	ContaminatEd land Remediation through Energy crops for Soil improvement to liquid biofuel Strategies
Call identifier	H2020-LC-SC3-2018-2019-2020
Grant Agreement N°	101006717
Coordinator	National Technical University of Athens
Work package	WP3 – Clean biofuel production and separation of contaminants
Work package leader	KIT
Related tasks	Task 3.1: Definition of process requirements in biofuel conversion & separation technologies and risk assessment
Deliverable title	Process specifications for SCWG and FP and decontamination technologies integration
Deliverable nature	Report
Dissemination level	PU
Lead Beneficiary	KIT
Contributing partners	CERTH, CNR, SHER
Authors	Boukis, Nikolaos (KIT); Giudicianni, Paola (CNR); Hurtado Castaño, Yira (SHER); Karagiannakis, George (CERTH); Koutsonikolas, Dimitris (CERTH); Lavoie, Jean-Michel (SHER); Plakas, Konstantinos (CERTH); Ragucci, Raffaele (CNR); Sabia, Pino (CNR); Skevis, George (CERTH); Stoll, I. Katharina (KIT)
Reviewers	Katsourinis, Dimitris (NTUA); Lavoie, Jean-Michel (SHER); Stathopoulos, Nikolaos (EXERGIA)
Version	F.1.5 (final)
Total number of pages	112
Issue date	28/7/2021

**All rights reserved:** The document is proprietary of the CERESiS consortium members. No copying or distributing, in any form or by any means, is allowed without the prior written agreement of the owner of the property rights. This document reflects only the authors' view. The European Community is not liable for any use that may be made of the information contained herein.

REVISION HISTORY			
Version	Date	Author(s)	Changes made
1.0	14/07/2021	Lavoie, Jean-Michel (SHER)	Revision of draft deliverable
1.1	16/07/2021	Katsourinis, Dimitris (NTUA)	Revision of draft deliverable
1.2	16/07/2021	Stoll, I. Katharina (KIT)	Implementation of comments in 1.0
1.3	23/07/2021	Boukis, Nikolaos (KIT); Giudicianni, Paola (CNR); Hurtado Castaño, Yira (SHER); Karagiannakis, George (CERTH); Koutsonikolas, Dimitris (CERTH); Lavoie, Jean-Michel (SHER); Plakas, Konstantinos (CERTH); Ragucci, Raffaele (CNR); Sabia, Pino (CNR); Skevis, George (CERTH); Stoll, I. Katharina (KIT)	Implementation of comments in 1.1
1.4	27/7/2021	Rentizelas, Athanasios (NTUA)	Revision of deliverable
1.5	28/7/2021	Plakas, Konstantinos (CERTH); Stoll, I. Katharina (KIT)	Implementation of comments in 1.4

# LIST OF CONTENT

<b>NOMENCLATURE .....</b>	<b>4</b>
<b>1 EXECUTIVE SUMMARY .....</b>	<b>7</b>
<b>2 BIOMASS SAMPLING SCHEME.....</b>	<b>8</b>
2.1 Fundamentals on biomass composition.....	8
2.2 Biomass overview and basic feedstock requirements.....	10
2.3 Biomass distribution.....	11
2.4 List of References.....	13
<b>3 HYDROTHERMAL GASIFICATION (SCWG) BASED TECHNOLOGY PATHWAY .....</b>	<b>14</b>
3.1 Supercritical water gasification (SCWG).....	14
3.1.1 Fundamentals and influential parameters of SCWG.....	14
3.1.2 Feedstock preparation .....	19
3.1.3 Salt behaviour and separation of solids.....	21
3.1.4 Tar removal .....	25
3.2 Decontamination technologies.....	27
3.2.1 Membrane gas absorption (MGA) .....	27
3.2.2 Electrocoagulation-flotation (EC) and electrochemical oxidation (EO) .....	33
3.2.3 ECF solid by-product (sludge) treatment and reuse options .....	39
3.3 Biofuel synthesis.....	41
3.3.1 Reforming/Water Gas Shift .....	41
3.3.2 Fischer-Tropsch-Synthesis and distillation .....	42
3.4 List of References.....	48
<b>4 FAST PYROLYSIS (FP) BASED TECHNOLOGY PATHWAY .....</b>	<b>63</b>
4.1 Fast pyrolysis (FP).....	63
4.1.1 Pyrolysis fundamentals and influential parameters of FP .....	63
4.1.2 FP reactor.....	67
4.1.3 Pyrolysis vapors cleaning and condensation .....	70
4.1.4 Market survey .....	72
4.2 MILD combustion .....	74
4.3 Bio-oil decontamination (microfiltration) and reuse options .....	78
4.3.1 Microfiltration.....	78
4.3.2 Char reuse options.....	83
4.4 List of References.....	90

<b>5</b>	<b>BIOMASS TECHNOLOGY MATRIX .....</b>	<b>96</b>
<b>6</b>	<b>RISK ASSESSMENT AND MITIGATION MEASURES .....</b>	<b>100</b>
	6.1 SCWG-based technology pathway .....	100
	6.2 FP-based technology pathway.....	103
<b>7</b>	<b>CONCLUSION.....</b>	<b>105</b>
	<b>LIST OF FIGURES .....</b>	<b>107</b>
	<b>LIST OF TABLES.....</b>	<b>109</b>
<b>ANNEX 1</b>	<b>BIOMASS DISTRIBUTION .....</b>	<b>110</b>
<b>ANNEX 2</b>	<b>SCWG FEEDSTOCK COMPOSITION .....</b>	<b>112</b>

## NOMENCLATURE

AAEM:	Alkali and Alkaline Earth Metals
AC:	Alternating current
AD:	Arundo donax
AGL:	Acid Gas Loading
AM:	Andropogon minarum
ASF:	Anderson-Schulz-Flory Distribution
B:	Brescia
BDD:	Boron Doped Diamond
BTM:	Biomass technology matrix
CCLR:	Coagulation Charge Loading Rate
CEC:	Cation Exchange Capacity
CERTH:	The Centre for Research & Technology, Hellas
CGC:	Cold gas cleaning
CHP:	Combined Heat and Power
CNR:	Consiglio Nazionale delle Ricerche
COD:	Chemical Oxygen Demand
CVD:	Chemical Vapor Deposition
DC:	Direct Current
DEA:	Diethanolamine
DoE:	Design of Experiments
DP:	Degree of Polymerization
DTA:	Differential Thermal Analyses
ECF:	Electrocoagulation Flotation
EDA:	Electron Donor Acceptor
EO:	Electrochemical Oxidation
ERSAF:	Ente Regionale Per I Servizi All'Agricoltura E Alle Foreste
ESP:	Electrostatic Precipitator
FESEM-EDX:	Field Emission Scanning Electron Microscopy and Energy-Dispersive X-ray spectrometry
FFR:	Feed Flow Rate
FLOX:	FLameless OXidation
FP:	Fast Pyrolysis
FT:	Fischer-Tropsch Synthesis
FTIR:	Fourier-Transform InfraRed spectroscopy
G:	Guaiacyl
GDE:	Gas Diffusion Electrode
H:	Hydroxyphenyl
HGC:	Hot gas cleaning
HiTAC:	High-Temperature Air Combustion
HM:	Heavy Metals
HMI:	Human Machine Interface
HTC:	Hydrothermal Carbonization

HTL:	Hydrothermal Liquefaction
HU:	Unburned Hydrocarbons
HZ:	Hazel
ICP:	Inductively Coupled Plasma
KIT:	Karlsruhe Institute of Technology
LENA:	Laboratory plant for the energetic exploitation of agricultural matter
LHV:	Lower Heating Value
LMW:	Low Molecular Weight
LTC:	Low Temperature Combustion
LUCY:	Lab Unit CYclonic burner
MC:	Miscanthus
MDEA:	Methyl diethanolamine
MF:	Microfiltration
MFC:	Mass Flow Controller
MGA:	Membrane Gas Absorption
MH:	Metal hydrogen bond
MILD:	Moderate or Intense Low-oxygen Dilution
MP-P:	Monopolar- parallel
ORP:	Oxidation Reduction Potential
P:	Thermal Power
PCB:	Polychlorinated biphenyl
PCCD:	Polychlorinated dibenzodioxins
PCDF:	Polychlorinated dibenzofurans
PLC:	Programmable Logic Controller
PM:	Particulate Matter
PP:	Pennisetum purpureum
PTE:	Potential Toxic Elements
PTFE:	Polytetrafluoroethylene
PV:	Panicum virgatum
PVDF:	Polyvinylidene Fluoride
RCG:	Reed canary grass
REA:	Renewable Energy Agency
RSM:	Response Surface Methodology
S:	Syringyl
SCADA:	Supervisory Control And Data Acquisition
SCWG:	Supercritical Water Gasification
SCWO:	Supercritical Water Oxidation
SEM:	Scanning Electron Microscopy
SHER:	Sherbrooke (Université de Sherbrooke)
SO:	Saccharum officinalis
SR:	Saccharum robustus
SRC:	Short rotation coppice
SS:	Suspended solids
TC:	Tetracycline
TCLP:	Toxicity Characteristic Leaching Procedure

TGA:	Thermal Gravimetric Analysis
TGC:	Treating Gas Capacity
TIC:	Total Inorganic Carbon
TOC:	Total Organic Carbon
TP:	Technology pathway
TUR:	Turbidity
UFG:	Universidade Federal de Goiás
UNITUS:	Università degli Studi della Tuscia
UoS:	University of Strathclyde
VIN:	Vineyard
WGC:	Warm gas cleaning
WGS:	Water gas shift
WP:	Work package
XRD:	X-Ray Diffraction



## 1 EXECUTIVE SUMMARY

This deliverable focuses on process specification of the CERESiS technological pillar (WP3). This includes the two conversion routes, supercritical water gasification (SCWG) and fast pyrolysis (FP), as well as the respective decontamination technologies and the subsequent biofuel production, as depicted in Figure 1-1. Additionally, a concept for the collaboration with the phytoremediation pillar (WP2) will be proposed.

Aims and scope of this report can be summarized as followed:

- Definition of a biomass sampling scheme: sample distribution based on characterization results
- Definition of the overall process chain for both technology pathways (TP): specification of SCWG and FP operation parameters
- Integration with decontamination technologies and biofuel production
- Presentation of a multi-parametric biomass technology matrix (BTM)
- Assessment of technological risks and proposal of mitigation measures

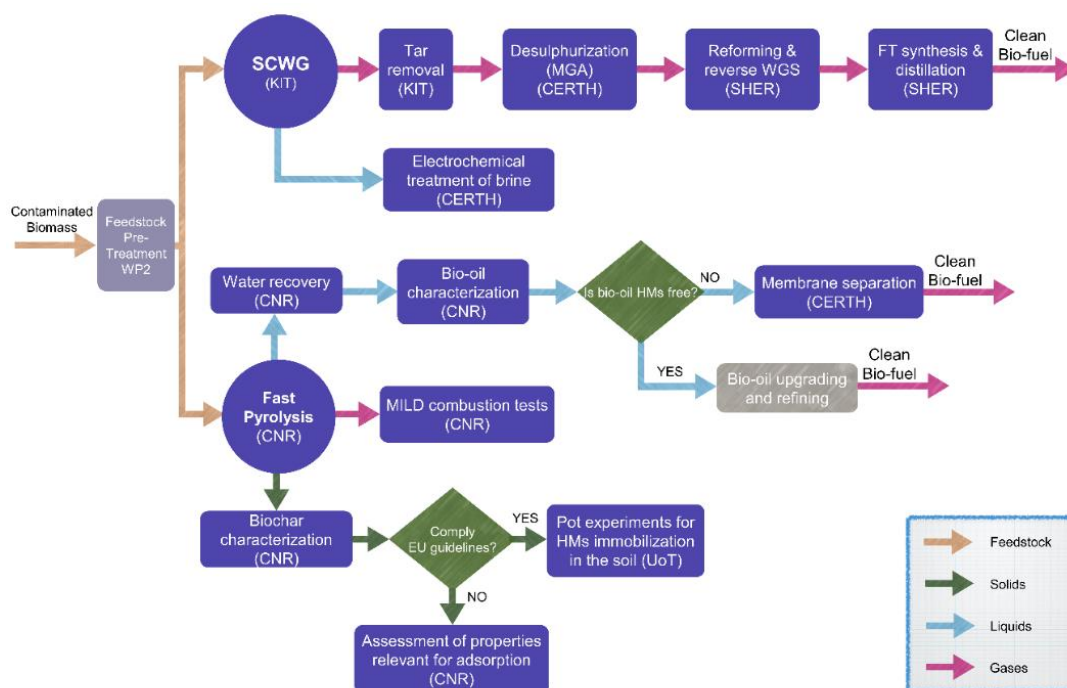


**Figure 1-1: Overview of the CERESiS technological pillar (WP3): Supercritical water gasification (TP1) and Fast Pyrolysis (TP2) based technology pathway.**

The information given in this report represents the current state of knowledge. The biomass technology matrix described below will evolve throughout the course of the project as new insights are going to be generated. The BTM will be adapted accordingly.

## 2 BIOMASS SAMPLING SCHEME

In this section, basic biomass characteristics and the workflow between WP2 (phytoremediation pillar) and WP3 (technological pillar) will be described. This includes an overview of expected biomass samples throughout the course of CERESiS, feedstock requirements and conceptual strategies for biomass distribution between TP1 and 2.

### 2.1 Fundamentals on biomass composition

Many databases collecting peer-reviewed data reported elemental and proximate analyses of several biomasses (Vassilev et al., 2010, Phyllis2). The analysis of these databases shows a considerable variability in the content of C, H, N, S, O, volatile matter, fixed carbon and ash, and in the ash composition. The variability is reduced if biomass species are grouped in families or sub-families and some common traits can be observed for woody and herbaceous families, the latter further divided into grasses, straws, fruit husks/shells sub-families (Vassilev et al., 2010).

The main components of plant biomass are cellulose, hemicellulose and lignin, long-chain natural polymers. Cellulose is a linear macromolecular polysaccharide consisting of cellobiose units linked by  $\beta$ -1,4-glycosidic bonds to form long chains with a high degree of polymerization (DP) (average DP comprised between 9,000-10,000). Hemicelluloses are found in both primary and secondary cell walls and are composed of short branched polysaccharides chains (500–3000 sugar units) cross-linked to other cell wall constituents. Hemicelluloses have a heteropolymeric structure made up mainly by six-carbon sugars as mannose, galactose, glucose, and 4-O-methyl-d-glucuronic acid and the five-carbon sugars as xylose and arabinose. Most of the sugars within the hemicellulose backbone are linked through  $\beta$ -1,4-glycosidic bonds. In many cases, the hydroxyl groups in the ring structure are replaced by methoxyl and acetoxyl groups. Hemicelluloses, usually, are named according to the main sugar unit type, so they are divided into four general groups: xylans, mannans, xyloglucans, and mixed-linkage  $\beta$ -glucans (Scheller and Ulvskov, 2010). Hemicellulose accounts for about one third of total biomass dry weight and it is present along with cellulose in almost all terrestrial plant cell walls. The hemicellulose distribution varies in softwoods and hardwood. Galacto-glucomannan and glucomannan prevail in softwood, while xylans are present in lower amounts. Hardwood and herbal plants hemicellulose consists mainly (more than 90%) of 4-O-methyl-D-glucurono-D-xylan units, whereas the glucurono-arabino-xylan is the dominant form in annual plants, like straw and grass (Scheller and Ulvskov, 2010).

Lignin is a natural biopolymer making up to 10–25 wt.% of plant biomass. It is a complex, dense, amorphous, secondary cell wall racemic heteropolymer embedding the cellulosic microfibrils and it is responsible of the cell wall structural rigidity. Lignin is composed of p-hydroxyphenyl (H), guaiacyl (G), and syringyl (S) monomers (monolignols) produced from p-coumaryl, coniferyl, and sinapyl alcohols, respectively. The three hydroxycinnamyl alcohol monomers are characterized by a different degree of methoxylation increasing

from 0 to 2 in the order of p-coumaryl, coniferyl and sinapyl alcohols. In the lignin network, the different monomeric units are bonded together through C-O-C bonds or C-C linkages. The proportion of the three monolignols differs among different regions in the cell wall, among cell types, and among plant species. G units predominate in gymnosperm lignin; G and S units predominate in angiosperms, while grass lignin is composed of H, G, and S units (Naseem et al., 2016).

Usually, cellulose, hemicellulose, and lignin account for more than 90% of the entire lignocellulosic biomass; however, other species should be considered such as pectin, extractives and inorganics. The relative content of the above-mentioned components depends not only on the type of biomass or plant organ, but also on the specific constraints of the growing site and the harvesting time as revealed by the available databases reporting the components analysis of many examples of the same species (Vassilev et al., 2012, Phyllis2, Debiagi et al., 2015).

In addition to the organic fraction, biomass often contains variable levels of inorganic elements. As reported in Giudicianni et al. (2021), Kirkbey (2012) provided an overview of the “essential mineral elements” (Arnon and Stout, 1939) in higher plants defined as essential elements in completing plant lifecycle, not replaceable by another element, and participating directly in plant metabolism. They are classified as macronutrients and micronutrients according to the concentration needed for plants life. Besides C, H and O forming the organic molecules, macronutrients comprise N, S, P, K, Ca, and Mg, whereas Fe, Mo, B, Cu, Mn, Zn, Ni, and Cl, are considered micronutrients and their concentration ranges from 0.1 to 200 mg/kg (Marschner, 2011). Macronutrients and micronutrients are grouped in four classes according to their biochemical behavior and physiological functions. N and S belongs to the first group and are mainly involved (together with C, H and O) in the formation of the organic building blocks of the plant (amino acids, proteins, enzymes and nucleic acids). S is absorbed as sulfate by the plant roots and transported to the leaves where it is transformed and incorporated into the protein structure of the plant. P, B and Si, constituting the second group, are typically present in form of esters and participate in energy transfer reactions. The third group comprises K, Na, Ca, Mg, Mn and Cl, which are mostly involved in establishing electrochemical potential. Finally, the fourth group is formed by Fe, Cu, Zn and Mo, which contribute in facilitating the electron transport. Actually, Co, Na and Si, together with other inorganic elements, such as Al and Se, cannot be included in the category of the “essential mineral elements”, but are considered only beneficial for plants since they are not required by all plants but can promote plant growth and may be essential for particular taxa (Pilon-Smits et al., 2009).

Inside plants, HMs can possess various forms, e.g. impurities in cellulose, bonds with organic matter, ionic species, defects in salt or crystal structures, and impurities in sulphate, nitrate, etc. (Dastyar et al., 2019; Vassilev et al., 2014). Almost all HMs, except Fe, Cu, and Al, have been detected along with cellulosic or water-insoluble structures (Dastyar et al., 2019; Vassilev et al., 2014). Depending on the type of HM and plant, the distribution of metals varies significantly among different parts of the plant (root, shoot and leaves) (Laval-Gilly et al., 2017; Yao et al., 2012; Zhang et al., 2013). (Dastyar et al., 2019).

## 2.2 Biomass overview and basic feedstock requirements

Throughout the course of CERESiS, the samples of contaminated biomass will be provided by the four partners in WP2 (UoS, UNITUS, UFG and REA) as well as the newly acquired stakeholder ERSAF. To the current state of knowledge, 11 different plant species on 19 harvest sites will potentially be considered for phytoremediation trials (Figure 2-1). Harvest periods will be between 11/2020 and 12/2023. Contamination categories include potentially toxic elements (PTE: Cd, Zn, V, Pb, Cu, Cr, Ni, Sb, Co, Mn, Th, As, Hg, Sn) and organic contaminants, e.g. PCBs, dioxins or furans. The contamination level will be individually classified (WP2) as low, medium or high. The information provided in Figure 2-1 results from meetings and agreements with WP2 partners.

<b>WP2 partner</b>	UoS				UNITUS				UFG				REA				ERSAF																					
<b>Plant species</b>	MC	RCG			SRC			VIN			HZ			AM			PP			SO			SR			AD			PV									
<b>Site</b>	i	ii	iii	iv	v	vi	vii	viii	ix(a)	ix(b)	x(a)	x(b)	xi(a)	xi(b)	xii(a)	xii(b)	xiii	xiv	B																			
<b>Harvest period</b>	2020		2021												2022												2023											
	11	12	1	2	3	4	5	6	7	8	9	10	11	12	1	2	3	4	5	6	7	8	9	10	11	12	1	2	3	4	5	6	7	8	9	10	11	12
<b>Contamination category</b>	PTE												Organic contaminants																									
<b>Contamination level</b>	low						medium						high																									

**Figure 2-1: Biomass sample overview: possible combinations of WP2 partner, plant species, harvest site and period and contamination category and level.** MC: Miscanthus, RCG: Reed canary grass, SRC: Short rotation coppice, VIN: Vineyard, HZ: Hazel, AM: Andropogon minarum, PP: Pennisetum purpureum, SO: Saccharum officinalis, SR: Saccharum robustus, AD\*: Arundo donax, PV\*: Panicum virgatum, B: Brescia.

\* These biomass samples were offered externally to the consortium from stakeholder ERSAF and were cultivated in the agricultural areas of SIN “Brescia-Caffaro” (B), Italy. Contamination by PCB, PCDD-PCDF, arsenic and mercury, mainly deriving from the past activities of the chemical plant Caffaro spa.

In order to generate wide-ranging results during the project, the intention is to test a broad variety of combinations shown in Figure 2-1. Especially biomass samples with a high contaminant load are considered to be of particular interest. To characterize the samples, WP2 partners will conduct the necessary analytical work. Depending on soil properties, elemental and proximate analyses will be performed to provide information on the following

(i) for all samples:

- Dry matter/H<sub>2</sub>O content
- Volatile matter
- Fixed carbon

- Ash content
- C, H, N, O, Cl, F, S
- Contaminants (potentially toxic elements: Cd, Zn, V, Pb, Cu, Cr, Ni, Sb, Co, Mn, Th, As, Hg, Sn)
- trace elements considered relevant to SCWG and/or FP \*

(ii) for selected samples (where relevant):

- Organic contaminants (if present)
- Alkali and earth alkali metals
- Ash composition
- Other specials

\* e.g. Fe, Si and P weren't originally considered as part of the basic screening in the GA, but are relevant due to the formation of complexes with HMs during pyrolysis (affecting the devolatilization behaviour, see Section o) and salts during SCWG (see Section 3.1.3).

In addition, a first feedstock pretreatment will be performed to homogenize the sample, facilitate drying and to meet the basic requirements of the subsequent conversion technologies. For SCWG, wet biomass samples are more applicable whereas for FP, biomass samples must be dried. If the samples are unstable (biological degradation), drying can become necessary even for SCWG samples. A mechanical size reduction (particle size < 5 cm) is essential in both cases. The basic feedstock requirements of SCWG and Fast Pyrolysis are summarized in Table 2-1.

**Table 2-1: Basic feedstock requirements of SCWG and Fast Pyrolysis.**

Conversion technology	Moisture Content	Particle size	Feedstock amount
<b>SCWG</b>	Preferably undried**	<b>Undried:</b> chips (as small as possible) <b>Dried:</b> powder	depending on moisture content, probably ~3-5 kg per sample
<b>Fast Pyrolysis</b>	<10 wt.%	Powder (4 mm) Chips (max. length 1 cm)	To be defined after the definition of the test matrix

\*\* First experiments revealed that in case of fibrous or woody materials, drying and milling (1mm particle size) will most likely be necessary for successful operation of the SCWG lab plant. See also Section 3.1 . Field H<sub>2</sub>O measurements will allow for dried, preserved biomass to be rewetted to near original condition.

## 2.3 Biomass distribution

The conceptual workflow between WP2 and WP3 with regard to sample distribution is depicted in Figure 2-2. When a biomass sample is harvested, WP2 partners will provide basic sample information. Data sheets will be distributed to relevant partners through the project's adopted communication channels. This information will be complemented with analytical data, as soon as the analytical work is completed. To avoid storage difficulties, stable biomass samples can be shipped to WP3 partners before a complete set of data is available.

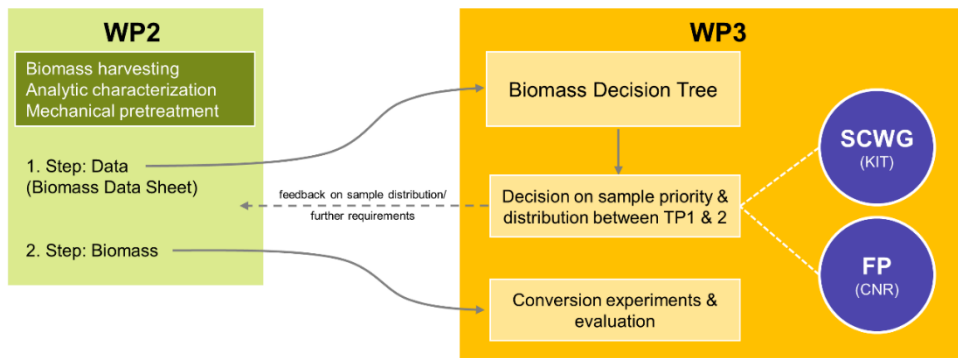


Figure 2-2: Conceptual workflow between WP2 und WP3.

The sample distribution between TP1 and TP2 and prioritization of treatment will then depend on

- Availability of biomass
- Capacity of laboratory plants
- Biomass sample characteristics

These aspects are taken into account in a purpose-built “Biomass Decision Tree” (Figure 2-3, see also Annex 1 Biomass Distribution), which will be applied to distribute the biomass samples between TP1 and TP2. At least one sample of each biomass species will be considered for conversion. The biomass decision tree allows prioritizing samples that qualify as interesting, e.g. samples with a high contaminant load, a new combination of characteristics (Figure 2-1) or a special feature. The classification largely depends on the availability of a complete set of biomass data provided by WP2 partners. Upon request, it will also be possible to reserve FP/SCWG testing capacity for anticipated samples of interest, in order to avoid omitting biomass species that will arise towards the end of the project (i.e. newly planted biomass).

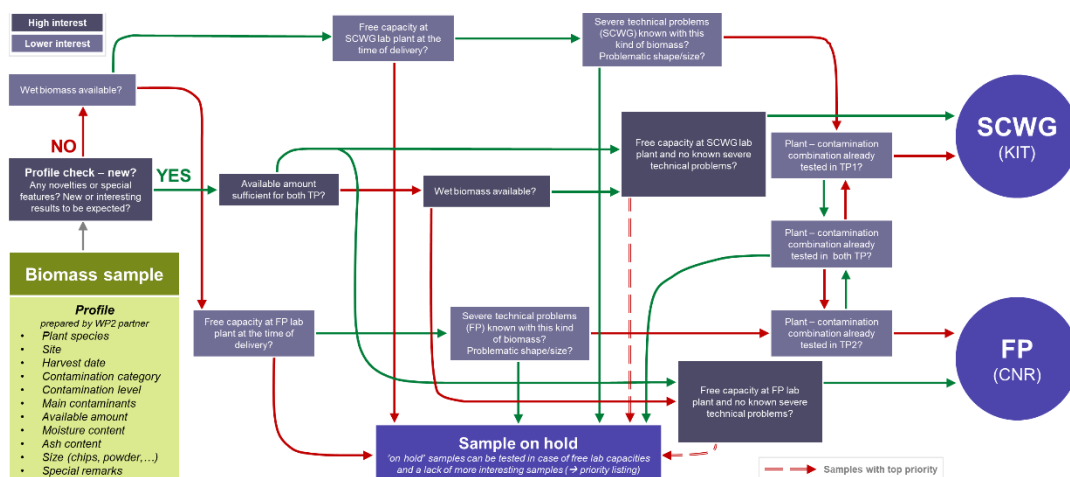


Figure 2-3: Biomass Decision Tree: Prioritization and distribution of biomass samples between TP1 and TP2.

## 2.4 List of References

---

- Arnon, D. I.; Stout, P. R. (1939). 'The essentiality of certain elements in minute quantity for plants with special reference to copper'. *Plant Physiology*, 14, p371.
- Dastyar, W., Raheem, A., He, J., Zhao, M., (2019). 'Biofuel Production Using Thermochemical Conversion of Heavy Metal-Contaminated Biomass (HM CB) Harvested from Phytoextraction Process'. *Chemical Engineering Journal* 358, 759–785.
- Debiagi, P. E. A.; Pecchi C.; Gentile, G.; Frassoldati, A.; Cuoci, A.; Faravelli, T.; Ranzi, E. (2015). 'Extractives extend the applicability of multistep kinetic scheme of biomass pyrolysis'. *Energy and Fuel*, 29, p6544-6555.
- Giudicianni, P., Gargiulo, V., Grottola, C. M., Alfè, M., Ferreiro, A. I., Mendes, M. A. A., Ferreiro, A. I., Ragucci, R. (2021). 'Inherent metal elements in biomass pyrolysis: A review', *Energy & Fuels*, 35(7), p5407-5478.
- Kirkbey, E. (2012). 'Introduction, definition and classification of nutrients'. In *Marschner's mineral nutrition of higher plants*, Academic Press, p3-5.
- Laval-Gilly, P., Henry, S., Mazziotti, M., Bonnefoy, A., Comel, A., Falla, J., (2017). 'Miscanthus x Giganteus Composition in Metals and Potassium After Culture on Polluted Soil and Its Use as Biofuel'. *Bioenerg. Res.* 10, 846–852.
- Marschner, H. (2011). 'Marschner's mineral nutrition of higher plants'. Academic Press.
- Naseem, A.; Tabasum, S.; Zia, K.M.; Zuber, M.; Ali, M.; Noreen, A. (2016). 'Lignin-derivatives based polymers, blends and composites: a review'. *International Journal of Biological Macromolecules*, 93, p296-313.
- Phyllis2, Energy research Centre of the Netherlands, database for biomass and waste; <https://www.ecn.nl/phyllis2> (accessed June 20, 2021).
- Pilon-Smits, E. A.; Quinn, C. F.; Tapken, W.; Malagoli, M.; Schiavon, M. (2009). 'Physiological functions of beneficial elements'. *Current Opinion in Plant Biology*, 12, p267-274.
- Scheller H. V.; Ulvskov P. (2010). 'Hemicelluloses'. *Annual Review of Plant Biology*, 61 (1), p263-289
- Vassilev, S. V.; Baxter, D.; Andersen, L. K.; Vassileva, C. G (2010). 'An overview of the chemical composition of biomass'. *Fuel*, 89 (5), p913-933.
- Vassilev, S. V.; Baxter, D.; Andersen, L. K.; Vassileva, C. G.; Morgan, T. J. (2012). 'An overview of the organic and inorganic phase composition of biomass'. *Fuel*, 94, p1-33.
- Vassilev, S.V., Vassileva, C.G., Baxter, D., (2014). 'Trace element concentrations and associations in some biomass ashes'. *Fuel* 129, 292–313.
- Yao, Z., Li, J., Xie, H., Yu, C., (2012). 'Review on Remediation Technologies of Soil Contaminated by Heavy Metals'. *Procedia Environmental Sciences* 16, 722–729.
- Zhang, H., Tian, Y., Wang, L., Zhang, L., Dai, L., (2013). 'Ecophysiological characteristics and biogas production of cadmium-contaminated crops'. *Bioresource Technology* 146, 628–636.

## 3 HYDROTHERMAL GASIFICATION (SCWG) BASED TECHNOLOGY PATHWAY

In this section, the overall process chain for technology pathway 1 will be defined and an initial screening of technologies will be performed. This includes supercritical water gasification and tar removal (KIT) (Section 3.1), desulphurization of the produced gas and saline wastewater treatment (CERTH) (Section 3.2) as well as the assessment of the feasibility of gas reforming and catalytic biofuel synthesis (reverse water gas shift reaction and Fischer-Tropsch-Synthesis, SHER) (Section 3.3). Key influential parameters for process performance will be identified for every technology, while considering the destruction of organic contaminants and separation/fixation of inorganics. The results will be summarized in a biomass technology matrix, displaying all technologies and influential parameters (Section 5).

### 3.1 Supercritical water gasification (SCWG)

---

#### 3.1.1 Fundamentals and influential parameters of SCWG

In hydrothermal conversion processes, biomass can be converted without prior drying, using water at high temperatures and increased pressure as reaction medium. The SCWG process exploits the special features of supercritical water, which comprise a low viscosity and density as well as a non-polar behaviour, promoting mixing and reaction with organic compounds (Galkin and Lunin, 2005; Kruse and Dinjus, 2007). This requires an operating pressure >221 bar (usually 250–300 bar) as well as temperatures well above 400 °C (up to 700 °C). The SCWG product gas is a mixture consisting mainly of H<sub>2</sub>, CH<sub>4</sub> and CO<sub>2</sub>, with smaller amounts of C<sub>2</sub>-C<sub>3</sub> compounds and CO (Boukis and Stoll, 2021; Kruse et al., 2013).

Since the early 2000s, the Karlsruhe Institute of Technology (KIT; former Research Center Karlsruhe) has been operating a dedicated pilot plant for SCWG, known as “VERENA” (Boukis et al., 2010, 2017a; Möbius et al., 2012, 2013). Parallel to the pilot plant, KIT also operates a lab-scale facility named “LENA” (German acronym: “laboratory plant for the energetic exploitation of agricultural matter”), which will be employed during the course of CERESiS. The lab-scale plant is equipped with a piston-like feeding system capable of handling even viscous feed slurries or solid particles. (Boukis and Stoll, 2021). Typical operating conditions are 280 bar and 650 °C, maximum feed rate is 1 kg/h. A scheme of the laboratory plant at KIT is shown in Figure 3-1. A description of the basic set-up and components can be found in (Boukis et al., 2015). The configuration of the reaction system is under continuous development.



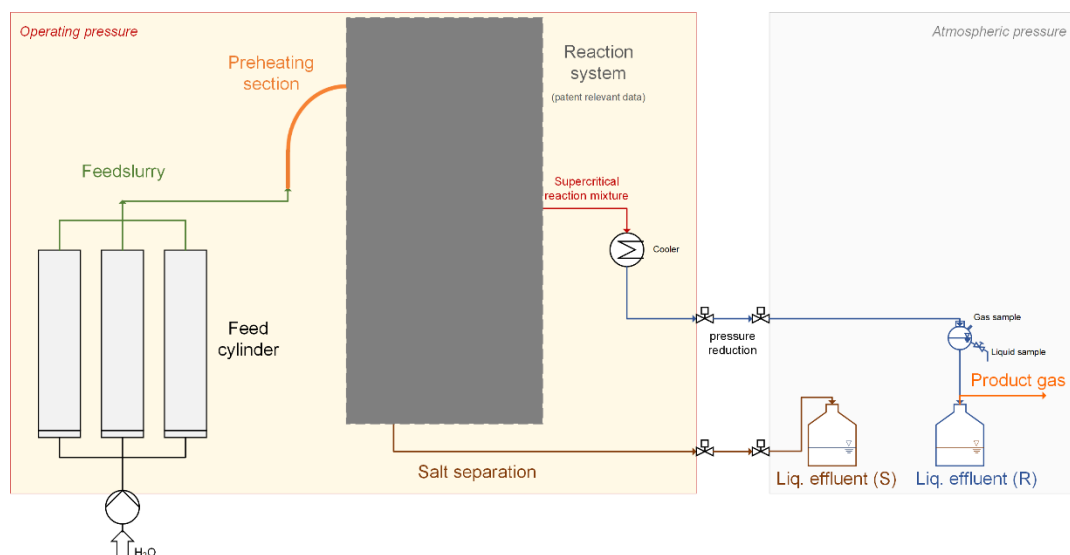
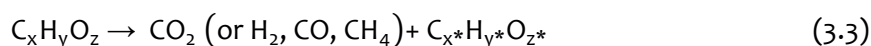
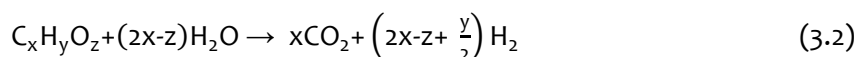
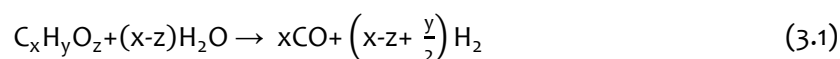


**Figure 3-1: Schematic description of the SCWG laboratory plant at KIT.**

For laboratory experiments, biomass is mixed with water and additives to create a slurry with a moisture content > 80 % (see 3.1.2 (feedstock preparation)). The slurry is filled in a feed cylinder and led to a preheating section, where sub- or near-critical conditions are achieved (300 – 450 °C). Hydrothermal gasification takes place in the subsequent reaction zone comprising one or more tubular reactor(s) ( $T > 500$  °C). The process pressure (> 250 bar) is controlled by a backpressure regulator. One important aspect in process design is the separation of solids (salts), which is described in detail in section 3.1.3 (Salt behaviour and separation of solids). This typically (but not necessarily) leads to two liquid streams, the reactor effluent (R) and a brine (S).

During gasification with supercritical water, the macromolecules contained in the biomass are first broken down into smaller intermediates, which are then converted into gases (Guan et al., 2012). In the first step, the biopolymers cellulose, hemicellulose, and lignin and proteins are hydrolysed in supercritical water and decomposed into their monomers. Through various reactions, these are further converted into a variety of smaller intermediates (acids, aldehydes, furfurals, phenols...), from which gases are formed. Here, possible conversion routes include the reaction with water (steam reforming) (Eq. (3.1) and (3.2)) or the formation of gases directly from intermediates as the molecules decompose (Eq. (3.3)) (Pavlovič et al., 2013; Resende and Savage, 2010; Yakaboylu et al., 2015c), for example, by decarboxylation (Waldner and Vogel, 2005; Watanabe et al., 2001).



In the gas phase, the water-gas shift and methanation reactions cause a shift in the relative proportions of the individual gas species. Compared to conventional gasification, in SCWG the equilibrium of the water-gas-shift reaction (Eq. (3.4)) is shifted to the side of the products due to the high water concentration. This results in the high H<sub>2</sub> yield and the low CO content in the gas mixture. (Resende and Savage, 2010; Yakaboylu et al., 2015c).



Resende and Savage (2010) identified the steam reforming reaction to be a significant source of hydrogen using reaction rate and sensitivity analysis. According to this study, CO, CO<sub>2</sub> and CH<sub>4</sub> are primarily formed directly from the various intermediates during non-catalytic gasification (radical reactions (Lu et al., 2006)). CH<sub>4</sub> is probably also formed by methanation of CO and CO<sub>2</sub> (Eqs. (3.5) and (3.6)) (Boukis et al., 2003). This reaction is promoted by the use of heterogeneous catalysts (e.g. nickel) (Azadi et al., 2012; Waldner and Vogel, 2005).



Various reactions can also produce coke or tar from aromatic intermediates (Karayildirim et al., 2008; Kruse, 2008; Reddy et al., 2014), although in small amounts compared to conventional “dry” gasification (Chuntanapum and Matsumura, 2010; Galkin and Lunin, 2005). Influential factors are type and composition of biomass (Karayildirim et al., 2008), temperature and heating rate (Matsumura et al., 2006; Müller and Vogel, 2012). During heat-up, process conditions of hydrothermal carbonization (HTC) and liquefaction (HTL) are passed and corresponding products are formed, some of which cannot be converted in the subsequent gasification step (Kruse, 2008). Commonly, polymerization reactions of unsaturated intermediates such as furfurals or phenols are employed as an explanation for coke and tar formation (Matsumura et al., 2006, 2005; Yong and Matsumura, 2012).

Hydrothermal technology offers a broad range of possible applications in the field of waste management (Zhan et al., 2020). Toxic organic compounds like PCBs can effectively be treated via supercritical water oxidation (SCWO) (Roshchin et al., 2017; Weber et al., 2002), a process developed in the 1980s by M. Modell for the conversion of organic wastes, using SCW and an oxidant (Peterson et al., 2008). At lower, subcritical temperatures, oxidative conditions also accelerate the degradation of dioxins and furans. With increasing temperature (> 200 °C), PCDDs and PCDFs could also be decomposed under non-oxidative conditions (Jin et al., 2013). It can therefore be assumed that organic contaminants contained in the CERESiS biomass will, at least partly, be decomposed during SCWG. As the concentrations are expected to be very low, a comprehensive analysis will be difficult due to detection limits of available analytical methods.

## Influential parameters of SCWG

### Temperature

The reaction temperature has a crucial role in SCWG (Lu et al., 2012; Reddy et al., 2014). Since the overall process is endothermic, high temperatures are advantageous from a thermodynamic point of view (Guo et al., 2007). As the temperature increases, radical reaction mechanisms dominate in supercritical water, which promotes the formation of gaseous products during biomass decomposition (Y. Guo et al., 2010). (D'Jesús Montilva et al., 2006; Guo et al., 2007; Lee et al., 2002; Lu et al., 2012, 2006) also report an increase in gasification efficiency with an increase in temperature for various feedstock and operating conditions. A high heating rate can also reduce the formation of coke and tars and improve gas yield (Hendry et al., 2011; Matsumura et al., 2006; Sinag et al., 2004).

### Pressure

The significance of pressure is less clear. D'Jesús Montilva et al., 2006) and (Hao et al., 2003) observed no effect of pressure variation on the amount of gas produced. In contrast, others reported decreased H<sub>2</sub> yield with increase in pressure (Kruse et al., 2000; Madenoğlu et al., 2013; Zhiyong and Xiuyi, 2015). (D'Jesús Montilva, 2007) suggests a small influence of pressure at higher temperatures, since the reactions taking place in this range are temperature controlled. (Lu et al., 2012) refer to the change in physical properties of supercritical water when the pressure is varied. Due to the increase in density with increasing pressure, water forms a "solvent cage" around the dissolved molecules and thus acts as a barrier to reactions of these molecules with each other (coking, polymerization). Simultaneously, reactions with water (steam reforming, water-gas shift) are promoted. (Lu et al., 2012).

### Reactor residence time

Various research groups observed a higher total gas yield or gasification efficiency with extended residence time in the reactor (Cao et al., 2011; Lu et al., 2006; Muangrat et al., 2010; Zhiyong and Xiuyi, 2015). (D'Jesús Montilva et al., 2006) describe an increase up to a temperature-dependent maximum value. No further improvement in efficiency can be obtained when the residence time is further increased. The gas composition is also affected by the reaction time, (Byrd et al., 2008), (D'Jesús Montilva, 2007) and (Boukis et al., 2017b) report a higher methane and lower hydrogen content in the gas composition at larger residence times. In comparison, (Lee et al., 2002) could not detect any influence of the residence time (conversion of glucose in supercritical water).

### Structure of biomass

The main components of biomass are cellulose, hemicellulose and lignin, as described in Section 2.1 In order to determine the influence of biomass structure, several studies focus on the hydrothermal conversion of these biomass model compounds (Madenoglu et al., 2016; Osada et al., 2004; Saisu et al., 2003; Yoshida and Matsumura, 2001) and the comparison with/of real biomasses (Ding et al., 2014; Kang et al., 2016; Salimi et al., 2016; Yanik et al., 2007; Yoshida et al., 2004). Gasification of biomasses with higher amount of

cellulose and hemicellulose was found to produce higher amounts of hydrogen, whereas the presence of lignin decreases the H<sub>2</sub> yield (Salimi et al., 2016). It is unclear whether the composition of lignin has an influence on gas production (Yanik et al., 2007; Yoshida et al., 2004).

#### Dry matter content of the feed slurry

Under the same operating conditions, gasification of feed material with a higher biomass concentration is more difficult (Guo et al., 2007; Lu et al., 2012). Regardless of the feed material, the gasification efficiency (L. Guo et al., 2010) and H<sub>2</sub> yield decrease with increasing dry matter content (Cao et al., 2011; Guo et al., 2007). (Antal et al., 2000) name high temperatures, a high heating rate and the use of catalysts as prerequisites for efficient gasification at high dry matter content.

#### Catalyst

In terms of the use of catalysts, there are two different process variants described in literature. One possibility is the application of noble metal catalysts (Azadi et al., 2012; Elliott, 2008; Waldner and Vogel, 2005), which enables a lower reaction temperature (<500 °C) and results in a higher methane content in the product gas. In the second option, earth alkali salts (e.g. carbonates) are employed as additives (Boukris et al., 2017a; Kruse et al., 2000; Muangrat et al., 2010; Onwudili, 2013). This requires higher reaction temperatures and leads to an increased hydrogen content in the product gas.

In order to achieve higher conversion rates at low temperatures, heterogeneous catalysts are widely used, especially when methane is the target product (Matsumura et al., 2005). Several authors report improved gasification efficiency by using ruthenium, nickel, or activated carbon (Azadi et al., 2012; Behnia et al., 2016; Byrd et al., 2008; Frusteri et al., 2017; Minowa and Ogi, 1998; Molino et al., 2017; Waldner and Vogel, 2005). It was shown that Ni-catalysts promote reactions such as steam reforming and methanation (Frusteri et al., 2017; Minowa and Inoue, 1999; Minowa and Ogi, 1998; Waldner and Vogel, 2005). A more detailed overview on catalysed SCWG can be found in (Azadi and Farnood, 2011) and (Y. Guo et al., 2010).

Alkali salts are known to increase the gasification yield (Kruse et al., 2000; Kruse and Faquir, 2007; Muangrat et al., 2010; Onwudili, 2013; Sinađ et al., 2003; Xu et al., 2013) and reduce coke formation (Onwudili, 2013; Sinađ et al., 2003). Taking K<sub>2</sub>CO<sub>3</sub> as an example, the catalytic effect is explained via the formation of potassium formate, the decay of which eventually produces H<sub>2</sub> and CO<sub>2</sub> (Onsager, 1996; Yanik et al., 2008). In summary, alkali salts promote the conversion of CO via the water–gas shift reaction, generating higher H<sub>2</sub> yields (and additionally CO<sub>2</sub>) (Kruse and Dinjus, 2005).

In SCWG experiments at the KIT lab facility LENA, potassium salts are usually employed as catalyst (c(K<sup>+</sup>): 500 – max. 10000 mg/kg feed slurry). Depending on the process parameters described above, gasification efficiency, product gas composition and production rate (~ 5 – 70 NL/h) vary. Phase separation of product gas and reactor effluent occurs after the reactor, where the supercritical reaction mixture is depressurized and cooled down

(1,013 bar, 25 °C). Samples of the product gas are withdrawn with a syringe and injected into a gas chromatograph (Hewlett Packard 5890), which determines the volume fractions of H<sub>2</sub>, CO, CH<sub>4</sub>, CO<sub>2</sub>, C<sub>2</sub>H<sub>4</sub>, C<sub>2</sub>H<sub>6</sub>, C<sub>3</sub>H<sub>6</sub> and C<sub>3</sub>H<sub>8</sub>. An estimated concentration range is listed in Table 3-1.

**Table 3-1: Estimated concentration range of SCWG product gas species.**

Gas species	H <sub>2</sub>	CH <sub>4</sub>	CO <sub>2</sub>	C <sub>2-3</sub>	CO	S compounds
Concentration range / vol.-%	20 – 40	10 – 30	30 – 50	1 – 15	0 – 2	< 1000 ppm

Gasification efficiency additionally affects the wastewater quality (effluent R). At lower conversion rates, the amount of organic compounds (total organic carbon, TOC) increases (D’Jesús Montilva, 2007) (see Table 3-7, Section 3.2 for exemplary composition of effluent R).

Experimental target throughout CERESiS will be the efficient separation of contaminants, which requires the development of a suitable process configuration for solid separation (see Section 3.1.3). Additionally, operating parameters will be optimized, focusing on temperature profiles, catalyst addition and residence time. Table 3-2 summarizes the foreseen operating conditions of the SCWG lab plant at KIT.

**Table 3-2: Range of operational conditions at KIT’s SCWG laboratory plant “LENA”**

Operating parameter	Range
<b>Temperature</b> - preheater - reactor	200 – 500 °C 500 – 750 °C
<b>Pressure</b>	250 – 300 bar
<b>Feed rate</b>	100 – 800 g/h
<b>Dry matter content</b>	5 – 15 %
<b>Catalyst*</b>	0 – 10000 ppm K <sup>+</sup>

\* The use of additional catalysts will eventually also be considered, depending on experimental results

### 3.1.2 Feedstock preparation

Depending on the composition and, especially, the size and texture of the feed material, a mechanical pretreatment is obligatory for successful SCWG operation. Another typical aspect of feed preparation for SCWG experiments is the addition of alkali salts as catalyst. Xanthene is added to the slurry to increase viscosity and prevent sedimentation of solid particles. Dry matter content of the feed slurry is below 20 wt.-%, typically between 5 and 12 wt.-%.

For fresh, moist biomass (plant parts, grasses), the mechanical pretreatment (at pilot-scale) starts with a coarse size reduction, followed by additional pretreatment steps. At first, a cutting mill is typically used to obtain biomass particles of few mm. With a second milling step using a colloid mill, the size of the particles can be further reduced. For example, with corn silage, 84 wt.% of the biomass particles were smaller than 0.5 mm after the second pretreatment step (Boukris et al., 2005). Another option is the utilization of a macerator or a meat grinder. For biomass and organic waste materials that already comprise only smaller particles (e.g., industrial sludge, sewage sludge, or brewer's spent grain), the use a colloid mill is sufficient. Generally, a particle size of less than 1 mm is recommended for the feed slurry that is led to the reactor. (Boukris and Stoll, 2021).

First lab-scale experiments in the course of CERESiS revealed that additional feed pretreatment will most likely be necessary for hydrothermal gasification of the plant species listed in Section 2.2 Several pretreatment methods for lignocellulosic biomass are already described in literature, an overview is provided in Table 3-3. In terms of SCWG, an alkaline hydrolysis using KOH seems to be the most convenient, as it simultaneously provides the homogeneous catalyst. This method will therefore be favoured at the beginning of the experimental investigations. Additional technologies will be considered if necessary.

**Table 3-3: Overview on pretreatment methods for lignocellulosic biomass.**

Pretreatment method	Advantages/Disadvantages	Literature
<b>Mechanical treatment</b> Size reduction (chipping, milling, grinding, ...)	+ reduce particle size and increase surface - low conversion efficiencies - energy intensive process	(Kumari and Singh, 2018; Kwon et al., 2016; Singh et al., 2016)
<b>Acid hydrolysis</b> Treatment with (diluted) acid, hydronium ions break and attack inter- and intramolecular interactions	+ simple to realize in the laboratory + concentrated sulfuric acid (H <sub>2</sub> SO <sub>4</sub> ) is very effective in cellulose hydrolysis + hemicellulose well soluble - toxic & corrosive process - degradation due to high temperatures	(Kim et al., 2016; Kumar et al., 2009; Lee et al., 2014; Singh et al., 2016; Tao et al., 2011)
<b>Alkaline hydrolysis</b> Treatment with alkali (NaOH, KOH, ...), biomass structure is destroyed by hydrolysis of the ester bonds	+ simple to realize in the laboratory + KOH: simultaneous addition of SCWG catalyst (K <sup>+</sup> ) + removes lignin + gentler than acid treatment - formation of irrecoverable salts - not suitable for softwood biomass	(Janke et al., 2016; Kumar et al., 2009; Singh et al., 2016)
<b>Biological treatment</b> Enzymes or fungi break down lignin, hemicellulose and polyphenols	+ mild operating parameters + lignin is degraded - low hydrolysis rate - expensive at larger scale	(Ali et al., 2017; Baba et al., 2017; Saritha et al., 2012; Singh et al., 2016; Widsten and Kandelbauer, 2008; Xu et al., 2009; Yu et al., 2009; Ziemiński et al., 2012)

<b>Orangosolv</b> An organic solvent with inorganic acids is used to break the lignin and hemicellulose bonds.	+ Hydrolysis of lignin and hemicellulose - Solvents must be recovered (high energy consumption) - Cellulose does not dissolve in solvent	(Kumar et al., 2009; Lee et al., 2014; Singh et al., 2016)
<b>Microwave irradiation</b> Heating via irradiation, alters the ultra-structure of cellulose & degrades or partially removes hemicelluloses and lignin. Can be combined with alkaline or acid treatment.	+ high uniformity and selectivity + short process time + less energy requirement compared to the traditional heating	(Kumari and Singh, 2018; Li et al., 2016; Singh et al., 2016)
<b>Pulsed-Electric-Field treatment (PEF)</b> High voltage impulses lead to structural changes in the cell wall and cell membrane. This increases permeability of the plant tissue.	+ low energy requirements (ambient conditions) + disruption of plant cells - high temperature, ash production	(Kumar et al., 2009)
<b>Supercritical CO<sub>2</sub></b> Supercritical CO <sub>2</sub> is directed across biomass. CO <sub>2</sub> penetrates biomass. During the subsequent pressure release, the biomass explodes. CO <sub>2</sub> also forms carbonic acid, which attacks hemicellulose.	+ cost-effective (CO <sub>2</sub> = cheap) + moderate temperatures + high loadings possible - high pressure device - no disruption of lignin and hemicellulose	(Daza Serna et al., 2016; Kumar et al., 2009; Singh et al., 2016)
<b>Ozonolyse</b> Lignin disintegration by oxidation using ozone. Fixed bed is more effective than an aqueous suspension.	+ reduces lignin content + milder operational conditions - high ozone demand - expensive	(Kumari and Singh, 2018; Singh et al., 2016)
<b>Ionic liquid</b> Cellulose dissolves in ionic liquid, 3D network of lignin is broken down	+ lowers the robustness of the biomass - expensive ionic liquids - difficult recovery of the liquid	(Lee et al., 2014; Singh et al., 2016; You et al., 2016)
<b>Ammonia fiber expansion (AFEX)</b> Biomass is exposed to ammonia under high pressure, which leads to swelling of the cellulose. Subsequent pressure reduction leads to explosive decompression. In addition, lignin is disintegrated.	+ moderate temperatures + increase of accessible surface area - does not sufficiently remove hemicellulose and lignin → not sufficient for lignin-rich biomasses	(Chundawat et al., 2020; Kumar et al., 2009; Singh et al., 2016)
<b>Steam Explosion</b> Saturated water vapor is directed at biomass under high pressure & penetrates biomass. Subsequent sudden expansion leads to explosion in the biomass	+ more energy efficient than mechanical processes + less corrosion, because only water is used - incomplete destruction of the lignin complex	(Medina et al., 2016; Singh et al., 2016)

### 3.1.3 Salt behaviour and separation of solids

The precipitation of salts is of particular importance in gasification under supercritical water conditions (Boukis et al., 2009; Schubert et al., 2010a; Yakaboylu et al., 2015a). Due to the reduced solubility, salts can cause blockages, especially in gasification processes with a fixed-bed catalyst, small pipe diameters and low flow velocities, or in combination with coke. The salt concentration of the biomass used, the type of salts formed, and the kinetics of crystal formation are crucial factors while reactor geometry and fluid dynamics also play a decisive role (Kruse, 2009, 2008). The management of the salt issue is an essential aspect in the technical implementation of a SCWG process (Boukis et al., 2009; Kruse, 2008; Matsumura et al., 2005). Crucial with respect to separation is the phase

behaviour of salts in supercritical and subcritical aqueous solution (Schubert et al., 2012, 2010a, 2010b).

Biomass contains various salts or salt-forming elements. Typically, these are N, K, P, S, Cl, Ca, Mg, Na and Si (Ekpo et al., 2016; Yanagida et al., 2008; Zhao et al., 2012) (see section 2.1). Due to their crucial influence on the SCWG process, several research groups have studied the behaviour of these components (Acelas et al., 2014; Bircan et al., 2013, 2011; Ekpo et al., 2016; Yakaboylu et al., 2015b; Yanagida et al., 2009; Zhang et al., 2012; Zhao et al., 2012; Zhu et al., 2011). During gasification with supercritical water, the macromolecules contained in the biomass are first broken down into smaller intermediates, which are then converted into gases (Guan et al., 2012). Cells are broken and organically bound heteroatoms such as N, P, Cl and S are converted to the corresponding inorganic acids (e.g. HCl, H<sub>2</sub>SO<sub>4</sub> or H<sub>3</sub>PO<sub>4</sub>), which are neutralized to their corresponding salts (Acelas et al., 2014; Schubert, 2010). Furthermore, inorganic components may be present in the feedstock as free ions (K<sup>+</sup>, Ca<sup>2+</sup>, Mg<sup>2+</sup>, ...) (Larcher, 2001; Zhao et al., 2012), which dissolve during biomass decomposition and form various salts. Table 3-4 describes the typical behavior (distribution between solid and liquid phase) of selected elements during a SCWG process. The concentration of these elements in the feed slurry is typically quantified in order to evaluate potential salt formation.

In contaminated biomass, heavy metals (Zn, Cu, Cd, Pb, Cr, Ni, Fe, Hg, As, ...) need to be considered as solid-forming elements as well. HMs can possess various forms inside the plant (see section 2.1). The fate of HMs has been under investigation during hydrothermal treatment of sewage sludge (Huang and Yuan, 2016; Li et al., 2012; Liew et al., 2021; Sawai et al., 2014; Weng et al., 2020), which is a very popular feedstock for SCW technology (Qian et al., 2016). In contrast to pyrolysis or conventional gasification, SCWG is not commonly in the picture for thermochemical conversion of contaminated biomass (Dastyar et al., 2019). Only recently, a few studies dealing with SCWG-based valorization of phytoremediation (or phycoremediation) – derived biomass were published (Leong et al., 2021; Li et al., 2018; Su et al., 2021). These investigations suggest that during SCWG, with increasing temperature, HMs are immobilized in solid deposits (Huang and Yuan, 2016; Li et al., 2018; Su et al., 2021), like salts and char. In addition, it can be assumed that HM will also be present in the liquid effluent(s) (see Section 3.2.2). The fate of heavy metals during SCWG will be a focus throughout the course of CERESiS.

As mentioned above, the presence of salts can cause clogging in hydrothermal processes (Boukris et al., 2005; Elliott et al., 2004; Kruse, 2008), increase the corrosion rate (Hodes et al., 2004; Kritzer et al., 1999), and lead to catalyst deactivation (Waldner et al., 2007; Yamaguchi et al., 2008). The first technical approaches for salt separation were developed in the 1980s and 90s for SCWO processes (Supercritical Water Oxidation: process for the conversion of (toxic) organic wastewater using supercritical water and an oxidant (Peterson et al., 2008)). A useful overview on this topic can be found in (Marrone et al., 2004).



**Table 3-4: Behaviour of N, K, P, Mg, Ca, S and Si during a SCWG process.**

Element	Present form in biomass	Present form after SCWG
<b>N</b>	org. bound: protein, nucleic acids; NO <sub>3</sub> <sup>-</sup> -Ion	Dissolved in the liquid phase: NH <sub>4</sub> <sup>+</sup>
<b>K</b>	K <sup>+</sup> -Ion	Dissolved in the liquid phase: K <sup>+</sup>
<b>P</b>	org. bound: protein, nucleotides, phosphoric acid esters Ion (H <sub>2</sub> PO <sub>4</sub> <sup>-</sup> , HPO <sub>4</sub> <sup>2-</sup> )	Solid form: hydroxyapatite, phosphates $P_{org} \xrightarrow{H_2O} PO_4^{3-} \rightarrow Ca_{10}(PO_4)_6(OH)_2$ $Ca^{2+} + H_2PO_4^- \rightarrow Ca_3(PO_4)_2$ $Mg^{2+} + H_2PO_4^- \rightarrow Mg_3(PO_4)_2$ Dissolved in the liquid phase: H <sub>2</sub> PO <sub>4</sub> <sup>-</sup> and HPO <sub>4</sub> <sup>2-</sup>
<b>S</b>	org. bound: protein, ester SO <sub>4</sub> <sup>2-</sup> - Ion	Partly in solid form: sulfates Dissolved in the liquid phase: SO <sub>4</sub> <sup>2-</sup> and SO <sub>3</sub> <sup>2-</sup> Traces of SO <sub>2</sub> and H <sub>2</sub> S in the gas phase
<b>Mg</b>	org. bound: protein (chelation) Mg <sup>2+</sup> -Ion	Solid form: magnesium phosphate (see P), -carbonate and -silicate $Mg^{2+} + CO_2 \rightarrow MgCO_3$ $Mg^{2+} + SiO_2 \cdot nH_2O \rightarrow MgSiO_3$ Dissolved in the liquid phase: Mg <sup>2+</sup>
<b>Ca</b>	org. bound: chelation Ca <sup>2+</sup> -Ion	Solid form: Hydroxyapatite (see P); also calcium carbonate, silicate and sulfate $Ca^{2+} + CO_2 \rightarrow CaCO_3$ $Ca^{2+} + SiO_2 \cdot nH_2O \rightarrow CaSiO_3$
<b>Si</b>	SiO <sub>2</sub> · nH <sub>2</sub> O, silicic acid (Si(OH) <sub>4</sub> )	Solid form: Silicate (see Mg and Ca), Dissolved in the liquid phase: SiO <sub>2</sub>

An example of salt separation in a gasification process is the MODAR reactor (Hong et al., 1989; Marrone et al., 2004). Here, the biomass slurry is fed at the top of the reaction zone, salts precipitate and sink to a lower, subcritical zone of the reactor, where they are dissolved again and separated as a concentrated salt mixture at the bottom of the vessel. In a process configuration at the Paul Scherrer Institute (PSI) in Switzerland, a concentrated brine is separated upstream of the gasification reactor, in a salt separator which is installed downstream of a preheater unit. The design is comparable to a MODAR reactor. The salt-free slurry is then led to a methanation reactor (Schubert et al., 2010a; Zöhner et al., 2014). In another process layout, the biomass slurry is fed to the salt separator from the bottom through a riser tube. The brine is discharged at the bottom. (De Boni et al., 2015; Reimer et al., 2016).

In the VERENA pilot plant at KIT (Figure 3-2), salt separation is performed at the bottom of the downflow reactor, while wastewater and product gas are led to the top via a thin tube (Boukis et al., 2007, 2005). To achieve a more efficient separation, a high-temperature cyclone was installed upstream of the reactor (Boukis et al., 2009). A preheater adjusts the temperature of the fluid from about 400 °C up to 480 °C. The cyclone separates salts, which have formed solids suspended in the supercritical water or dense brines, before

precipitation on the tubing wall. The linear velocity of the feed stream at a temperature of 400 °C is in the range of 2 m/s and reaches approximately 4 m/s at 450 °C. This is due to the lower density of supercritical water at higher temperatures. The resulting man-made gravity is 10 to 30 g and enables a fast separation. The solids from the cyclone are removed in a discontinuous mode by very short pressure releases from 280 bar to ambient pressure with a high throughput. The salt separation at this position is not obligatory. In case of feed materials with a low fraction of inorganic components or in process configurations with a different preheater design, it is possible to omit the salt separation at this stage of the process. (Boukis and Stoll, 2021).

In experiments at lab-scale, salt/solid separation is performed by a similar rapid pressure release, either located downstream of the reactor (D'Jesús et al., 2005) or in-between preheating and reaction system (Boukis et al., 2017b). In short-term experiments, the collection of solids in a filter housing should be feasible. These are most likely the possibilities that will be considered during the course of CERESiS. The configuration of salt separation, the process conditions and the feedstock material determine the composition of this brine stream described in Section 3.1.1. Thus, the composition shows great variations, as shown exemplarily in Section 3.2.2. In case of incomplete gasification, a high amount of organic carbon is to be expected (liquid phase: TOC > 1 g/L; unconverted tars). In experiments with brewer's spent grain, an increased fraction of Mg, Ca, P and Si could be detected in the solid residue of the salt separator. (Boukis et al., 2017b). Additionally, a higher concentration of dissolved inorganic salts (up to 100 mg/L, depending on feedstock) in comparison to the reactor effluent (R, Figure 3-1) is likely. It should be noted that due to the nature of the SCWG process (mixing of biomass with large amounts of water), concentrations of trace elements are diluted (< 10 mg/L) and therefore detection and element balances can be a challenge. An exception is K, which is found in comparatively high concentrations (> 100 mg/L) due to its addition as a catalyst.

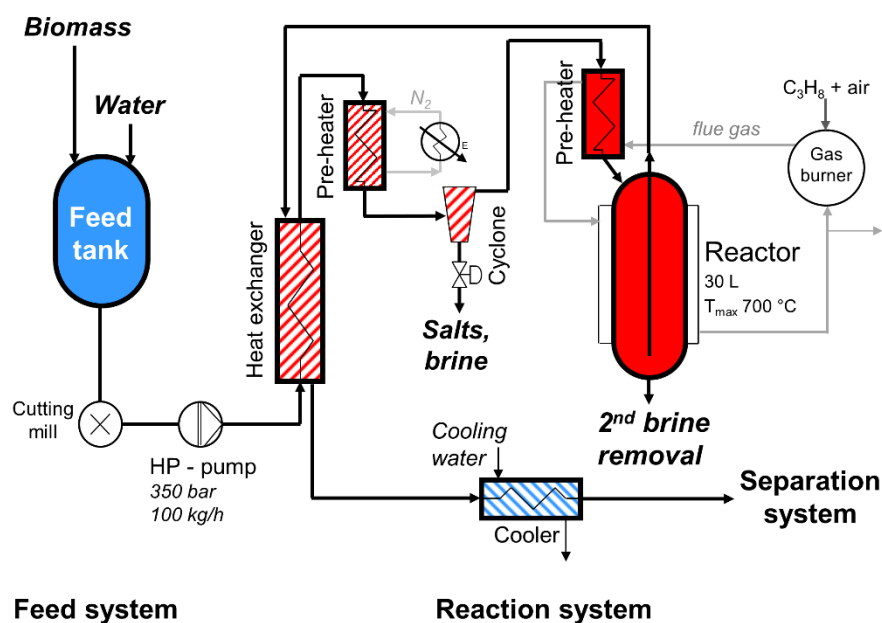


Figure 3-2: Schematic description of the feed and reaction system of the SCWG pilot plant VERENA at KIT. After (Boukis and Stoll, 2021).

### 3.1.4 Tar removal

Tars can be a byproduct of SCWG, as described in section 3.1.1. Tar contained in the product gas can be a problem in the subsequent membrane process (MGA) and should therefore be removed. Several strategies for tar removal are reviewed and discussed in literature (Anis and Zainal, 2011; Milne et al., 1998; Singh et al., 2014; Woolcock and Brown, 2013; Zeng et al., 2020), since tars are a significant problem in conventional biomass gasification. In general, removal methods can be divided into physical, chemical or biological approaches (Zeng et al., 2020). Woolcock and Brown (2013) additionally propose a differentiation between cold (CGC), warm (WGC) and hot (HGC) gas clean up. Biological techniques are presumably not applicable in the case of CERESiS (longer treatment time, lower removing capacity (Zeng et al., 2020), difficult to implement at the KIT laboratory plant) and will thus not be considered. On the other hand, technologies that can employ other products of thermochemical conversion of biomass, such as bio-oil (Bhoi et al., 2015) and bio-char (Nakamura et al., 2015) are of special interest. Naturally, a combination of different removal methods is possible (e.g. Paethanom et al., 2012).

In terms of conventional gasification, chemical approaches for tar removal include partial oxidation and steam reforming (Milne et al., 1998), which can be implemented to the gasifying process. Another option is plasma cracking (Anis and Zainal, 2011) or thermal cracking, a process requiring very high temperatures (approx. 900 – 1500 °C) (Han and Kim, 2008; Milne et al., 1998). Depending on the type of gasifier, these temperatures are already achieved during gasification (Zhang et al., 2020) (but not in case of SCWG). Temperature requirements for tar destruction can be reduced to some extent by the use of a catalyst (metallic or char, an overview can be found in literature (Zeng et al., 2020; Zhang et al.,

2020)). These catalysts ought to be strong and effective in removing tar, resistant to deactivation and sintering as well as inexpensive and easily regenerated (Han and Kim, 2008; Sutton et al., 2001). Additionally, the different process conditions of conventional gasification and SCWG need to be considered. In previous experimental studies at KIT, a fixed bed of char inserted for catalytic purposes was gasified under SCWG reaction conditions (650 °C, 280 bar). Catalytic tar removal at SCWG conditions using char as catalyst is therefore not applicable. On the other hand, studies investigating catalytic tar removal by char have been performed successfully at 800 - 900 °C in pyrolysis gas atmosphere, reaching a tar removal efficiency of 98 % (Monteiro Nunes et al., 2007; Zeng et al., 2020). In general, the catalytic activity of char depends on its properties (kind, origin, structure of carbon and surface, catalytic active site) and process conditions (temperature, atmosphere, residence time) (Zeng et al., 2020). For example, at lower temperatures (400 – 600 °C) and an inert atmosphere (helium), only 0 - 30 % of wood tar vapors could be converted (Boroson et al., 1989).

Physical tar removal methods can be divided into two categories, wet and dry cleaning technologies (Anis and Zainal, 2011). Typical equipment includes (Anis and Zainal, 2011; Milne et al., 1998):

#### Dry technologies

- Cyclone
- Rotating particle separator
- Electrostatic precipitator
- Different kind of filters (bag, baffle, ceramic, fabric/tube, sand bed, ...)

#### Wet technologies

- Spray tower
- Packed column scrubber
- Impingement scrubber
- Venturi scrubber
- Wet electrostatic precipitator
- Wet cyclone

Although physical removal methods are simple and effective, the energy stored in tars cannot be easily recovered. An additional drawback of all wet gas cleaning systems is the production of contaminated wastewater. (Milne et al., 1998; Zeng et al., 2020). Wet electrostatic separators are very costly compared the other technologies (Milne et al., 1998). The particle or droplet size influences separation efficiency as well as energy consumption. Smaller particles are generally more difficult to remove (Anis and Zainal, 2011) and require higher specific energy inputs (Milne et al., 1998). In case of fabric, ceramic, and metallic filters, the temperature of the gas can also have a significant effect, since gaseous tars ( $T > 150$  °C) can potentially pass through the filter (Milne et al., 1998).

With regard to CERESiS, an important aspect will be the actual amount of tar that will be contained in the SCWG product gas. Since the reaction mixture is depressurized and cooled down (atmospheric pressure, 25 °C), a large fraction will probably condense and

accumulate in the wastewater (effluent stream R). Throughout the experimental studies, efforts will be made to evaluate the tar content in the product gas. If the amount of tar is significant, a suitable method for the removal will be selected and implemented in the KIT laboratory plant. An appropriate filtering device is most likely expected to be sufficient.

## 3.2 Decontamination technologies

### 3.2.1 Membrane gas absorption (MGA)

The MGA process is the method selected for further assessment regarding its H<sub>2</sub>S removal efficiency from the SCWG gas effluent. More details on the selection procedure and analysis of the advantages and challenging aspects of the method have been presented in Deliverable D1.2.

#### Experimental setup

A CERTH's pre-existing bench-scale MGA experimental test unit was modified accordingly in order to be used for the needs of the CERESiS project (Figure 3-3). The experimental unit consists of three different sections: (i) the Feed section, (ii) the Membrane contactor section, (iii) the Residue/Analysis section. The unit setup can be operated either with liquid recycle representing a semi-batch operation mode or on a once-through mode representing a continuous operation mode.

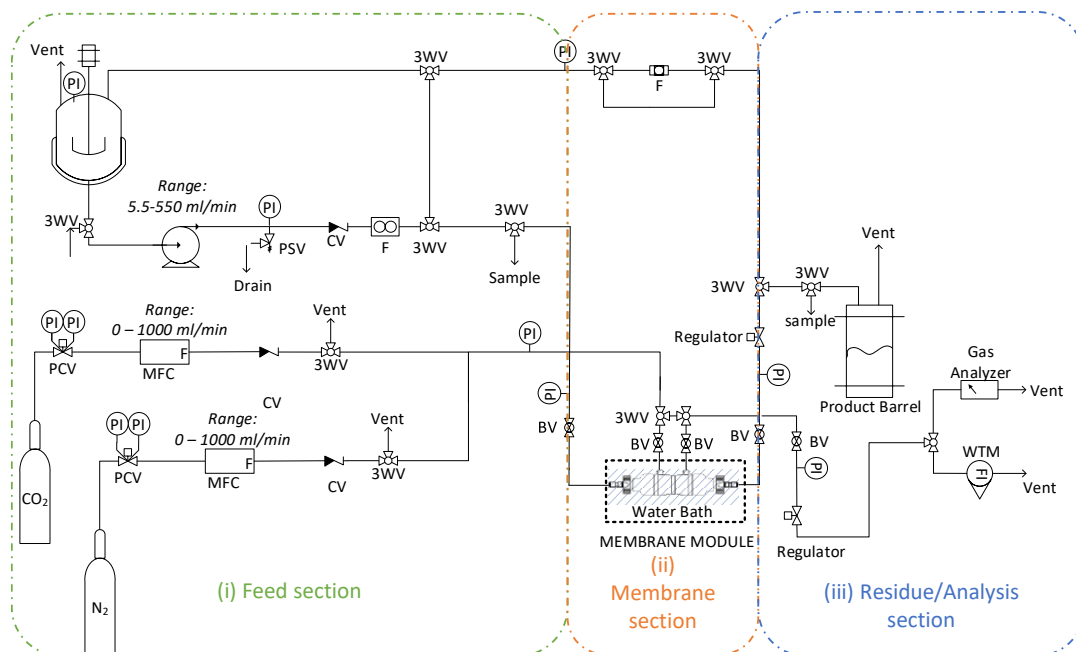


**Figure 3-3: Schematic depiction of the bench-scale membrane reactor/precipitator experimental unit setup.**

(i) **Feed section:** Liquid solvents preparation takes place in a 6 l Stainless Steel (SS316) feed tank equipped with a pressure gauge and safety valve. Liquid solvent is being fed with a high precision gear pump (Ismatec ISM446B), through a float ball flowmeter (0-0.5 l/min). Through a 3-way valve, the liquid phase either recirculates into the mixing vessel, or it is directed to the Membrane contactor section. Feed gas is being supplied through two different compressed gas cylinders (containing either single gases or gas mixtures) using two independent Mass Flow Controllers (MFCs) (Bronkhorst F-201CV-20K-AAD-22-V) at flow rates up to approximately 2 slpm. Through a series of valves, the Feed gas can be either sent directly to the Residue/Analysis section for feed flow and composition measurements or to the Membrane module for H<sub>2</sub>S capture and subsequently to the Analysis section.

(ii) **Membrane contactor section:** Two different types of commercial 3M Liqui-Cel membrane module will be employed in the tests (Figure 3-4 and Figure 3-5). Gas phase is fed in the lumen side of the fibers while liquid solvent in the shell side. Gas and liquid flows are fed in a counter-current parallel flow mode in the MM1.7x5.5 membrane module and in cross flow mode in the MM0.5x1 membrane module. Some details on the membrane module characteristics are presented in Table 3-5. Gas and liquid pressures are continuously monitored with pressure gauges in each side of the membrane module (i.e. entry and exit). Pressure regulating valves are used at the outlets of both gas and liquid phases in order to control the pressures of the two flows.

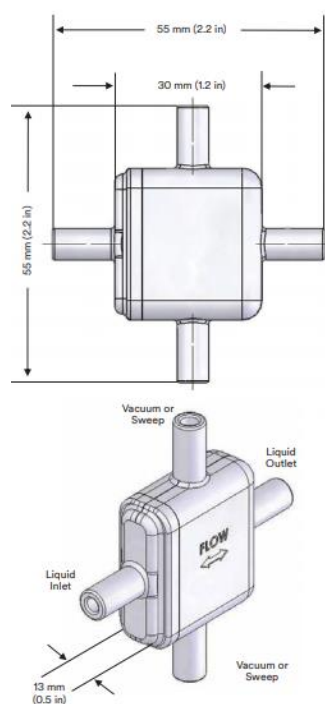


**Figure 3-4: Schematic representation of the Liqui-Cel 0.5x1 Mini Module.**

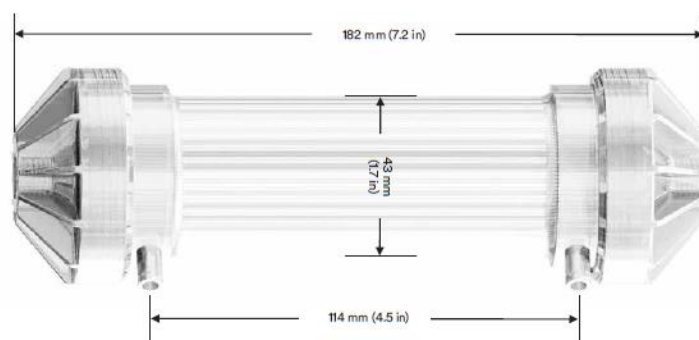


Figure 3-5: Schematic representation of the Liqui-Cel 1.7x5.5 Mini Module.

Table 3-5: Main characteristics of the two selected membrane modules

Module characteristics	MM 0.5x1	MM 1.7x5.5
Dimensions (mm)	13x30x30 (LxHxW)	162x42.5 (LxD)
Weight (g)	10	142
Housing material	Polycarbonate	Polycarbonate
Membranes material	Polypropylene X50 hollow fibers	Polypropylene X50 hollow fibers
Hollow fiber dimensions ( $\mu\text{m}$ )	300/220 (OD/ID)	300/220 (OD/ID)
Membranes pore size (nm)	40	40
Membranes porosity (%)	40	40
Number of hollow fibers	700	7400
Active surface area ( $\text{m}^2$ )	0.01 (OD based)	0.79 (OD based)
Potting material	Epoxy	Polyurethane
Gas-Liquid flows arrangement	Cross flow	Parallel flow

Different type of membrane modules can be selected in the case that any stability or efficiency issues arise.

**(iii) Residue/Analysis section:** In the residue/analysis section, the liquid phase effluent is collected into the product barrel, and the treated gas is sent for on-line composition analysis (Hubei Cubic-Ruiyi Instruments CO. Gas Analyzer – A dedicated gas analyzer has been procured by the project and expecting delivery by the end of M9) and flow measurement (RITTER GAS METER).

### Experimental procedure

The experimental procedure consists of the following consecutive steps:

- Preparation of the liquid solvent and loading into the tank
- Preparation of the gas mixture using the two MFCs
- Analysis of composition and measurement of the total flow of the feed gas
- Feeding gas and liquid flows to the membrane module
- Regulate liquid pressure about 0.5 bar higher than the gas pressure to prevent gas dispersion into the liquid phase
- Real time analysis of composition and measurement of the total gas flow in the gas effluent
- Monitoring the effect of process parameters variation (e.g. changing gas and liquid flow rates, G/L ratio, mode of operation, etc.) on process performance

### Experimental test matrix

A range of conditions and process parameters have been selected to be experimentally assessed. This experimental test matrix is presented in Table 3-6. This set of conditions and process parameters can be adjusted and/or modified based on the test result, as these will become available.

**Table 3-6: Selected set of experimental conditions that will be tested (initial estimations)**

Process parameters / conditions	Range of values
<b>Solvents</b>	MDEA, DEA, NaOH
<b>Solvent concentration</b>	0.25-2 M
<b>Liquid feed flow rates</b>	25 – 2500 ml/min
<b>Gas flow rates</b>	0.02-2 sl/min
<b>Gas composition</b>	H <sub>2</sub> S concentrations up to 1500 ppm at binary and simulated gas mixtures
<b>Mode of operation</b>	Once-through / Liquid Recycle

In any case, the exact set of experimental conditions that will be tested will be adjusted according to the capacities of the two selected membrane modules described above.

### Analysis of the experimental results

The main performance indicator of the process is the H<sub>2</sub>S removal efficiency. This can be calculated using Eq. (3.7)

$$H_2S \text{ removal } (\%) = \frac{(Q_{g(STP)}^{in} x_{H_2S}^{in} - Q_{g(STP)}^{out} x_{H_2S}^{out})}{Q_{g(STP)}^{in} x_{H_2S}^{in}} \times 100\% \quad (3.7)$$



Similarly, since CO<sub>2</sub> is typically being removed to some extent in parallel with H<sub>2</sub>S from the gas mixture, the CO<sub>2</sub> removal efficiency can be calculated as (Eq. (3.8)):

$$CO_2 \text{ removal (\%)} = \frac{(Q_{g(STP)}^{in} x_{CO_2}^{in} - Q_{g(STP)}^{out} x_{CO_2}^{out})}{Q_{g(STP)}^{in} x_{CO_2}^{in}} \times 100\% \quad (3.8)$$

where, Q is the total gas flow rate (l/s<sub>(STP)</sub>) and x are the relevant gas molar fraction values.

The quantities of H<sub>2</sub>S and CO<sub>2</sub> transferred from the gas phase to the liquid solvent is a measure of how “saturated” the solvent is at the module’s exit. This gives an indication if there is any additional potential of the solvent to be further used (e.g. by recycling) or has to be sent for regeneration. The Acid Gas Loading (AGL) of the solvent can be calculated by Eq. (3.9)

$$AGL = \frac{(F_g^{in} x_{H_2S}^{in} - F_g^{out} x_{H_2S}^{out}) + (F_g^{in} x_{CO_2}^{in} - F_g^{out} x_{CO_2}^{out})}{Q_l C_s} \quad (3.9)$$

where, AGL is the Acid Gas Loading of the solvent (mol<sub>acid-gases</sub>/mol<sub>solvent</sub>), F is the total gas molar flow rate (mol/s), x are the relevant gas molar fractions, Q<sub>l</sub> is the liquid flow rate (l/s) and C<sub>s</sub> is the solvent concentration (mol/l).

If the tests are conducted in the Liquid Recycle operating mode all the above mentioned performance indicators become time dependent.

If the tests are conducted in the once-through mode of operation, another important process performance indicator is the Treating Gas Capacity (TGC) of the membrane module, defined as (Eq. (3.10)):

$$TGC = \frac{Q_g^{in}}{A} \quad (3.10)$$

where, TGC is the Treating Gas Capacity (m<sup>3</sup>·m<sup>-2</sup>·h<sup>-1</sup>), Q<sub>g</sub><sup>in</sup> is the total gas feed flow rate (m<sup>3</sup>/h<sub>(STP)</sub>) and A is the membrane active surface area (m<sup>2</sup>).

In case the system is operated in the Liquid Recycle operating mode, the TGC can be estimated by Eq. (3.11):

$$TGC = \frac{V_g^{treated}}{A \cdot t_s} \quad (3.11)$$

where, V<sub>g</sub><sup>treated</sup> is the total gas volume treated till the time that the liquid solvent becomes saturated and needs to be regenerated (m<sup>3</sup><sub>(STP)</sub>) and t<sub>s</sub> is the time needed until solvent becomes saturated (h).

Analysis of mass transfer phenomena

A comprehensive analysis of the mass transfer phenomena taking place in the process is presented below in order to assist in the assessment of the process performance at different experimental conditions (Mavroudi et al., 2003).

Mass transfer is determined by the consecutive steps in the three phases shown schematically in Figure 3-1, i.e. diffusion of gaseous component *i* from the bulk gas to the membrane wall, diffusion through the pores of the membrane to the membrane-liquid interface, and dissolution into the liquid absorbent, followed by liquid phase diffusion/chemical reaction. Hence, the overall liquid phase mass transfer resistance,  $1/K_{overall}$  (s/cm), can be expressed by a resistance-in-series model (Eq. (3.12)):

$$\frac{1}{K_{overall}} = \frac{H_i}{k_{i,gas}} + \frac{H_i}{k_{i,membrane}} + \frac{1}{Ek_{i,liquid}} \tag{3.12}$$

where,  $k_{i,gas}$  is the gas side mass transfer coefficient (cm/s),  $k_{i,membrane}$  is the membrane mass transfer coefficient (cm/s),  $k_{i,liquid}$  is the liquid phase mass transfer coefficient (cm/s),  $H_i$  is the dimensionless Henry’s constant, and  $E$  is an enhancement factor due to the chemical reaction.

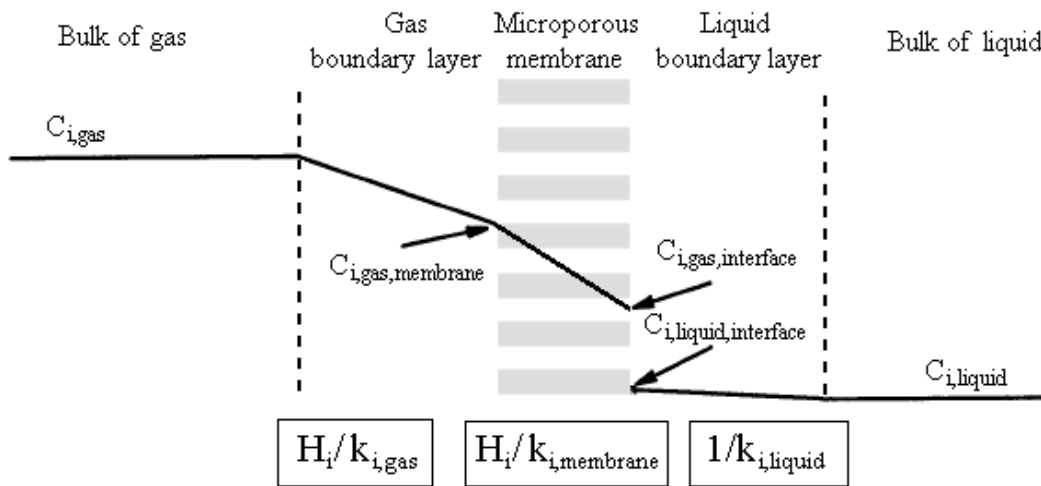


**Figure 3-6: Mass transfer regions and transport resistances in a membrane contactor.**

The overall gas phase based mass transfer coefficient,  $K_{OG}$  (m/s), (accounting for all mass transfer resistances, i.e. lumen, membrane and shell side) can be estimated from experimental data, based on Eqs. (3.13) and (3.14) (Karoo, 1992).

$$K_{OG,i} = \frac{F_g^{in} R_g T}{AP_g} \left[ (X_i^{in} - X_i^{out}) - \ln \frac{X_i^{out}}{X_i^{in}} \right] \tag{3.13}$$

$$X_i = \frac{x_i}{1-x_i} \tag{3.14}$$

where,  $F$  is the total feed mixture molar flowrate ( $\text{mol/s}$ ),  $R_g$  is the gas constant ( $\text{atm}\cdot\text{m}^3\cdot\text{mol}^{-1}\cdot\text{K}^{-1}$ ),  $T$  is the temperature (K),  $A$  is the contact surface ( $\text{m}^2$ ),  $P_g$  is the pressure (atm), and  $x_i$  is the mole fraction of component  $i$  ( $\text{CO}_2$  or  $\text{H}_2\text{S}$ ), used to calculate the adjusted mole fractions  $X_i$ .

### 3.2.2 Electrocoagulation-flotation (EC) and electrochemical oxidation (EO)

Typically, the SCWG process leads to two liquid streams, the reactor effluent (R) and a brine (S) (Figure 3-1). Depending on their composition and HM loading, the two streams will be separately or combined treated by means of a hybrid process which combines two well-known electrochemical techniques, the electrocoagulation – flotation (ECF) and the electrochemical oxidation (EO). Both processes take advantage of the high conductivity and the presence of inorganic ions (sulphates, chlorides) in the two streams which result to reduced energy consumption (due to the decreased ohmic resistance and thus, the low voltage that needs to be applied), and the in situ production of chemical reagents (coagulants, strong oxidants) which favor the separation/elimination of the target contaminants (HMs, organic pollutants). Details on the attributes, the technical characteristics, the mechanisms and the parameters that affect the effectiveness of the two processes can be found in Deliverable D1.2.

#### Liquid influents composition

It is understood that the characterization of the biomass feed (contaminant load, alkali and earth alkali metals, Cl, F, Fe, etc.) and of the two SCWG liquid streams is detrimental to the design of the respective experimental work. The composition of the two streams can vary significantly, depending on the feedstock, the process conditions and the configuration of the salt separation. In case of incomplete gasification, a high amount of organic carbon is expected in (R) (liquid phase:  $\text{TOC} > 1 \text{ g/L}$ ; unconverted tars), whereas a higher concentration of dissolved inorganic salts (up to  $100 \text{ mg/L}$ , depending on feedstock) is likely in (S), in comparison to the reactor effluent (R, Figure 3-1). Concerning the heavy metals (Zn, Cu, Cd, Pb, Cr, Ni, Fe, Hg, As, etc.), their distribution may vary significantly among the different parts of the plant. According to the preceding discussion (3.1.3(3)), during SCWG with increasing temperature, HM are immobilized in solid deposits, like salts and char. However, their presence in (S) and (R) is also likely, since HM can be dissolved in water in form of ionic species or as complexes with organic matter. An additional issue to be considered is the possible presence of tar in the wastewater (R). Since the reaction mixture is depressurized and cooled down (atmospheric pressure,  $25 \text{ }^\circ\text{C}$ ), a large fraction will probably condense and accumulate in (R).

Table 3-7 describes the composition of the SCWG reactor effluent (R) and brine (S) in case of previous experimental work carried out in the KIT laboratory plant with sewage sludge and brewer's spent grain (initial composition of the feedstocks can be found in Annex 2, respectively). The values of the organic and inorganic content are indicative of the SCWG process and are expected to greatly differ with those expected in CERESiS in case of the feedstock (plant species) mentioned in Figure 2-1. However, the concentration values in

Table 3-7 underline the differences between the two liquid streams and the potential for a combined or separate treatment by the hybrid ECF/EO process.

**Table 3-7: Composition of liquid effluents during a SCWG process.**

SCWG treatment of sewage sludge						
all values in mg/L	Reactor effluent (R)			Brine (S)		
	MIN	MAX	MID	MIN	MAX	MID
TC	162	10905	6969	388	12709	4852
TIC	100	8420	5089	0	1058	278
TOC (C)	133	3444	1985	323	11650	4573
NO <sub>3</sub>	0	208	26	0	209	20
NH <sub>4</sub>	1764	13983	8970	10	2476	798
TN	2098	9400	6193	100	7150	1405
P	6.30	647.00	189.76	12.6	2674	691
PO <sub>4</sub>	40.60	1849.00	493.23	32.9	5169	1614
S	20.70	1865.00	301.90	29.4	574	208
SO <sub>4</sub>	19.90	180.00	87.89	26.6	700	288
Ca	0.50	18.60	4.72	3.55	30.6	10
K	25.90	1576.00	677.22	81	4275	1367
Mg	0.48	19.20	3.98	1.56	147	28
Na	3.48	29.90	11.54	3.4	130	45
Si	12.10	719.00	64.79	9.5	95.5	50
Al	0.00	0.70	0.15	0	1.09	0
As	0.00	0.00	0.00	0	0.32	0
Cd	0.00	0.00	0.00	0	0	0
Cu	0.00	0.00	0.00	0	0.06	0
Pb	0.00	0.00	0.00	0	0	0
Zn	0.00	0.05	0.01	0	2.62	0
Cr	0.00	0.00	0.00	0	0	0
Fe	0.00	3.51	0.57	0.29	16.4	5
Mo	0.00	0.20	0.01	0	3.32	1
Ni	0.00	6.40	0.13	0	108	9
Cl	21.31	226.00	56.65	29.4	87.5	46
Hg	0.00	0.00	0.00	0	0	0
Phenolindex	86.00	537.00	354.94	7	518	117

SCWG treatment of brewer's spent grain						
all values in mg/L	Reactor effluent (R)			Brine (S)		
	MIN	MAX	MID	MIN	MAX	MID
TC	1896	6492	4273	1064	14011	3938
TIC	1517	4585	3154	0	1000	245
TOC	229	2625	1124	1064	13841	3797
TN	1876	5054	3627	100	2227	571
Al	0.10	0.35	0.19	0.10	1.00	0.28
Ca	0.60	8.46	2.38	3.50	192.00	43.13
Cr	0.10	0.10	0.10	0.10	1.00	0.19
Fe	0.02	1.57	0.53	0.05	2.10	0.63
K	0.24	1320.00	373.59	0.05	3114.00	1167.52
Cu	0.10	68.00	12.25	0.10	454.00	108.18
Mg	0.11	15.20	2.31	38.90	482.00	186.10
Mn	0.01	0.09	0.04	0.21	2.00	0.97
Mo	0.20	1.45	0.26	0.20	2.00	0.42
Na	0.10	0.51	0.23	0.07	1.00	0.33
Ni	0.20	0.75	0.22	0.20	2.00	0.38
P	2.00	123.00	28.61	51.00	778.50	322.13
S	2.00	28.50	10.03	15.40	185.00	66.80
Si	6.60	70.00	30.74	21.50	99.50	48.49
Zn	0.02	0.05	0.04	0.02	0.34	0.12

### Experimental setups

The decontamination of the SCWG liquid stream(s) by the hybrid ECF/EO process ((S) alone or in combination with (R)) will be investigated by CERTH with the aid of two bench-scale ECF and EO setups. A special ECF setup has been designed for the scope of CERESiS project aiming to the effective removal of HM and dissolved organics. Specifically, a monopolar-parallel (MP-P) electrode setup has been designed, in which two anodes are connected to each other and to the external DC supply, and the same thing applies to cathode electrodes (Figure 3-7). In this configuration, the current is divided between the electrodes resulting in a lower potential difference if compared to the electrodes connected in series. This design can help testing two different processes: a) ECF with two sacrificial anodes, and b) ECF and EO in parallel connection in a single setup, consisting of one sacrificial anode (Al or Fe) and one non-active electrode of high oxygen overpotential (e.g. boron doped diamond-BDD). In the latter configuration, the current is divided between the electrodes

resulting in a lower potential difference if compared to the electrodes connected in series. The choice of the appropriate electrode configuration will be determined by the removal efficiency and treatment cost in response to modern zero liquid discharge standards.

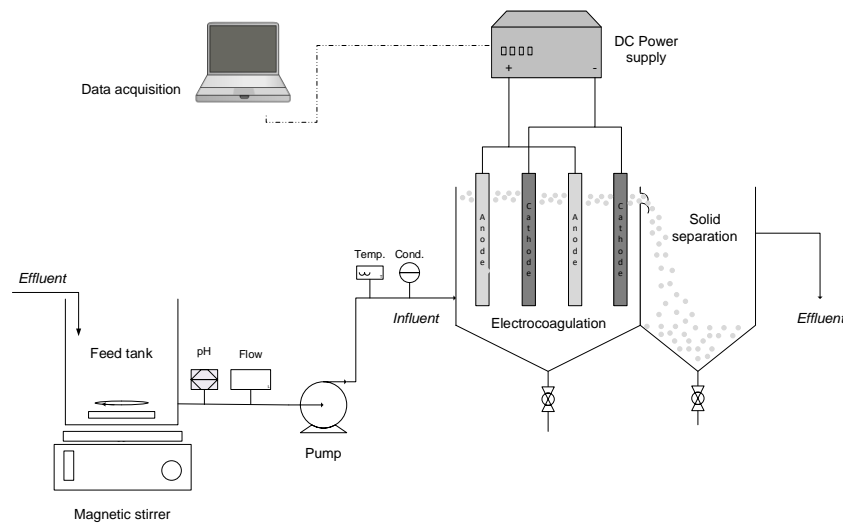


**Figure 3-7: Schematic illustration of the ECF setup.**

The EO investigation will be carried out at CERTH with the aid of a bench-scale electrochemical oxidation set-up which comprises a plate-and-frame electrochemical cell (Micro Flow Cell by ElectroCell, Denmark), a 1 L feed water tank, a recirculation pump and a power supply (Figure 3-8a). Sensors are located at inlet and outlet of the cell, measuring operating variables, such as flow rate, pH, temperature, oxidation-reduction potential (ORP) and pressure. The experimental set-up is equipped with a Supervisory Control And Data Acquisition (SCADA) system for collection and recording of the aforementioned operating parameters and for overall control through a PLC unit, a touch screen Human Machine Interface (HMI), and other expansion electronic modules. The distance between the electrodes in the cell is 4 mm and for better dispersion of the solution, a polyvinylidene fluoride (PVDF) spacer is used. Figure 3-8b shows the micro flow cell configuration and its distinctive parts.

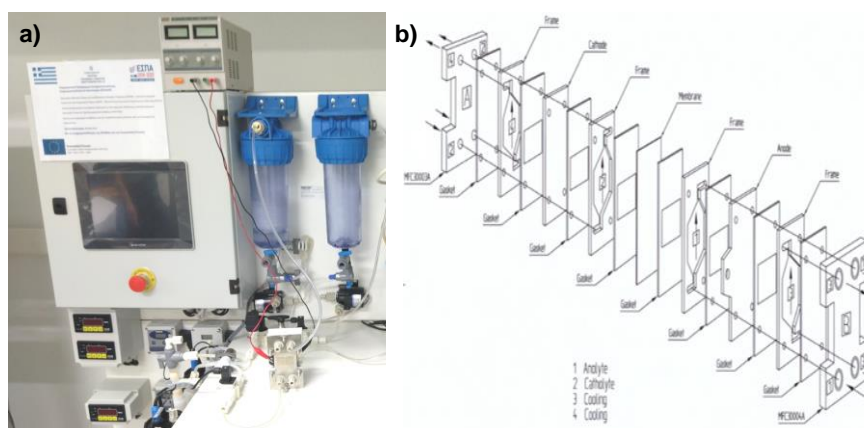


**Figure 3-8: a) Bench-scale electrochemical oxidation unit, and b) micro flow cell configuration.**

### Electrode materials

Selecting the proper electrode material is critical since it determines the reactions that would take place. As mentioned in D1.2, ECF tests will be carried out with different combinations of electrodes (Al-Al, Al-Fe, Fe-Fe, Fe-Al, SS-SS, Al-SS, and SS-Al) in an effort to evaluate and compare the performance of the process on the reduction of COD, turbidity (TUR) and heavy metals. In the case of EO, the effectiveness of two or three commercial high-O<sub>2</sub> overpotential anodes will be tested over the elimination of model organic contaminants (e.g. to be selected according to the characterization campaigns of the feedstock samples and the SCWG liquid streams), using a gas diffusion electrode (GDE), made of carbon-PTFE, as cathode.

### Design of experiments

The design of the experiments (DoE) and the optimization of both ECF and EO processes, will be carried out using the Response Surface Methodology (RSM). RSM finds wide scale application in drinking water treatment process such as electrochemical (Rajkumar and Muthukumar, 2017) and advanced oxidation process (Cherif et al., 2014). RSM is a set of statistical and mathematical tool for designing experiments and optimizing the effect process variables (Myers et al., 2002; Sharma et al., 2009; Tawabini et al., 2020a; 2020b). RSM reduces the number of trials and recognizes the influence of process parameters on the removal process. RSM has been successfully used for the optimization of process parameters like adsorbent dose, pH, metal ion concentration, reaction time etc., for bio-sorption of metals (Watson et al., 2016; Yousefi et al., 2019) and dyes (Bangaraiaha et al., 2019). In CERESiS project, the experimental design, statistical analysis, response surface plots, and optimization will be performed using Design Expert® v.11.1.2.0 software program (Stat-Ease, Inc., Minneapolis, MN, USA), according to the selected independent variables summarized in Table 3-8. The independent variables will be varied over three levels, between -1 and +1, at determined ranges chosen based on previous research (Tawabini et al., 2020a; 2020b; Plakas et al., 2019; Salmerón et al., 2019) and literature survey (D1.2).

**Table 3-8: Estimated experimental range and levels of independent variables for the ECF and EO testing**

ECF variable	Units	Level and range		
		Low (-1)	Central (o)	High (+1)
Current density ( <i>j</i> )	mA/cm <sup>2</sup>	5	52.5	100
pH	-	2	5	8
Electrolysis time	min	10	125	240
Coagulation Charge Loading Rate (CCLR)	C/L/min	100	550	1000
EO variable	Units	Level and range		
Current density ( <i>j</i> )	mA/cm <sup>2</sup>	50	125	200
pH	-	3	5	7
Feed flow rate ( <i>FFR</i> )	mL/min	300	600	900

For both EC and EO processes, other parameters affecting performance such as temperature, conductivity and presence of ions (ionic strength) in the feed solution will be also considered, depending on their ranges in the SCWG liquid influent(s).

#### Analysis of experimental results

In both electrochemical processes, the efficiency of the treatment, RE%, is calculated as:

$$RE = \frac{C_i - C_f}{C_i} \times 100 \quad (3.15)$$

where  $C_i$  and  $C_f$  (expressed in NTU in the case of turbidity or in mg/ in the case of HM, SS, or COD) are respectively the initial and the final concentration of the pollution parameter. The current density ( $j$ ), the charge loading ( $CL$ ) and the specific electrical energy consumption ( $SEEC$ ) are determined according to Eqs. (3.16)–(3.18) below:

$$j = \frac{I}{S} \quad (3.16)$$

$$CL = \frac{It}{VF} \quad (3.17)$$

$$SEEC = \frac{IUt}{V} \quad (3.18)$$

where  $I$  (A) is the current intensity,  $S$  (m<sup>2</sup>) the active electrode surface,  $V$  the volume of the solution,  $F$  (96,500 C) the Faraday constant,  $U$  (V) the voltage and  $t$  (h) the treatment time.

In EO, it is necessary to establish certain indexes including current efficiency and energy consumption for project evaluation and efficiency assessment towards the electrochemical treatment first. Current efficiency ( $\Phi$ ) is generally defined as the percentage of the experimental charge for the oxidation of organic compound to the total charge passed during electrolysis. Despite the fact that different expressions of current efficiency are proposed, the equations most commonly adopted in the literature are determined by Chemical Oxygen Demand (COD) and Total Organic Carbon (TOC) using the following relationships (Panizza and Cerisola, 2009):



$$\Phi = \frac{Q_{Exp}}{Q_{Total}} = \frac{COD_0 - COD_t}{8I \Delta t} FV \quad (3.19)$$

$$\Phi = \frac{\Delta TOC_{Exp}}{\Delta TOC_{theor}} \quad (3.20)$$

$$\Delta TOC_{theor} = \frac{It n_c M}{V n_e F} \times 10^3 \quad (3.21)$$

where  $COD_0$  and  $COD_t$  are the COD values at times 0 and t (in g O<sub>2</sub> / L), respectively, I is the current (A), F is Faraday's constant (96,485 C/mol), V is the electrolyte volume (L), and 8 is the oxygen equivalent mass (g/eq).  $\Delta TOC_{exp}$  and  $\Delta TOC_{theor}$  are the experimental and theoretical TOC change values during treatment time (mg/L), respectively,  $n_e$  is the number of electrons consumed in the mineralization of organic pollutant molecule,  $n_c$  is the number of carbon atoms in organic pollutant molecule, M is the molar mass of carbon (12 g/mol). The specific energy consumption ( $E_{sp}$ ), expressed in Wh/L (or Wh/kg<sub>COD</sub>, Wh/kg<sub>TOC</sub>), is the energy consumed to remove a unit volume (or mass COD, TOC) wastewater and can be calculated using the following relationships (Chaplin, 2014):

$$E_{sp} = \frac{U_c I t}{V} \quad (3.22)$$

$$E_{sp} = \frac{U_c I t}{V \Delta COD_{exp}} \quad (3.23)$$

$$E_{sp} = \frac{U_c I t}{V \Delta TOC_{exp}} \quad (3.24)$$

where  $U_c$  is the voltage (V), I is the applied current (A), t is the electrolysis time (h), and V is the solution volume (L);  $\Delta COD_{exp}$  and  $\Delta TOC_{exp}$  are the concentrations of the removed COD and TOC (mg/L). In a recent comprehensive review, Brillas and Garcia-Segura (2020) provide a benchmarking framework of novel electrochemical oxidation (EO) processes, based on the oxidation of phenol as model compound, and highlight the engineering challenges that need to be successfully addressed toward novel technology commercialization. Among such challenges, the satisfactory long-term performance in a realistic operational environment critically determines the technology readiness level of these technologies (Garcia-Segura et al., 2020). For example, the EO process, applied to brine wastes characterized by a high chloride content, resulted in improved performance for organic pollutants degradation, due to the formation of reactive chlorine species during electrolysis, thus designated as electrochlorination process (ECL) (Garcia-Segura et al., 2018; Mostafa et al., 2018; Tawabini et al., 2020).

### 3.2.3 ECF solid by-product (sludge) treatment and reuse options

The ECF treatment of the SCWG liquid stream(s) will result to the formation of a solid by-product, namely ECF sludge, at a mass rate which is expected to be lower than 2-3% (<2-3 kg/m<sup>3</sup>). As stated in D1.2, the main advantage of ECF over chemical coagulation/flocculation is that coagulation/flocculation uses chemical coagulants/flocculants such as metal salts or polyelectrolytes while in ECF the coagulants are generated *in situ* by the electrolytic oxidation of an appropriate anode material which results in much less sludge generation

(Aljaberi 2018; Mroczek et al., 2019). In addition to practicality, this is also an important point related to the economy of the process, since sludge generated using any water treatment method must be further treated. Furthermore, ECF sludge is also of better quality; i.e., lower water content, much larger and more stable flocs with better settleability. This is thought to be particularly true for Fe-ECF (Chen et al., 2002; Mollah et al., 2004; Zodi et al. 2011).

ECF sludge production will be affected by the SCWG brine characteristics such as the number of settleable solids and presences of destabilized matter due to coagulation and flocculation. As observed in literature, ECF time and applied current density will be the major factors influencing the quantity of the electrogenerated sludge, independently of the electrodes used (Fe, Al or SS). This can be explained by the increase of dissolved metal anodes with time and applied current (Faraday's law). Moreover, increasing flow rate may result in a decrease in amount of produced sludge, energy and electrode consumptions.

Despite the fact that a large number of studies on ECF treatment of various types of water and wastewater have been reported in the scientific literature, there are only a few works dealing with sludge treatment and reuse, and to our knowledge, there is no relevant publication on the treatment of SCWG liquid streams by ECF. Interesting remarks were made in the studies by Kushwaha et al. (2010) and Xu et al. (2002). In the first work, synthetic dairy wastewater had been treated by EC. The authors suggested (based on thermal gravimetric and differential thermal analyses; TGA and DTA) that EC sludge could be dried and used as fuel in boilers/incinerators or in fuel briquette production. A similar suggestion was presented by Kumar et al. (2009); EC sludge (heating value 5.3 MJ/kg) from the treatment of biodigester effluent from an alcohol distillery could be used in making blended fuel briquettes along with other organic fuels. In the latter study, real egg processing wastewater was treated by EC. In addition to good treatment results, valuable by-products (EC sludge) bearing high digestible protein and fat values were yielded. Also, Linares-Hernández et al. (2009) found that using Al and Fe anodes simultaneously outperformed (higher removal efficiencies, less sludge produced) the use of either metal alone, combining the advantages of both.

In the context of CERESiS project, the performance of ECF will be optimized in terms of HM removal efficiency, settleability and dewaterability of the EC sludge. Considering that sludge can be regarded as a valuable resource because of its high iron or aluminium content (expected to be as high as 50%), a preliminary sludge feasibility analysis will be performed for further reuse of the generated ECF sludge into useful applications. For this scope, the amount and the composition of that solid waste will be analyzed. Specifically, ECF sludge will be collected, dried and analyzed by X-ray diffraction (XRD) and scanning electron microscopy (SEM). Moreover, the heating value, the moisture content, ash and fixed carbon of the ECF generated sludge will be measured in an effort to assess the further application of this solid by-product; i.e., for blending material in coal or for catalysis (in case of high metal content) or in granulated bio ash-based fertilizer products in case the ECF sludge contains notable amounts of phosphorus and nitrogen.

The possible reuse and other ECF sludge treatment options (i.e., dewatering, filtration, incineration, landfill disposal) will be further discussed in D3.4, in which the detailed characteristics of the sludge generated during the respective R&D work will be defined.

## 3.3 Biofuel synthesis

---

Using SCWG, biomass can be transformed into a series of gases that can be used in a boiler, in a turbine, or an engine, after being adequately conditioned. At CERESiS, we want to use these gases as precursors for high-quality liquid fuels. Case in point, the gases obtained as a product of the SCWG process will be subjected to an electrocatalytic steam reforming process to produce syngas. The syngas will then be used as feedstock for the Fischer-Tropsch synthesis (FT), a process through which biofuels will be obtained.

### 3.3.1 Reforming/Water Gas Shift

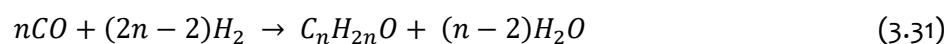
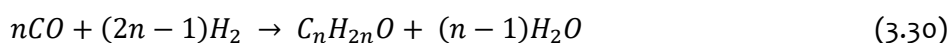
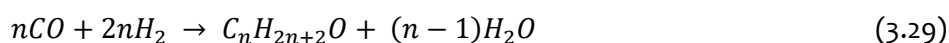
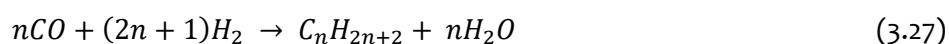
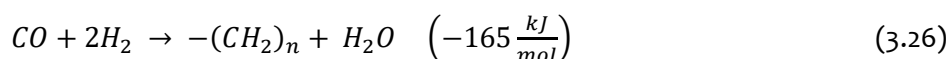
The main components of the gaseous products obtained from SCWG are H<sub>2</sub>, CO<sub>2</sub>, CH<sub>4</sub>, C<sub>2-3</sub> and CO and some impurities. The concentration depends on both the biomass used as feedstock and the operating conditions used (as mentioned in section 3.1.1.). The most critical pollutants are sulfur and ash. Using the results obtained from the SCWG process, a gas mixture will be emulated to carry out the reforming process. Converting these compounds to CO and H<sub>2</sub> can be accomplished using hydrocarbon reforming technologies such as steam, autothermal and partial oxidation. Depending on the concentration of CO<sub>2</sub> and CH<sub>4</sub> obtained, an electrocatalytic dry reforming process could be implemented (Banville et al., 2014, Rego de Vasconcelos and Lavoie, 2019). In a dry reforming process, CH<sub>4</sub> and CO<sub>2</sub> react to produce syngas with an H<sub>2</sub>/CO ratio of 1 (Eq 3.25).



The dry reforming process is a carbon dioxide sequestration method and valorization. However, the energy requirement of the technique is high ( $\Delta H = +247$  kJ/mol), and the syngas produced needs adjustment before the Fischer-Tropsch synthesis. Our team at SHER has successfully used electron-activated steel wool catalytic bed for dry reforming of methane operating under water-saturated methane and carbon dioxide in previous studies. That resulted in a 95+% conversion of the reactants to syngas, producing an average H<sub>2</sub>/CO ratio of 2 (Labrecque and Lavoie, 2011, Banville et al., 2013). This process utilizes electricity to supply heat directly to the catalyst surface through resistance heating. Each end of the catalytic packing is electrically connected to a DC supply through suitable feedthrough terminals. The experimental setup consists of a gas delivery system with steam generation and a catalytic test reactor with associated power supply and heat exchanger. The hot effluent gas leaving the reactor will be cooled in the feed/effluent heat exchanger and then passed through a dry ice/ethylene glycol cooled water trap prior to discharge to the atmosphere. The details of the experimental setup can be found elsewhere (Banville et al., 2014, Rego de Vasconcelos and Lavoie, 2019).

### 3.3.2 Fischer-Tropsch-Synthesis and distillation

Fischer – Tropsch synthesis is the name for the process in which carbon monoxide and hydrogen are hydrogenated to produce high molecular weight hydrocarbons following the overall reaction depicted in Eq. 3.26. The main products of the synthesis are olefins (Eq. 3.27) and paraffin (Eq. 3.28); by-products of the reaction are methane, lightweight hydrocarbons, oxygenates, and carbon monoxide (Eq. 3.27 – 3.32) (Dry, 2002b, Schulz, 1999). The process is in essence a surface polymerization reaction that provides better yields under severe conditions (temperature of 200 - 350 °C and pressures of 5 - 60 bar). The catalysts used in the synthesis are transition metals that possess a sufficiently high hydrogenation activity, such as nickel, ruthenium, cobalt, and iron. The reaction is exothermic and removing the reaction heat is one of the main concerns when designing the process to avoid methane production and catalyst deactivation. The system is pressurized because improving contact between the gaseous reactants with the solid catalyst surface increases the yield (Dry, 2002b, Davis, 2001, Davis, 2005, Iglesia et al., 1993). The FT products are further refined through hydrogenation or isomerization to produce fuels with a high hydrogen content, molecular uniformity, high function points, better combustion characteristics, lower sulfur content, and low content of aromatic compounds (Mahmoudi et al., 2017, Van Der Laan and Beenackers, 1999, Schulz, 1999, Demirbas, 2007, Lappas and Heracleous, 2016).



There is still no single reaction mechanism that explains the diversity of products obtained in the FT synthesis. The most accepted are carbide mechanism, CO insertion and the hydroxycarbene mechanism (Mahmoudi et al., 2017, Davis, 2001, Ail and Dasappa, 2016). In the carbide mechanism, the chain begins with dissociative chemisorption of CO. The oxygen in the surface reacts with hydrogen to produce water, while the carbon hydrogenates to produce CH<sub>2</sub> and CH<sub>3</sub> in consecutive reactions. CH<sub>3</sub> acts as chain started and the CH<sub>2</sub> in the surface is the monomer in the polymerization reaction. The chain grows with the successive incorporation of CH<sub>2</sub>. The chains termination is due to β-hybrid elimination or addition of hydrogen. This mechanism does not explain the formation of oxygenates and branched chains. In the second mechanism, the monomer is the chemisorbed CO and the metallic species in the surface (M-H) initiates the reaction. The CO insertion generates an acyl group that propagates the chain grow. The termination step is a hydrogenation or β-hybrid elimination. In the hydroxycarbene mechanism, the hydrogenation of chemisorbed CO generates a hydroxycarbene specie and chain grow

happens by coupling of two reactions, the condensation of the enolic specie and water elimination (Mahmoudi et al., 2017).

Two other reactions play an important role in the FT synthesis, methane formation (undesirable) and water gas shift (WGS). Methane formation (Eq. 3.32) is significant when the temperature of the process is increased, while WGS (Eq. 3.33) is relevant when the catalyst used is iron-base, and the H<sub>2</sub>/CO ratio is low because the by-product in the synthesis is CO<sub>2</sub> (Schulz et al., 1988).



Regardless of the mechanism, the reaction starts with CO chemisorption and is followed by the propagation and termination of the chain, generating carbon chains around 10 to 40 (Schulz et al., 1988). However, the distribution of products is independent of the carbon number, although the carbon numbers obtained in this process is determined by the probability of chain growth in the catalyst, which is known as the  $\alpha$  value in the Anderson-Schulz-Flory (ASF) relation (Eq. 3.34) (Dry, 2002b, Van Der Laan and Beenackers, 1999).

$$x_n = (1 - \alpha)\alpha^{n-1} \quad (3.34)$$

The hydrocarbon yield in the FT synthesis is a function of the chain growth probability. In turn, the chain growth probability is strictly dependent on the operating conditions, such as H<sub>2</sub>/CO ratio, temperature, pressure, type of catalyst, composition of the catalyst, type of reactor, and composition of the synthesis gas fed to the system. Thus, operating conditions can be used to manipulate the carbon number distribution (Dry, 2002a). For instance, lowering the H<sub>2</sub>/CO ratio increases the probability of chain growth because fewer hydrogens molecules are available for the hydrogenation of the chain, and selectivity shifts towards hydrocarbons with a higher carbon number. Indeed, an H<sub>2</sub>/CO ratio around 2 is within the optimal range for the process (Rauch et al., 2013, Eric and Michael, 2008, Demirbas, 2007).

Similarly, FT-synthesis occurs at temperatures between 150–300 °C, and an increase in temperature promotes the termination of the chain, which translates into a decrease in the probability of chain growth leading to undesired short chains hydrocarbons and methane, damage of the catalyst and carbon deposition. Reaction velocities and the conversion rate limit lower temperatures (Espinoza et al., 1999, Todici et al., 2016). Likewise, typical pressures for the FT synthesis are in the range of 5 to 60 bar because an increase in pressure leads to higher conversion rates and favors the formation of desired long-chain alkanes. However, if the pressure is too high, coke formation will cause catalyst deactivation, and the overall cost of the process increases because expensive high-pressure equipment is needed (Dry, 2002a, Dry, 2002b, Espinoza et al., 1999). Additionally, syngas produced from biomass rarely reach an H<sub>2</sub>/CO ratio of two, and it can have a high concentration of methane and CO<sub>2</sub>. In that case, using steam reforming and the water gas shift reaction (WGS), the CH<sub>4</sub> and CO<sub>2</sub> molecules are transform to CO and H<sub>2</sub> and the desired H<sub>2</sub>/CO ratio is set to the ideal level of two (Lappas and Heracleous, 2016).

Equally important is the type of reactor used in the FT synthesis. To that end, there are four types of reactors currently used on an industrial scale for FT synthesis: multitubular fixed bed reactor (FBR), slurry bubble column (SBCR), circulating fluidized bed reactor (CFB), and fluidized fixed bed reactor (FFB). The first two are used at low temperatures (220 – 250 °C), and the others are used for high-temperature processes (300 - 350 °C) (Guettel et al., 2008). Multitubular fixed bed and slurry bubble column reactors are used when the desired product is long-chain heavy hydrocarbons. They can be subjected to refining processes such as hydrocracking and isomerization to obtain high-quality gasoline and diesel. Consequently, using these two reactors has significant importance for the sustainability of the transport sector (Dry, 2002a). In SBCR reactors, two things make it challenging to apply on an industrial scale, (i) separation of the catalyst and the liquid wax, and (ii) prediction of the fluid dynamic behavior of the reactor which can result in cost-intensive pilot-plant studies for a successful scale-up (Espinoza et al., 1999). Meanwhile, for FBR reactors, heat transfer limitation is a significant disadvantage because it affects methane formation, low product selectivity, and a shorter lifetime of the catalyst. Another drawback for the FBR reactor is the high-pressure drop and low catalyst utilization caused by conventional pelletized catalyst configuration (Rauch et al., 2013, Ail and Dasappa, 2016). Nevertheless, syngas from biomass is generally produced in decentralized plants that do not have the production capacity of a natural gas or coal plant. Hence using a fixed bed reactor technology is the most efficient way to maximize the synthesis on the grounds that (i) this type of reactor are easy to operate; (ii) scale up can be easily accomplished by investigations on a single tube because in principle, parallel tubes behave similarly so; and (iii) there is no need for liquid-solid separation unit. Additionally, the disadvantages of an FBR reactor can be overcome by adopting the use of a structural catalyst (monolithic and foams). Structural catalysts can enhance mass transfer characteristics between synthesis gas, liquid products, and solid catalysts while maintaining isothermal operation (good axial and radial heat transfer) and reduce pressure drop in gas-liquid reactions (Hilmen et al., 2001, Tronconi et al., 2014, Visconti et al., 2009, Visconti et al., 2011, Parra-Cabrera et al., 2018, Bogdan and Michorczyk, 2020).

When it comes to catalysts, there are four transition metals with a sufficiently high hydrogenation activity to be employed in FTS processes, cobalt (Co), iron (Fe), nickel (Ni), and ruthenium (Ru). Still, only Co and Fe are considered industrial catalysts due to the high cost of Ru and the Ni very high CH<sub>4</sub> selectivity. Fe is the most applied catalyst among all catalysts due to its low price and availability. Furthermore, because the syngas generated from biomass has a low H<sub>2</sub>/CO ratio and water is always a by-product of the FT, Fe-base catalysts are better suited for biomass feedstocks as well as for CO<sub>2</sub>-rich feedstocks (Luque et al., 2012, Mehariya et al., 2020, Eric and Michael, 2008). In fact, many experimental studies detail the physical and chemical characteristics that can improve catalytic activity, selectivity and reduce the formation of unwanted products for Fe based catalyst. However, the challenges of developing more efficient, cheaper, and tailored Fe-based catalysts still exist because Co-based materials have better characteristics in terms of performance, selectivity, and lifetime (Tu et al., 2015, Mandal et al., 2018, Pant and Upadhyayula, 2017, Abrokwah et al., 2019, He et al., 2015, Javed et al., 2018, Li et al., 2019, Luo et al., 2019, Sineva et al., 2014, Daramola et al., 2017). That, coupled with the fact that fixed-bed reactors need

to improve the reaction rates and heat and mass transfer characteristics, is a research opportunity that has motivated the adoption of structured catalysts for CO hydrogenation (Tronconi et al., 2014, Visconti et al., 2011). Structured catalysts are ceramic or metallic substrates, pre-shaped in the form of a single continuous structure with stable geometry, often a monolithic honeycomb matrix (including many small parallel channels with openings in the order of one to few millimetres) or open cell foams (Hilmen et al., 2001, Giani et al., 2006, Tronconi et al., 2014, Visconti et al., 2009, Visconti et al., 2011, Kapteijn et al., 2005). Because structural catalysts present lower internal diffusional resistance and have a better heat transfer capacity, hot spots in the catalytic bed are limited, and sintering, carbon deposition, and reduction of the amount of catalyst active sites can be avoided (Kolaczkowski et al., 2016, Tronconi et al., 2014, Visconti et al., 2011, Harmel et al., 2018, Liu et al., 2012). A Fe-based structural catalyst can achieve lower pressure drop (by two orders of magnitude), smaller size reactors (compared to conventional pelletized catalysts), and significantly higher selectivities (Liu et al., 2020, Luo et al., 2019). Structural catalysts are prepared via electrodeposition, powder metallurgy, metal melt atomization, casting of metal melts into a porous ceramic mold, and additive manufacturing (3D printing). The material of the whole structure can come at as the active phase of the catalyst, or it can only be the support. If the structure is only the support, then the active phase can be deposited over it by washcoating or be "grown" on the surface of the support (Parra-Cabrera et al., 2018, Hilmen et al., 2001, Kolaczkowski et al., 2016).

### **Fischer-Tropsch Experimental Setup for the CERESiS Project**

With the previous considerations, the following describes the process specifications for the FT synthesis to develop in this work.

The FBR reactors resembles a shell and tube exchanger. The catalyst particles are packed in the tube. The reaction heat is removed by circulating a coolant that passes through the shell side. The temperature on the shell side is approximately 220 °C with operating pressures on the tube side of 20 bar. In the process depicted here, the tail gas is not recirculated to the FT reactor. This gas circuit configuration is the simplest and involves a single passage of the synthesis gas through the FT reactor. It is easy to build and operate, and there is no accumulation of inert compounds in the reactor or recirculation configurations that complicate the design. Although the unconverted syngas is not used to maximize the production of FT liquid fuels, it can be used as fuel gas in scaling up. After the FT reactor, the synthetic crude that emerges in two separate streams is recovered at low temperature. One is the liquid phase stream containing molten wax. The other is the gaseous stream that contains the lighter components of synthetic crude. The upgrading of the synthetic oil will be carried up with a classical hydrogenation technique using waste catalyst from the mining industry.

The reactor consists of two concentric stainless-steel cylinders. The inner cylinder has a diameter of 25 mm. The outer cylinder has a diameter of 32 mm. The reaction takes place in the inner cylinder. Nitrogen is circulated in the outer cylinder to control the temperature of the reactor. The reactor is equipped with several thermocouples to measure the catalytic bed's temperature. For its operation, the reactor is connected to a series of peripheral components shown and listed in Figure 3-9.

The gases (carbon monoxide, hydrogen, nitrogen, or syngas) are stored in a compressed gas cylinder. The components of the gas feed are pressure-regulating valves for each gas cylinder, followed by a mass flow controller, valves to ensure that each controller works correctly, check valves to control backflow. Then, a pressure gauge monitors the pressure at the reactor inlet, a relief valve used to limit stress in the system. Then a bypass valve to divert gas to the analysis section or to maintain an even pressure (preventing pressure build-up). A gas heater is set before the reactor to increase the gases temperature. After the catalytic reactor comes two separation units to recover the products obtained during the reaction. The first separation unit will collect wax, and the second will contain the lighter components of synthetic crude. A second pressure gauge follows the separation unit to monitor the pressure at the reactor exit. Then, a backpressure regulator installed at the end of the piping system provides an obstruction to flow and regulates upstream pressure. Finally, a gas flow counter to measure the volumetric flow rate of the gases that did not react or were produced during the reaction.

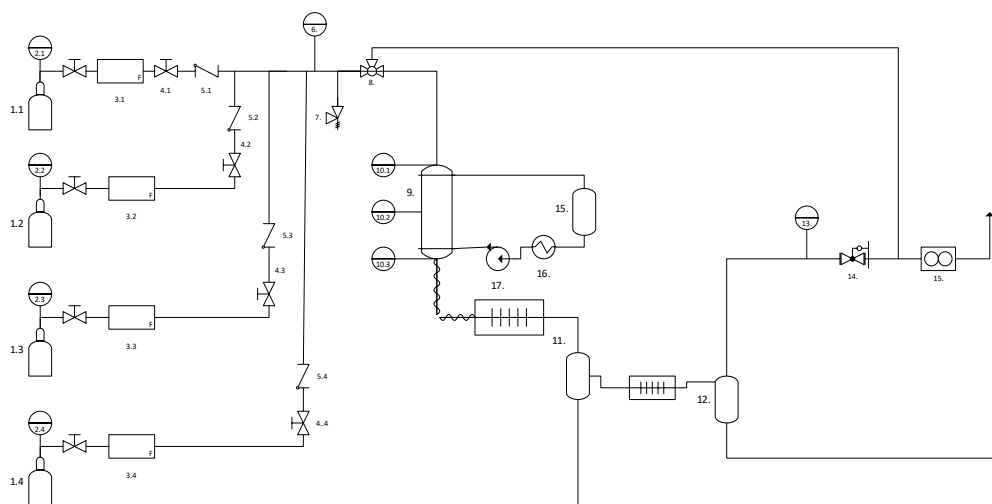


**Figure 3-9: Simplified Flow Diagram for Fisher-Tropsch reactor and peripheral components: 1. Gas cylinders; 2. Pressure regulators; 3. Mass flow controllers; 4. Valves; 5. Check valve; 6. A front pressure gauge; 7. Relief valve; 8. Bypass valve; 9. Tube and shell catalytic reactor; 10. Temperature sensors; 11. Separation column (hot trap); 12. Separation column (cold trap); 12. A back pressure gauge; 13. Backpressure regulator; 14. Gas flow counter; 15. Oil tank; 16. Heat exchanger; 17. Pump.**

The setup's operation parameters are as follows: The system's temperature range is 200 to 250 °C with an adjustable set point (generally fixed at 220 °C). Three thermocouples will monitor the temperature in the catalytic bed to prevent the temperature from rising. Nitrogen will be circulated for the external cylinder of the reactor. The maximum pressure of the system will be 20 bar, control with a backpressure regulator. However, if the pressure were to rise, a safety valve is installed in the setup. The gas flow rate will be kept between 1.8 and 18 litres per hour. The expected gas composition is 25 – 40% CO, 50 - 80% hydrogen, 10 – 30 % carbon dioxide, and 5 - 10% nitrogen.



Using this experimental setup, a tube and shell reactor loaded with a structural catalyst will be tested in the low-temperature Fischer–Tropsch synthesis and compared to commercial pelletized catalysts. The hope is that by using structured catalysts, a conventional packed-bed reactor approaches the ideal plug-flow behavior while enabling isothermal operation of highly exothermic reactions, facilitating the intraparticle mass transfer, and limiting pressure drop.

## 3.4 List of References

---

Abrokwah, R. Y., Rahman, M. M., Deshmane, V. G. & Kuila, D. (2019). Effect of titania support on Fischer-Tropsch synthesis using cobalt, iron, and ruthenium catalysts in silicon-microchannel microreactor. *Molecular Catalysis*, 478, 110566.

Acelas, N.Y., López, D.P., Brilman, D.W.F. (Wim), Kersten, S.R.A., Kootstra, A.M.J., (2014). Supercritical water gasification of sewage sludge: Gas production and phosphorus recovery. *Bioresource Technology* 174, 167–175. <https://doi.org/10.1016/j.biortech.2014.10.003>

Ail, S. S. & Dasappa, S. (2016). Biomass to liquid transportation fuel via Fischer Tropsch synthesis–Technology review and current scenario. *Renewable and sustainable energy reviews*, 58, 267-286.

Ali, S.S., Abomohra, A.E.-F., Sun, J., (2017). Effective bio-pretreatment of sawdust waste with a novel microbial consortium for enhanced biomethanation. *Bioresource Technology* 238, 425–432. <https://doi.org/10.1016/j.biortech.2017.03.187>

Aljaberi, F.Y., (2018). Studies of autocatalytic electrocoagulation reactor for lead removal from simulated wastewater. *Journal of Environmental Chemical Engineering* 6(5), 6069-6078. <https://doi.org/10.1016/j.jece.2018.09.032>.

Anis, S., Zainal, Z.A., (2011). Tar reduction in biomass producer gas via mechanical, catalytic and thermal methods: A review. *Renewable and Sustainable Energy Reviews* 15, 2355–2377. <https://doi.org/10.1016/j.rser.2011.02.018>

Antal, M.J., Allen, S.G., Schulman, D., Xu, X., Divilio, R.J., (2000). Biomass Gasification in Supercritical Water. *Ind. Eng. Chem. Res.* 39, 4040–4053. <https://doi.org/10.1021/ie0003436>

Azadi, P., Afif, E., Azadi, F., Farnood, R., (2012). Screening of nickel catalysts for selective hydrogen production using supercritical water gasification of glucose. *Green Chem.* 14, 1766. <https://doi.org/10.1039/c2gc16378k>

Azadi, P., Farnood, R., (2011). Review of heterogeneous catalysts for sub- and supercritical water gasification of biomass and wastes. *International Journal of Hydrogen Energy* 36, 9529–9541. <https://doi.org/10.1016/j.ijhydene.2011.05.081>

Baba, Y., Matsuki, Y., Mori, Y., Suyama, Y., Tada, C., Fukuda, Y., Saito, M., Nakai, Y., (2017). Pretreatment of lignocellulosic biomass by cattle rumen fluid for methane production: Bacterial flora and enzyme activity analysis. *Journal of Bioscience and Bioengineering* 123, 489–496. <https://doi.org/10.1016/j.jbiosc.2016.11.008>

Bangaraiaha, P.; Sarathbabu, B., (2019). Optimization of process parameters in removal of lead from aqueous solution through response surface methodology. *Chemical Engineering Communications*, 206(8), 986–993.

Banville, M., Labrecque, R. & Lavoie, J.-M. (2014). Dry reforming of methane under an electro-catalytic bed: effect of electrical current and catalyst composition. *WIT Transactions on Ecology and the Environment*, 186, 603-611.

Banville, M., Lee, R., Labrecque, R. & Lavoie, J. (2013). Interaction of CO<sub>2</sub>/CH<sub>4</sub> with steel WOOL in an electrocatalytic dry reforming reactor. *Energy Sust.* IV, 176, 17.

Behnia, I., Yuan, Z., Charpentier, P., Xu, C., (2016). Production of methane and hydrogen via supercritical water gasification of renewable glucose at a relatively low temperature: Effects of metal catalysts and supports. *Fuel Processing Technology* 143, 27–34. <https://doi.org/10.1016/j.fuproc.2015.11.006>

Bhoi, P.R., Huhnke, R.L., Kumar, A., Payton, M.E., Patil, K.N., Whiteley, J.R., (2015). Vegetable oil as a solvent for removing producer gas tar compounds. *Fuel Processing Technology* 133, 97–104. <https://doi.org/10.1016/j.fuproc.2014.12.046>

Bircan, S.Y., Kamoshita, H., Kanamori, R., Ishida, Y., Matsumoto, K., Hasegawa, Y., Kitagawa, K., (2011). Behavior of heteroatom compounds in hydrothermal gasification of biowaste for hydrogen production. *Applied Energy* 88, 4874–4878. <https://doi.org/10.1016/j.apenergy.2011.06.031>

Bircan, S.Y., Naruse, I., Matsumoto, K., Kitagawa, K., (2013). Production of Hydroxylapatite from Biowaste, Chicken Manure by Hydrothermal Process. *JSBS* 03, 74–78. <https://doi.org/10.4236/jsbs.2013.31010>

Bogdan, E. & Michorczyk, P. (2020). 3D Printing in Heterogeneous Catalysis—The State of the Art. *Materials*, 13, 4534.

Boroson, M.L., Howard, J.B., Longwell, J.P., Peters, W.A., (1989). Heterogeneous cracking of wood pyrolysis tars over fresh wood char surfaces. *Energy Fuels* 3, 735–740. <https://doi.org/10.1021/ef00018a014>

Boukis, N., Diem, V., Habicht, W., Dinjus, E., (2003). Methanol Reforming in Supercritical Water. *Ind. Eng. Chem. Res.* 42, 728–735. <https://doi.org/10.1021/ie020557i>

Boukis, N., Galla, U., D'Jesús, P., Müller, H., Dinjus, E., (2005). Gasification of Wet Biomass in Supercritical Water. Results of Pilot Plant Experiments, in: 14th European Conference on Biomass for Energy, Industrie and Climate Protection. Presented at the 14th European Conference on Biomass for Energy, Industrie and Climate protection, Paris, France, pp. 964–967.

Boukis, N., Galla, U., Müller, H., Dinjus, E., (2007). Biomass Gasification in supercritical water. Experimental progress achieved with the VERENA Pilot-Plant., in: 15th European Biomass Conference & Exhibition. Presented at the 15th European Biomass Conference & Exhibition, Berlin, Germany, pp. 1013–1016.

Boukis, N., Galla, U., Müller, H., Dinjus, E., (2009). Behaviour of inorganic salts during hydrothermal gasification of biomass, in: 17th European Biomass Conference & Exhibition. From Research to Industry and Markets. Presented at the 17th European Biomass Conference & Exhibition. From research to Industry and Markets, Hamburg, Germany.

Boukis, N., Hauer, E., Herbig, S., Sauer, J., Vogel, F., (2017a). Catalytic gasification of digestate sludge in supercritical water on the pilot plant scale. *Biomass Conv. Bioref.* 7, 415–424. <https://doi.org/10.1007/s13399-017-0238-x>

Boukis, N., Korving, L., Hauer, E., Herbig, S., Sauer, J., (2015). Gasification of Sewage Sludge in Supercritical Water, Experimental Results from the Gasification of Dutch Sewage Sludge, in: 23rd European Biomass Conference and Exhibition. ETA-Florence Renewable Energies, p. 5 Pages. <https://doi.org/10.5071/23RDEUBCE2015-1CO.5.2>

Boukis, N., Neumann, M., Galla, U., Dinjus, E., (2010). Gasification of Herbage in Supercritical Water, Experimental Results, in: 18th European Biomass Conference and Exhibition. ETA-Florence Renewable Energies, pp. 562–566. <https://doi.org/10.5071/18THEUBCE2010-OA4.2>

Boukis, N., Stoll, I.K., (2021). Gasification of Biomass in Supercritical Water, Challenges for the Process Design—Lessons Learned from the Operation Experience of the First Dedicated Pilot Plant. *Processes* 9, 455. <https://doi.org/10.3390/pr9030455>

Boukis, N., Stoll, I.K., Sauer, J., Fischer, J., Kansy, R., (2017b). Separation of Salts During the Gasification of Spent Grain in Supercritical Water, in: European Biomass Conference and Exhibition, Stockholm, Sweden, 12-15 June 2017. Presented at the 25th European Biomass Conference and Exhibition, ETA-Florence Renewable Energies, Florence, Italy, pp. 338–343. <https://doi.org/10.5071/25THEUBCE2017-2BP.2.2>

Brillas, E.; Garcia-Segura, S., (2020). Benchmarking recent advances and innovative technology approaches of fenton, photo-fenton, electro-fenton, and related processes: a review on the relevance of phenol as model molecule. *Separation and Purification Technology*, 237, 116337.

Byrd, A., Pant, K., Gupta, R., (2008). Hydrogen production from glycerol by reforming in supercritical water over Ru/Al<sub>2</sub>O<sub>3</sub> catalyst. *Fuel* 87, 2956–2960. <https://doi.org/10.1016/j.fuel.2008.04.024>

Cao, C., Guo, L., Chen, Y., Guo, S., Lu, Y., (2011). Hydrogen production from supercritical water gasification of alkaline wheat straw pulping black liquor in continuous flow system. *International Journal of Hydrogen Energy* 36, 13528–13535. <https://doi.org/10.1016/j.ijhydene.2011.07.101>

Chaplin, B.P., (2014). Critical review of electrochemical advanced oxidation processes for water treatment applications. *Environmental Science: Processes & Impacts*, 16, 1182–1203.

Chen, X., Chen, G., Yue, P.L., (2002). Investigation on the electrolysis voltage of electrocoagulation. *Chemical Engineering Science* 57(13), 2449–2455. [https://doi.org/10.1016/S0009-2509\(02\)00147-1](https://doi.org/10.1016/S0009-2509(02)00147-1).

Cherif, Y.; Yahiaoui, I.; Aissani-Benissad, F.; Madi, K.; Benmehdi, N.; Fourcade, F.; Amrane, A., (2014). Heat attachment method for the immobilization of TiO<sub>2</sub> on glass plates: application to photodegradation of basic yellow dye and optimization of operation parameters, using response surface methodology. *Industrial and Engineering Chemistry Research*, 53(10), 3813–3819.

Chundawat, S.P.S., Pal, R.K., Zhao, C., Campbell, T., Teymouri, F., Videto, J., Nielson, C., Wieferich, B., Sousa, L., Dale, B.E., Balan, V., Chipkar, S., Aguado, J., Burke, E., Ong, R.G., (2020). Ammonia Fiber Expansion (AFEX) Pretreatment of Lignocellulosic Biomass. *JoVE* 57488. <https://doi.org/10.3791/57488>

Chuntanapum, A., Matsumura, Y., (2010). Char Formation Mechanism in Supercritical Water Gasification Process: A Study of Model Compounds. *Ind. Eng. Chem. Res.* 49, 4055–4062. <https://doi.org/10.1021/ie901346h>

D'Jesús Montilva, P., Boukis, N., Kraushaar-Czarnetzki, B., Dinjus, E., (2006). Influence of Process Variables on Gasification of Corn Silage in Supercritical Water. *Ind. Eng. Chem. Res.* 45, 1622–1630. <https://doi.org/10.1021/ie050367i>

D'Jesús Montilva, P.M., (2007). Die Vergasung von realer Biomasse in überkritischem Wasser: Untersuchung des Einflusses von Prozessvariablen und Edukteigenschaften. Universität Karlsruhe (TH), Karlsruhe.

D'Jesús, P., Artiel, C., Boukis, N., Kraushaar-Czarnetzki, B., Dinjus, E., (2005). Influence of Educt Preparation on Gasification of Corn Silage in Supercritical Water. *Ind. Eng. Chem. Res.* 44, 9071–9077. <https://doi.org/10.1021/ie0508637>

Daramola, M. O., Matamela, K. & Sadare, O. O. (2017). Effect of CO<sub>2</sub> co-feeding on the conversion of syngas derived from waste to liquid fuel over a bi-functional Co/H-ZSM-5 catalyst. *Journal of environmental chemical engineering*, 5, 54-62.

Dastyar, W., Raheem, A., He, J., Zhao, M., (2019). Biofuel Production Using Thermochemical Conversion of Heavy Metal-Contaminated Biomass (HMCB) Harvested from Phytoextraction Process. *Chemical Engineering Journal* 358, 759–785. <https://doi.org/10.1016/j.cej.2018.08.111>

Davis, B. H. (2001). Fischer–Tropsch synthesis: current mechanism and futuristic needs. *Fuel processing technology*, 71, 157-166.

Davis, B. H. (2005). Fischer–Tropsch synthesis: overview of reactor development and future potentialities. *Topics in catalysis*, 32, 143-168.

Daza Serna, L.V., Orrego Alzate, C.E., Cardona Alzate, C.A., (2016). Supercritical fluids as a green technology for the pretreatment of lignocellulosic biomass. *Bioresource Technology* 199, 113–120. <https://doi.org/10.1016/j.biortech.2015.09.078>

De Boni, E., Reimer, J., Peng, G., Zöhrer, H., Vogel, F., (2015). Salt separator and method for producing a methane-contraining gas mixture from biomass by using a salt separator. *WO2015/135785A1*.

Demirbas, A. (2007). Converting biomass derived synthetic gas to fuels via Fisher-Tropsch synthesis. *Energy Sources, Part A: Recovery, Utilization, and Environmental Effects*, 29, 1507-1512.

Ding, N., Azargohar, R., Dalai, A.K., Kozinski, J.A., (2014). Catalytic gasification of cellulose and pinewood to H<sub>2</sub> in supercritical water. *Fuel* 118, 416–425. <https://doi.org/10.1016/j.fuel.2013.11.021>

Dry, M. E. (2002a). High quality diesel via the Fischer–Tropsch process—a review. *Journal of Chemical Technology & Biotechnology: International Research in Process, Environmental & Clean Technology*, 77, 43-50.

Dry, M. E. (2002b). The fischer–tropsch process: 1950–2000. *Catalysis today*, 71, 227-241.

Ekpo, U., Ross, A.B., Camargo-Valero, M.A., Williams, P.T., (2016). A comparison of product yields and inorganic content in process streams following thermal hydrolysis and hydrothermal processing of microalgae, manure and digestate. *Bioresource Technology* 200, 951–960. <https://doi.org/10.1016/j.biortech.2015.11.018>

Elliott, D.C., (2008). Catalytic hydrothermal gasification of biomass. *Biofuels, Bioproducts and Biorefining* 2, 254–265. <https://doi.org/10.1002/bbb.74>

Elliott, D.C., Neuenschwander, G.G., Hart, T.R., Butner, R.S., Zacher, A.H., Engelhard, M.H., Young, J.S., McCready, D.E., (2004). Chemical Processing in High-Pressure Aqueous Environments. 7. Process Development for Catalytic Gasification of Wet Biomass Feedstocks. *Ind. Eng. Chem. Res.* 43, 1999–2004. <https://doi.org/10.1021/ie034303o>

Eric, V. & Michael, C. (2008). Fischer-Tropsch catalysts for the biomass-to-liquid process. *Chem. Eng. Technol.* 31, 655.

Espinoza, R., Steynberg, A., Jager, B. & Vosloo, A. (1999). Low temperature Fischer–Tropsch synthesis from a Sasol perspective. *Applied Catalysis A: General*, 186, 13-26.

Frusteri, F., Frusteri, L., Costa, F., Mezzapica, A., Cannilla, C., Bonura, G., (2017). Methane production by sequential supercritical gasification of aqueous organic compounds and selective CO<sub>2</sub> methanation. *Applied Catalysis A: General* 545, 24–32. <https://doi.org/10.1016/j.apcata.2017.07.030>

Galkin, A.A., Lunin, V.V., (2005). Subcritical and Supercritical Water: A Universal Medium for Chemical Reactions. *ChemInform* 36. <https://doi.org/10.1002/chin.200527217>

Garcia-Segura, S.; Nienhauser, A.B.; Fajardo, A.S.; Bansal, R.; Coonrod, C.L.; Fortner, J.D.; Marcos-Hernández, M.; Rogers, T.; Villagran, D.; Wong, M.S.; Westerhoff, P., (2020). Disparities between experimental and environmental conditions: research steps toward making electrochemical water treatment a reality. *Current Opinions in Electrochemistry*, 22, 9–16.

Garcia-Segura, S.; Ocon, J.D.; Chong, M.N., (2018). Electrochemical oxidation remediation of real wastewater effluents — a review. *Process Safety & Environmental Protection*, 113, 48–67.

Giani, L., Cristiani, C., Groppi, G. & Tronconi, E. (2006). Washcoating method for Pd/γ-Al<sub>2</sub>O<sub>3</sub> deposition on metallic foams. *Applied Catalysis B: Environmental*, 62, 121-131.

Guan, Q., Wei, C., Savage, P.E., (2012). Kinetic model for supercritical water gasification of algae. *Phys. Chem. Chem. Phys.* 14, 3140. <https://doi.org/10.1039/c2cp23792j>

Guettel, R., Kunz, U. & Turek, T. (2008). Reactors for Fischer-Tropsch Synthesis. *Chemical Engineering & Technology: Industrial Chemistry-Plant Equipment-Process Engineering-Biotechnology*, 31, 746-754.

Guo, L., Cao, C., Lu, Y., (2010). Supercritical Water Gasification of Biomass and Organic Wastes, in: Benteke Momba, M.N. (Ed.), *Biomass. Sciyo*. <https://doi.org/10.5772/9774>

Guo, L., Lu, Y., Zhang, X., Ji, C., Guan, Y., Pei, A., (2007). Hydrogen production by biomass gasification in supercritical water: A systematic experimental and analytical study. *Catalysis Today* 129, 275–286. <https://doi.org/10.1016/j.cattod.2007.05.027>

Guo, Y., Wang, S.Z., Xu, D.H., Gong, Y.M., Ma, H.H., Tang, X.Y., (2010). Review of catalytic supercritical water gasification for hydrogen production from biomass. *Renewable and Sustainable Energy Reviews* 14, 334–343. <https://doi.org/10.1016/j.rser.2009.08.012>

Han, J., Kim, H., (2008). The reduction and control technology of tar during biomass gasification/pyrolysis: An overview. *Renewable and Sustainable Energy Reviews* 12, 397–416. <https://doi.org/10.1016/j.rser.2006.07.015>

Hao, X.H., Guo, L., Mao, X., Zhang, X.M., Chen, X.J., (2003). Hydrogen production from glucose used as a model compound of biomass gasified in supercritical water. *International Journal of Hydrogen Energy* 28, 55–64. [https://doi.org/10.1016/S0360-3199\(02\)00056-3](https://doi.org/10.1016/S0360-3199(02)00056-3)

Harmel, J., Peres, L., Estrader, M., Berliet, A., Maury, S., Fécant, A., Chaudret, B., Serp, P. & Soulantica, K. (2018). hcp-Co Nanowires Grown on Metallic Foams as Catalysts for Fischer–Tropsch Synthesis. *Angewandte Chemie*, 130, 10739–10743.

He, L., Zhang, Y. & Fan, M. (2015). Development of composited rare-earth promoted cobalt-based Fischer–Tropsch synthesis catalysts with high activity and selectivity. *Applied Catalysis A: General*, 505, 276–283.

Hendry, D., Venkitasamy, C., Wilkinson, N., Jacoby, W., (2011). Exploration of the effect of process variables on the production of high-value fuel gas from glucose via supercritical water gasification. *Bioresource Technology* 102, 3480–3487. <https://doi.org/10.1016/j.biortech.2010.11.003>

Hilmen, A.-M., Bergene, E., Lindvåg, O., Schanke, D., Eri, S. & Holmen, A. (2001). Fischer–Tropsch synthesis on monolithic catalysts of different materials. *Catalysis Today*, 69, 227–232.

Hodes, M., Marrone, P.A., Hong, G.T., Smith, K.A., Tester, J.W., (2004). Salt precipitation and scale control in supercritical water oxidation—Part A: fundamentals and research. *The Journal of Supercritical Fluids* 29, 265–288. [https://doi.org/10.1016/S0896-8446\(03\)00093-7](https://doi.org/10.1016/S0896-8446(03)00093-7)

Hong, G.T., Killilea, W.R., Thomason, T.B., (1989). Method for solids separation in a wet oxidation type process. US4822497A.

Huang, H., Yuan, X., (2016). The migration and transformation behaviors of heavy metals during the hydrothermal treatment of sewage sludge. *Bioresource Technology* 200, 991–998. <https://doi.org/10.1016/j.biortech.2015.10.099>

Iglesia, E., Reyes, S. C., Madon, R. J. & Soled, S. L. (1993). Selectivity control and catalyst design in the Fischer–Tropsch synthesis: sites, pellets, and reactors. *Advances in catalysis*, 39, 221–302.

Janke, L., Leite, A., Batista, K., Weinrich, S., Sträuber, H., Nikolausz, M., Nelles, M., Stinner, W., (2016). Optimization of hydrolysis and volatile fatty acids production from sugarcane filter cake: Effects of urea supplementation and sodium hydroxide pretreatment. *Bioresource Technology* 199, 235–244. <https://doi.org/10.1016/j.biortech.2015.07.117>

Javed, M., Cheng, S., Zhang, G., Dal, P., Cao, Y., Lu, C., Yang, R., Xing, C. & Shan, S. (2018). Complete encapsulation of zeolite supported Co based core with silicalite-1 shell to achieve high gasoline selectivity in Fischer–Tropsch synthesis. *Fuel*, 215, 226–231.

Jin, Y., Ma, X., Jiang, X., Liu, H., Li, X., Yan, J., (2013). Hydrothermal Degradation of Polychlorinated Dibenzo- p-dioxins and Polychlorinated Dibenzofurans in Fly Ash from Municipal Solid Waste Incineration under Non-oxidative and Oxidative Conditions. *Energy Fuels* 27, 414–420. <https://doi.org/10.1021/ef301325f>

Kang, K., Azargohar, R., Dalai, A.K., Wang, H., (2016). Hydrogen production from lignin, cellulose and waste biomass via supercritical water gasification: Catalyst activity and process optimization study. *Energy Conversion and Management* 117, 528–537. <https://doi.org/10.1016/j.enconman.2016.03.008>

Kapteijn, F., De Deugd, R. M. & Moulijn, J. A. (2005). Fischer–Tropsch synthesis using monolithic catalysts. *Catalysis Today*, 105, 350–356.

Karayıldırım, T., Sinağ, A., Kruse, A., (2008). Char and Coke Formation as Unwanted Side Reaction of the Hydrothermal Biomass Gasification. *Chem. Eng. Technol.* 31, 1561–1568. <https://doi.org/10.1002/ceat.200800278>

Karoor, S. (1992). Gas Separation Using Microporous Hollow Fiber Membranes. Ph.D. Dissertation, Stevens Institute of Technology: Hoboken, NJ.

Kim, D.Y., Kim, Y.S., Kim, T.H., Oh, K.K., (2016). Two-stage, acetic acid-aqueous ammonia, fractionation of empty fruit bunches for increased lignocellulosic biomass utilization. *Bioresource Technology* 199, 121–127. <https://doi.org/10.1016/j.biortech.2015.09.049>

Kolaczowski, S. T., Awdry, S., Smith, T., Thomas, D., Torkuhl, L. & Kolvenbach, R. (2016). Potential for metal foams to act as structured catalyst supports in fixed-bed reactors. *Catalysis Today*, 273, 221–233.

Kritzer, P., Boukis, N., Dinjus, E., (1999). Factors controlling corrosion in high-temperature aqueous solutions: a contribution to the dissociation and solubility data influencing corrosion processes. *Journal of Supercritical Fluids* 15, 205–227.

Kruse, A., (2008). Supercritical water gasification. *Biofuels, Bioprod. Bioref.* 2, 415–437. <https://doi.org/10.1002/bbb.93>

Kruse, A., (2009). Hydrothermal biomass gasification. *The Journal of Supercritical Fluids* 47, 391–399. <https://doi.org/10.1016/j.supflu.2008.10.009>

Kruse, A., Dinjus, E., (2005). Influence of Salts During Hydrothermal Biomass Gasification: The Role of the Catalysed Water-Gas Shift Reaction. *Zeitschrift für Physikalische Chemie* 219, 341–366. <https://doi.org/10.1524/zpch.219.3.341.59177>

Kruse, A., Dinjus, E., (2007). Hot compressed water as reaction medium and reactant. *The Journal of Supercritical Fluids* 39, 362–380. <https://doi.org/10.1016/j.supflu.2006.03.016>

Kruse, A., Faquir, M., (2007). Hydrothermal Biomass Gasification – Effects of Salts, Backmixing and Their Interaction. *Chem. Eng. Technol.* 30, 749–754. <https://doi.org/10.1002/ceat.200600409>

Kruse, A., Funke, A., Titirici, M.-M., (2013). Hydrothermal conversion of biomass to fuels and energetic materials. *Current Opinion in Chemical Biology* 17, 515–521. <https://doi.org/10.1016/j.cbpa.2013.05.004>

Kruse, A., Meier, D., Rimbrecht, P., Schacht, M., (2000). Gasification of Pyrocatechol in Supercritical Water in the Presence of Potassium Hydroxide. *Ind. Eng. Chem. Res.* 39, 4842–4848. <https://doi.org/10.1021/ie0001570>

Kumar, M., Ponselvan, F.I.A., Malviya, J.R., Srivastava, V.C., Mall, I.D., (2009). Treatment of biodigester effluent by electrocoagulation using iron electrodes. *Journal of Hazardous Materials* 165(1–3), 345–352. <https://doi.org/10.1016/j.jhazmat.2008.10.041>

Kumar, P., Barrett, D.M., Delwiche, M.J., Stroeve, P., (2009). Methods for Pretreatment of Lignocellulosic Biomass for Efficient Hydrolysis and Biofuel Production. *Ind. Eng. Chem. Res.* 48, 3713–3729. <https://doi.org/10.1021/ie801542g>

Kumari, D., Singh, R., (2018). Pretreatment of lignocellulosic wastes for biofuel production: A critical review. *Renewable and Sustainable Energy Reviews* 90, 877–891. <https://doi.org/10.1016/j.rser.2018.03.111>

Kushwaha, J.P., Srivastava, V.C., Mall, I.D., (2010). Organics removal from dairy wastewater by electrochemical treatment and residue disposal. *Separation and Purification Technology* 76(2), 198–205. <https://doi.org/10.1016/j.seppur.2010.10.008>.

Kwon, J.H., Kang, H., Sang, B.-I., Kim, Y., Min, J., Mitchell, R.J., Lee, J.H., (2016). Feasibility of a facile butanol bioproduction using planetary mill pretreatment. *Bioresource Technology* 199, 283–287. <https://doi.org/10.1016/j.biortech.2015.08.074>

Labrecque, R. & Lavoie, J.-M. (2011). Dry reforming of methane with CO<sub>2</sub> on an electron-activated iron catalytic bed. *Bioresource technology*, 102, 11244–11248.

Lappas, A. & Heracleous, E. (2016). Production of biofuels via Fischer–Tropsch synthesis: biomass-to-liquids. *Handbook of biofuels production*. Elsevier.

Larcher, W., (2001). *Ökophysiologie der Pflanzen: Leben, Leistung und Streßbewältigung der Pflanzen in ihrer Umwelt*; 6. Neubearb. Aufl. ed, UTB für Wissenschaft. Ulmer, Stuttgart.

Laval-Gilly, P., Henry, S., Mazziotti, M., Bonnefoy, A., Comel, A., Falla, J., (2017). Miscanthus x Giganteus Composition in Metals and Potassium After Culture on Polluted Soil and Its Use as Biofuel. *Bioenerg. Res.* 10, 846–852. <https://doi.org/10.1007/s12155-017-9846-3>

Lee, H.V., Hamid, S.B.A., Zain, S.K., (2014). Conversion of Lignocellulosic Biomass to Nanocellulose: Structure and Chemical Process. *The Scientific World Journal* 2014, 1–20. <https://doi.org/10.1155/2014/631013>

Lee, I.-G., Kim, M.-S., Ihm, S.-K., (2002). Gasification of Glucose in Supercritical Water. *Ind. Eng. Chem. Res.* 41, 1182–1188. <https://doi.org/10.1021/ie010066i>

Leong, Y.K., Chen, W.-H., Lee, D.-J., Chang, J.-S., (2021). Supercritical water gasification (SCWG) as a potential tool for the valorization of phycoremediation-derived waste algal biomass for biofuel generation. *Journal of Hazardous Materials* 418, 126278. <https://doi.org/10.1016/j.jhazmat.2021.126278>

Li, D., Rohani, V., Fabry, F., Ramaswamy, A. P., Sennour, M. & Fulcheri, L. (2019). Experimental study on plasma-catalytic synthesis of hydrocarbons from syngas. *Applied Catalysis A: General*, 588, 117269.

Li, H., Qu, Y., Yang, Y., Chang, S., Xu, J., (2016). Microwave irradiation – A green and efficient way to pretreat biomass. *Bioresource Technology* 199, 34–41. <https://doi.org/10.1016/j.biortech.2015.08.099>

Li, J., Chen, J., Chen, S., (2018). Supercritical water treatment of heavy metal and arsenic metalloids-bioaccumulating-biomass. *Ecotoxicology and Environmental Safety* 157, 102–110. <https://doi.org/10.1016/j.ecoenv.2018.03.069>

Li, L., Xu, Z.R., Zhang, C., Bao, Jianping., Dai, X., (2012). Quantitative evaluation of heavy metals in solid residues from sub- and super-critical water gasification of sewage sludge. *Bioresource Technology* 121, 169–175. <https://doi.org/10.1016/j.biortech.2012.06.084>

Liew, C.-S., Kiatkittipong, W., Lim, J.-W., Lam, M.-K., Ho, Y.-C., Ho, C.-D., Ntwampe, S.K.O., Mohamad, M., Usman, A., (2021). Stabilization of heavy metals loaded sewage sludge: Reviewing conventional to state-of-the-art thermal treatments in achieving energy sustainability. *Chemosphere* 277, 130310. <https://doi.org/10.1016/j.chemosphere.2021.130310>

Linares-Hernández, I., Barrera-Díaz, C., Roa-Morales, G., Bilyeu, B., Ureña-Núñez, F., (2009). Influence of the anodic material on electrocoagulation performance. *Chemical Engineering Journal* 148(1), 97–105. <https://doi.org/10.1016/j.cej.2008.08.007>.

Liu, P., Zhang, D., Dai, Y., Lin, J., Li, Y. & Wen, C. (2020). Microstructure, mechanical properties, degradation behavior, and biocompatibility of porous Fe-Mn alloys fabricated by sponge impregnation and sintering techniques. *Acta Biomaterialia*, 114, 485–496.



Liu, W., Wang, Y., Wilcox, W. & Li, S. (2012). A compact and high throughput reactor of monolithic-structured catalyst bed for conversion of syngas to liquid fuels. *AIChE journal*, 58, 2820-2829.

Lu, Y., Guo, L., Ji, C., Zhang, X., Hao, X., Yan, Q., (2006). Hydrogen production by biomass gasification in supercritical water: A parametric study. *International Journal of Hydrogen Energy* 31, 822–831. <https://doi.org/10.1016/j.ijhydene.2005.08.011>

Lu, Y., Guo, L., Zhang, X., Ji, C., (2012). Hydrogen production by supercritical water gasification of biomass: Explore the way to maximum hydrogen yield and high carbon gasification efficiency. *International Journal of Hydrogen Energy* 37, 3177–3185. <https://doi.org/10.1016/j.ijhydene.2011.11.064>

Luo, M., Xu, S., Gu, Q., Di, Z., Liu, Q. & Zhao, Z. (2019). Co-Al nanosheets derived from LDHs and their catalytic performance for syngas conversion. *Journal of colloid and interface science*, 538, 440-448.

Luque, R., De La Osa, A. R., Campelo, J. M., Romero, A. A., Valverde, J. L. & Sanchez, P. (2012). Design and development of catalysts for Biomass-To-Liquid-Fischer-Tropsch (BTL-FT) processes for biofuels production. *Energy & Environmental Science*, 5, 5186-5202.

Madenoglu, T., Sađlam, M., Yüksel, M., Ballice, L., (2013). Simultaneous effect of temperature and pressure on catalytic hydrothermal gasification of glucose. *The Journal of Supercritical Fluids* 73, 151–160. <https://doi.org/10.1016/j.supflu.2012.10.004>

Madenoglu, T., Sađlam, M., Yüksel, M., Ballice, L., (2016). Hydrothermal gasification of biomass model compounds (cellulose and lignin alkali) and model mixtures. *The Journal of Supercritical Fluids* 115, 79–85. <https://doi.org/10.1016/j.supflu.2016.04.017>

Mahmoudi, H., Mahmoudi, M., Doustdar, O., Jahangiri, H., Tsolakis, A., Gu, S. & Lechwyszynski, M. (2017). A review of Fischer Tropsch synthesis process, mechanism, surface chemistry and catalyst formulation. *Biofuels Engineering*, 2, 11-31.

Mandal, S., Maity, S., Gupta, P. K., Mahato, A., Bhanja, P. & Sahu, G. (2018). Synthesis of middle distillate through low temperature Fischer-Tropsch (LTFT) reaction over mesoporous SDA supported cobalt catalysts using syngas equivalent to coal gasification. *Applied Catalysis A: General*, 557, 55-63.

Marrone, P.A., Hodes, M., Smith, K.A., Tester, J.W., (2004). Salt precipitation and scale control in supercritical water oxidation—part B: commercial/full-scale applications. *The Journal of Supercritical Fluids* 29, 289–312. [https://doi.org/10.1016/S0896-8446\(03\)00092-5](https://doi.org/10.1016/S0896-8446(03)00092-5)

Matsumura, Y., Harada, M., Nagata, K., Kikuchi, Y., (2006). Effect of heating rate of biomass feedstock on carbon gasification efficiency in supercritical water gasification. *Chemical Engineering Communications* 193, 649–659. <https://doi.org/10.1080/00986440500440157>

Matsumura, Y., Minowa, T., Potic, B., Kersten, S., Prins, W., Vanswaaij, W., Vandebeld, B., Elliott, D., Neuenschwander, G., Kruse, A., (2005). Biomass gasification in near- and super-critical water: Status and prospects. *Biomass and Bioenergy* 29, 269–292. <https://doi.org/10.1016/j.biombioe.2005.04.006>

Mavroudi, M.; Kaldis, S.P.; Sakellariopoulos, G.P. (2003). Reduction of CO<sub>2</sub> Emissions by a Membrane Contacting Process. *Fuel*, 82, 2153–2159.

Medina, J.D.C., Woiciechowski, A., Filho, A.Z., Nigam, P.S., Ramos, L.P., Soccol, C.R., (2016). Steam explosion pretreatment of oil palm empty fruit bunches (EFB) using autocatalytic hydrolysis: A biorefinery approach. *Bioresource Technology* 199, 173–180. <https://doi.org/10.1016/j.biortech.2015.08.126>

Mehariya, S., Iovine, A., Casella, P., Musmarra, D., Figoli, A., Marino, T., Sharma, N. & Molino, A. (2020). Fischer-Tropsch synthesis of syngas to liquid hydrocarbons. *Lignocellulosic Biomass to Liquid Biofuels*. Elsevier.

Milne, T.A., Evans, R.J., Abatzoglou, N., (1998). Biomass Gasifier “Tars”: Their Nature, Formation, and Conversion (No. NREL/TP-570-25357, ON: DE00003726, 3726). <https://doi.org/10.2172/3726>

Minowa, T., Inoue, S., (1999). Hydrogen production from biomass by catalytic gasification in hot compressed water. *Renewable Energy* 16, 1114–1117. [https://doi.org/10.1016/S0960-1481\(98\)00436-4](https://doi.org/10.1016/S0960-1481(98)00436-4)

Minowa, T., Ogi, T., (1998). Hydrogen production from cellulose using a reduced nickel catalyst. *Catalysis Today* 45, 411–416. [https://doi.org/10.1016/S0920-5861\(98\)00277-6](https://doi.org/10.1016/S0920-5861(98)00277-6)

Möbius, A., Boukis, N., Galla, U., Dinjus, E., (2012). Gasification of pyrolygneous acid in supercritical water. *Fuel* 94, 395–400. <https://doi.org/10.1016/j.fuel.2011.11.023>

Möbius, A., Boukis, N., Sauer, J., (2013). Gasification of biomass in supercritical water (SCWG). *Materials and processes for energy: communicating current research and technological developments* 264–268. <https://doi.org/10.13140/2.1.3147.3603>

Molino, A., Migliori, M., Blasi, A., Davoli, M., Marino, T., Chianese, S., Catizzone, E., Giordano, G., (2017). Municipal waste leachate conversion via catalytic supercritical water gasification process. *Fuel* 206, 155–161. <https://doi.org/10.1016/j.fuel.2017.05.091>

Mollah, M.Y.A., Morkovsky, P., Gomes, J.A.G., Kesmez, M., Parga, J., Cocke, D.L., (2004). Fundamentals, present and future perspectives of electro-coagulation. *Journal of Hazardous Materials* 114(1–3), 199–210. <https://doi.org/10.1016/j.jhazmat.2004.08.009>.

Monteiro Nunes, S., Paterson, N., Dugwell, D.R., Kandiyoti, R., (2007). Tar Formation and Destruction in a Simulated Downdraft, Fixed-Bed Gasifier: Reactor Design and Initial Results. *Energy Fuels* 21, 3028–3035. <https://doi.org/10.1021/ef070137b>

Mostafa, E.; Reinsberg, P.; Garcia-Segura, S.; Baltruschat, H., (2018). Chlorine species evolution during electrochlorination on boron-doped diamond anodes: In-situ electrogeneration of Cl<sub>2</sub>, Cl<sub>2</sub>O and ClO<sub>2</sub>. *Electrochimica Acta*, 281, 831–840.

Mroczek, E.K., Graham, D., Bacon, L., (2019). Removal of arsenic and silica from geothermal fluid by electrocoagulation. *Journal of Environmental Chemical Engineering* 7(4), 103232. <https://doi.org/10.1016/j.jece.2019.103232>.

Muangrat, R., Onwudili, J.A., Williams, P.T., (2010). Alkali-promoted hydrothermal gasification of biomass food processing waste: A parametric study. *International Journal of Hydrogen Energy* 35, 7405–7415. <https://doi.org/10.1016/j.ijhydene.2010.04.179>

Müller, J.B., Vogel, F., (2012). Tar and coke formation during hydrothermal processing of glycerol and glucose. Influence of temperature, residence time and feed concentration. *The Journal of Supercritical Fluids* 70, 126–136. <https://doi.org/10.1016/j.supflu.2012.06.016>

Myers, R. H. & Montgomery, D. C. Montgomery, (2002). *Response Surface Methodology*, 2nd edition, Wiley Int.

Nakamura, S., Siritwat, U., Yoshikawa, K., Kitano, S., (2015). Development of Tar Removal Technologies for Biomass Gasification using the By-products. *Energy Procedia* 75, 208–213. <https://doi.org/10.1016/j.egypro.2015.07.305>

Onsager, O., (1996). Hydrogen production from water and CO via alkali metal formate salts. *International Journal of Hydrogen Energy* 21, 883–885. [https://doi.org/10.1016/0360-3199\(96\)00031-6](https://doi.org/10.1016/0360-3199(96)00031-6)

Onwudili, J.A., (2013). Catalytic hydrothermal gasification of algae for hydrogen production: Composition of reaction products and potential for nutrient recycling. *Bioresource Technology* 127, 72–80.

Osada, M., Sato, T., Watanabe, M., Adschiri, T., Arai, K., (2004). Low-Temperature Catalytic Gasification of Lignin and Cellulose with a Ruthenium Catalyst in Supercritical Water. *Energy Fuels* 18, 327–333. <https://doi.org/10.1021/ef034026y>

Paethanom, A., Nakahara, S., Kobayashi, M., Prawisudha, P., Yoshikawa, K., (2012). Performance of tar removal by absorption and adsorption for biomass gasification. *Fuel Processing Technology* 104, 144–154. <https://doi.org/10.1016/j.fuproc.2012.05.006>

Panizza, M.; Cerisola, G., (2009). Direct and mediated anodic oxidation of organic pollutants. *Chemical Reviews*, 109, 6541–6569.

Pant, K. K. & Upadhyayula, S. (2017). Synthesis of C<sub>5</sub>+ hydrocarbons from low H<sub>2</sub>/CO ratio syngas over silica supported bimetallic Fe-Co catalyst. *Catalysis Today*, 291, 133-145.

Parra-cabrera, C., Achille, C., Kuhn, S. & Ameloot, R. (2018). 3D printing in chemical engineering and catalytic technology: structured catalysts, mixers and reactors. *Chemical Society Reviews*, 47, 209-230.

Pavlovič, I., Knez, Ž., Škerget, M., (2013). Hydrothermal Reactions of Agricultural and Food Processing Wastes in Sub- and Supercritical Water: A Review of Fundamentals, Mechanisms, and State of Research. *J. Agric. Food Chem.* 61, 8003–8025. <https://doi.org/10.1021/jf401008a>

Peterson, A.A., Vogel, F., Lachance, R.P., Fröling, M., Antal, Jr., M.J., Tester, J.W., (2008). Thermochemical biofuel production in hydrothermal media: A review of sub- and supercritical water technologies. *Energy Environ. Sci.* 1, 32. <https://doi.org/10.1039/b810100k>

Plakas, K.V.; Mantza, A.; Sklari, S.D.; Zaspalis, V.T.; Karabelas, A.J., (2019). Heterogeneous Fenton-like oxidation of pharmaceutical diclofenac by a catalytic iron-oxide ceramic microfiltration membrane. *Chemical Engineering Journal*, 373, 700-708.

Qian, L., Wang, S., Xu, D., Guo, Y., Tang, X., Wang, L., (2016). Treatment of municipal sewage sludge in supercritical water: A review. *Water Research* 89, 118–131. <https://doi.org/10.1016/j.watres.2015.11.047>

Rajkumar, K.; Muthukumar, M., (2017). Response surface optimization of electro-oxidation process for the treatment of C.I. Reactive Yellow 186 dye: reaction pathways. *Applied Water Science*, 7(2), 637–652.

Rauch, R., Kiennemann, A. & Sauciuc, A. (2013). Fischer-Tropsch synthesis to biofuels (BtL process). *The Role of Catalysis for the Sustainable Production of Bio-fuels and Bio-chemicals*. Elsevier.

Reddy, S.N., Nanda, S., Dalai, A.K., Kozinski, J.A., (2014). Supercritical water gasification of biomass for hydrogen production. *International Journal of Hydrogen Energy* 39, 6912–6926. <https://doi.org/10.1016/j.ijhydene.2014.02.125>

Rego De Vasconcelos, B. & Lavoie, J.-M. (2019). Recent advances in power-to-X technology for the production of fuels and chemicals. *Frontiers in chemistry*, 7, 392.

Reimer, J., Peng, G., Viereck, S., De Boni, E., Breinl, J., Vogel, F., (2016). A novel salt separator for the supercritical water gasification of biomass. *The Journal of Supercritical Fluids* 117, 113–121. <https://doi.org/10.1016/j.supflu.2016.06.009>

Resende, F.L.P., Savage, P.E., (2010). Kinetic model for noncatalytic supercritical water gasification of cellulose and lignin. *AIChE J. NA-NA*. <https://doi.org/10.1002/aic.12165>

Roshchin, A.V., Grigor'ev, V.S., Strelets, A.V., Nikolaev, A.I., Raevskaya, E.G., Usin, V.V., Korneeva, T.N., (2017). Supercritical hydrothermal degradation of hazardous organic wastes with a view to utilizing the potential energy of gaseous products. *Russ. J. Phys. Chem. B* 11, 555–560. <https://doi.org/10.1134/S1990793117040108>

Saisu, M., Sato, T., Watanabe, M., Adschiri, T., Arai, K., (2003). Conversion of Lignin with Supercritical Water–Phenol Mixtures. *Energy Fuels* 17, 922–928. <https://doi.org/10.1021/ef0202844>

Salimi, M., Safari, F., Tavasoli, A., Shakeri, A., (2016). Hydrothermal gasification of different agricultural wastes in supercritical water media for hydrogen production: a comparative study. *Int J Ind Chem* 7, 277–285. <https://doi.org/10.1007/s40090-016-0091-y>

Salmerón, I.; Plakas, K.V.; Oller, I.; Sirés, I.; Maldonado, M.I.; Karabelas, A.J.; Malato, S., (2019). Optimization of electrocatalytic H<sub>2</sub>O<sub>2</sub> production at pilot plant scale for solar-assisted water treatment. *Applied Catalysis B: Environmental*, 242, 327-336.

Saritha, M., Arora, A., Lata, (2012). Biological Pretreatment of Lignocellulosic Substrates for Enhanced Delignification and Enzymatic Digestibility. *Indian J Microbiol* 52, 122–130. <https://doi.org/10.1007/s12088-011-0199-x>

Sawai, O., Nunoura, T., Yamamoto, K., (2014). Supercritical water gasification of sewage sludge using bench-scale batch reactor: advantages and drawbacks. *J Mater Cycles Waste Manag* 16, 82–92. <https://doi.org/10.1007/s10163-013-0144-7>

Schubert, M., (2010). Catalytic hydrothermal gasification of biomass: salt recovery and continuous gasification of glycerol solutions. ETH Zurich, Zurich, Switzerland. <https://doi.org/10.3929/ETHZ-A-006212308>

Schubert, M., Aubert, J., Müller, J.B., Vogel, F., (2012). Continuous salt precipitation and separation from supercritical water. Part 3: Interesting effects in processing type 2 salt mixtures. *The Journal of Supercritical Fluids* 61, 44–54. <https://doi.org/10.1016/j.supflu.2011.08.011>

Schubert, M., Regler, J.W., Vogel, F., (2010a). Continuous salt precipitation and separation from supercritical water. Part 1: Type 1 salts. *The Journal of Supercritical Fluids* 52, 99–112. <https://doi.org/10.1016/j.supflu.2009.10.002>

Schubert, M., Regler, J.W., Vogel, F., (2010b). Continuous salt precipitation and separation from supercritical water. Part 2. Type 2 salts and mixtures of two salts. *The Journal of Supercritical Fluids* 52, 113–124. <https://doi.org/10.1016/j.supflu.2009.10.003>

Schulz, H. (1999). Short history and present trends of Fischer–Tropsch synthesis. *Applied Catalysis A: General*, 186, 3-12.

Schulz, H., Beck, K. & Erich, E. (1988). Mechanism of the Fischer Tropsch process. *Studies in Surface Science and Catalysis*. Elsevier.

Sharma, Y. C.; Srivastava, V.; Singh, V.K.; Kaul, S.H.; Weng, C.H., (2009). Nanoadsorbents for the removal of metallic pollutants from water and wastewater. *Environmental Technology*, 30(6), 583–609.

Sinag, A., Kruse, A., Rathert, J., (2004). Influence of the Heating Rate and the Type of Catalyst on the Formation of Key Intermediates and on the Generation of Gases During Hydrolysis of Glucose in Supercritical Water in a Batch Reactor. *Industrial & Engineering Chemistry Research* 43, 502–508. <https://doi.org/10.1021/ie030475+>

Sinaž, A., Kruse, A., Schwarzkopf, V., (2003). Key Compounds of the Hydrolysis of Glucose in Supercritical Water in the Presence of K<sub>2</sub>CO<sub>3</sub>. *Ind. Eng. Chem. Res.* 42, 3516–3521. <https://doi.org/10.1021/ie030079r>

Sineva, L. V., Khatkova, E. Y., Kriventseva, E. V. & Mordkovich, V. Z. (2014). Effect of introduced zeolite on the Fischer–Tropsch synthesis over a cobalt catalyst. *Mendeleev Communications*, 24, 316-318.

Singh, R., Krishna, B.B., Kumar, J., Bhaskar, T., (2016). Opportunities for utilization of non-conventional energy sources for biomass pretreatment. *Bioresource Technology* 199, 398–407. <https://doi.org/10.1016/j.biortech.2015.08.117>

- Singh, R.N., Singh, S.P., Balwanshi, J.B., (2014). Tar removal from Producer Gas: A Review. *Research Journal of Engineering Sciences* 3, 16–22.
- Su, W., Liu, P., Cai, C., Ma, H., Jiang, B., Xing, Y., Liang, Y., Cai, L., Xia, C., Le, Q.V., Sonne, C., Lam, S.S., (2021). Hydrogen production and heavy metal immobilization using hyperaccumulators in supercritical water gasification. *Journal of Hazardous Materials* 402, 123541. <https://doi.org/10.1016/j.jhazmat.2020.123541>
- Sutton, D., Kelleher, B., Ross, J.R.H., (2001). Review of literature on catalysts for biomass gasification. *Fuel Processing Technology* 73, 155–173. [https://doi.org/10.1016/S0378-3820\(01\)00208-9](https://doi.org/10.1016/S0378-3820(01)00208-9)
- Tao, L., Aden, A., Elander, R.T., Pallapolu, V.R., Lee, Y.Y., Garlock, R.J., Balan, V., Dale, B.E., Kim, Y., Mosier, N.S., Ladisch, M.R., Falls, M., Holtzapple, M.T., Sierra, R., Shi, J., Ebrik, M.A., Redmond, T., Yang, B., Wyman, C.E., Hames, B., Thomas, S., Warner, R.E., (2011). Process and techno-economic analysis of leading pretreatment technologies for lignocellulosic ethanol production using switchgrass. *Bioresource Technology* 102, 11105–11114. <https://doi.org/10.1016/j.biortech.2011.07.051>
- Tawabini, B.S.; Plakas, K.V.; Fraim, M.; Safi, E.; Oyehan, T.; Karabelas, A.J., (2020a). Assessing the efficiency of a pilot-scale GDE/BDD electrochemical system in removing phenol from high saline waters. *Chemosphere*, 239, 124714.
- Tawabini, B.S.; Plakas, K.V.; Karabelas, A.J., (2020b). A pilot study of BTEX removal from highly saline water by an advanced electrochemical process. *Journal of Water Process Engineering*, 37, 101427.
- Todic, B., Nowicki, L., Nikacevic, N. & Bukur, D. B. (2016). Fischer–Tropsch synthesis product selectivity over an industrial iron-based catalyst: Effect of process conditions. *Catalysis Today*, 261, 28–39.
- Tronconi, E., Groppi, G. & Visconti, C. G. (2014). Structured catalysts for non-adiabatic applications. *Current Opinion in Chemical Engineering*, 5, 55–67.
- Tu, J., Ding, M., Zhang, Y., Li, Y., Wang, T., Ma, L., Wang, C. & Li, X. (2015). Synthesis of Fe<sub>3</sub>O<sub>4</sub>-nanocatalysts with different morphologies and its promotion on shifting C<sub>5</sub>+ hydrocarbons for Fischer–Tropsch synthesis. *Catalysis Communications*, 59, 211–215.
- Van Der Laan, G. P. & Beenackers, A. (1999). Kinetics and selectivity of the Fischer–Tropsch synthesis: a literature review. *Catalysis Reviews*, 41, 255–318.
- Vassilev, S.V., Vassileva, C.G., Baxter, D., (2014). Trace element concentrations and associations in some biomass ashes. *Fuel* 129, 292–313. <https://doi.org/10.1016/j.fuel.2014.04.001>
- Visconti, C. G., Tronconi, E., Groppi, G., Lietti, L., Iovane, M., Rossini, S. & Zennaro, R. (2011). Monolithic catalysts with high thermal conductivity for the Fischer–Tropsch synthesis in tubular reactors. *Chemical Engineering Journal*, 171, 1294–1307.
- Visconti, C. G., Tronconi, E., Lietti, L., Groppi, G., Forzatti, P., Cristiani, C., Zennaro, R. & Rossini, S. (2009). An experimental investigation of Fischer–Tropsch synthesis over washcoated metallic structured supports. *Applied Catalysis A: General*, 370, 93–101.
- Waldner, M.H., Krumeich, F., Vogel, F., (2007). Synthetic natural gas by hydrothermal gasification of biomass Selection procedure towards a stable catalyst and its sodium sulfate tolerance. *The Journal of Supercritical Fluids*, 43, 91–105.
- Waldner, M.H., Vogel, F., (2005). Renewable Production of Methane from Woody Biomass by Catalytic Hydrothermal Gasification. *Ind. Eng. Chem. Res.* 44, 4543–4551. <https://doi.org/10.1021/ie050161h>
- Watanabe, M., Inomata, H., Smith, R.L., Arai, K., (2001). Catalytic decarboxylation of acetic acid with zirconia catalyst in supercritical water. *Applied Catalysis A: General* 219, 149–156. [https://doi.org/10.1016/S0926-860X\(01\)00677-9](https://doi.org/10.1016/S0926-860X(01)00677-9)

Watson, M.A.; Tubić, A.; Agbaba, J.; Nikić, J.; Maletić, S.; Jazić, J.M.; Dalmacija, B., (2016). Response surface methodology investigation into the interactions between arsenic and humic acid in water during the coagulation process. *Journal of Hazardous Materials*, 312, 150–158.

Weber, R., Yoshida, S., Miwa, K., (2002). PCB Destruction in Subcritical and Supercritical Water Evaluation of PCDF Formation and Initial Steps of Degradation Mechanisms. *Environ. Sci. Technol.* 36, 1839–1844. <https://doi.org/10.1021/es0113910>

Weng, Z., Kanchanatip, E., Hantoko, D., Yan, M., Su, H., Zhang, S., Wang, G., (2020). Improving supercritical water gasification of sludge by oil palm empty fruit bunch addition: Promotion of syngas production and heavy metal stabilization. *Chinese Journal of Chemical Engineering* 28, 293–298. <https://doi.org/10.1016/j.cjche.2019.08.004>

Widsten, P., Kandelbauer, A., (2008). Adhesion improvement of lignocellulosic products by enzymatic pre-treatment. *Biotechnology Advances* 26, 379–386. <https://doi.org/10.1016/j.biotechadv.2008.04.003>

Woolcock, P.J., Brown, R.C., (2013). A review of cleaning technologies for biomass-derived syngas. *Biomass and Bioenergy* 52, 54–84. <https://doi.org/10.1016/j.biombioe.2013.02.036>

Xu, C., Ma, F., Zhang, X., (2009). Lignocellulose degradation and enzyme production by *Irpeax lacteus* CD2 during solid-state fermentation of corn stover. *Journal of Bioscience and Bioengineering* 108, 372–375. <https://doi.org/10.1016/j.jbiosc.2009.04.023>

Xu, L.J., Sheldon, B.W., Larick, D.K., Carawan, R.E., (2002). Recovery and utilization of useful by-products from egg processing wastewater by electrocoagulation. *Poultry Science* 81(6), 785–792. <https://doi.org/10.1093/ps/81.6.785>.

Xu, Z.R., Zhu, W., Gong, M., Zhang, H.W., (2013). Direct gasification of dewatered sewage sludge in supercritical water. Part 1: Effects of alkali salts. *International Journal of Hydrogen Energy* 38, 3963–3972. <https://doi.org/10.1016/j.ijhydene.2013.01.164>

Yakaboylu, O., Harinck, J., Smit, K., de Jong, W., (2015a). Supercritical Water Gasification of Biomass: A Literature and Technology Overview. *Energies* 8, 859–894. <https://doi.org/10.3390/en8020859>

Yakaboylu, O., Harinck, J., Smit, K.G., de Jong, W., (2015b). Supercritical Water Gasification of Biomass: A Detailed Process Modeling Analysis for a Microalgae Gasification Process. *Ind. Eng. Chem. Res.* 54, 5550–5562. <https://doi.org/10.1021/acs.iecr.5b00942>

Yakaboylu, O., Yapar, G., Recalde, M., Harinck, J., Smit, K.G., Martelli, E., de Jong, W., (2015c). Supercritical Water Gasification of Biomass: An Integrated Kinetic Model for the Prediction of Product Compounds. *Ind. Eng. Chem. Res.* 54, 8100–8112. <https://doi.org/10.1021/acs.iecr.5b02019>

Yamaguchi, A., Hiyoshi, N., Sato, O., Osada, M., Shirai, M., (2008). Lignin Gasification over Supported Ruthenium Trivalent Salts in Supercritical Water. *Energy Fuels* 22, 1485–1492. <https://doi.org/10.1021/ef8001263>

Yanagida, T., Minowa, T., Nakamura, A., Matsumura, Y., Noda, Y., (2008). Behavior of Inorganic Elements in Poultry Manure during Supercritical Water Gasification. *J. Jpn. Inst. Energy* 87, 731–736. <https://doi.org/10.3775/jie.87.731>

Yanagida, T., Minowa, T., Shimizu, Y., Matsumura, Y., Noda, Y., (2009). Recovery of activated carbon catalyst, calcium, nitrogen and phosphate from effluent following supercritical water gasification of poultry manure. *Bioresource Technology* 100, 4884–4886. <https://doi.org/10.1016/j.biortech.2009.05.042>

Yanik, J., Ebale, S., Kruse, A., Saglam, M., Yuksel, M., (2007). Biomass gasification in supercritical water: Part 1. Effect of the nature of biomass. *Fuel* 86, 2410–2415. <https://doi.org/10.1016/j.fuel.2007.01.025>

Yanik, J., Ebale, S., Kruse, A., Saglam, M., Yüksel, M., (2008). Biomass gasification in supercritical water: II. Effect of catalyst. *International Journal of Hydrogen Energy* 33, 4520–4526. <https://doi.org/10.1016/j.ijhydene.2008.06.024>

Yao, Z., Li, J., Xie, H., Yu, C., (2012). Review on Remediation Technologies of Soil Contaminated by Heavy Metals. *Procedia Environmental Sciences* 16, 722–729. <https://doi.org/10.1016/j.proenv.2012.10.099>

Yong, T.L.-K., Matsumura, Y., (2012). Reaction Kinetics of the Lignin Conversion in Supercritical Water. *Ind. Eng. Chem. Res.* 51, 11975–11988. <https://doi.org/10.1021/ie300921d>

Yoshida, T., Matsumura, Y., (2001). Gasification of Cellulose, Xylan, and Lignin Mixtures in Supercritical Water. *Ind. Eng. Chem. Res.* 40, 5469–5474. <https://doi.org/10.1021/ie0101590>

Yoshida, T., Oshima, Y., Matsumura, Y., (2004). Gasification of biomass model compounds and real biomass in supercritical water. *Biomass and Bioenergy* 26, 71–78. [https://doi.org/10.1016/S0961-9534\(03\)00063-1](https://doi.org/10.1016/S0961-9534(03)00063-1)

You, T.-T., Zhang, L.-M., Xu, F., (2016). Progressive deconstruction of *Arundo donax* Linn. to fermentable sugars by acid catalyzed ionic liquid pretreatment. *Bioresource Technology* 199, 271–274. <https://doi.org/10.1016/j.biortech.2015.08.152>

Yousefi, M.; Nabizadeh, R.; Alimohammadi, M.; Mohammadi, A.A.; Mahvi, A.H., 2019. Performance of granular ferric hydroxide process for removal of humic acid substances from aqueous solution based on experimental design and response surface methodology. *Methods X*, 6, 35–42.

Yu, J., Zhang, J., He, J., Liu, Z., Yu, Z., (2009). Combinations of mild physical or chemical pretreatment with biological pretreatment for enzymatic hydrolysis of rice hull. *Bioresource Technology* 100, 903–908. <https://doi.org/10.1016/j.biortech.2008.07.025>

Zeng, X., Ueki, Y., Yoshiie, R., Naruse, I., Wang, F., Han, Z., Xu, G., (2020). Recent progress in tar removal by char and the applications: A comprehensive analysis. *Carbon Resources Conversion* 3, 1–18. <https://doi.org/10.1016/j.crcon.2019.12.001>

Zhan, L., Jiang, L., Zhang, Y., Gao, B., Xu, Z., (2020). Reduction, detoxification and recycling of solid waste by hydrothermal technology: A review. *Chemical Engineering Journal* 390, 124651. <https://doi.org/10.1016/j.cej.2020.124651>

Zhang, H., Tian, Y., Wang, L., Zhang, L., Dai, L., (2013). Ecophysiological characteristics and biogas production of cadmium-contaminated crops. *Bioresource Technology* 146, 628–636. <https://doi.org/10.1016/j.biortech.2013.07.148>

Zhang, H.W., Zhu, W., Xu, Z.R., Gong, M., (2012). Distributions of Carbon Nitrogen and Phosphorus in the Products from SCWG of Cyanobacteria. *AMR* 518–523, 326–331. <https://doi.org/10.4028/www.scientific.net/AMR.518-523.326>

Zhang, Y., Wan, L., Guan, J., Xiong, Q., Zhang, S., Jin, X., (2020). A Review on Biomass Gasification: Effect of Main Parameters on Char Generation and Reaction. *Energy Fuels* 34, 13438–13455. <https://doi.org/10.1021/acs.energyfuels.0c02900>

Zhao, L., Zhang, J., Sheng, C.D., Wang, K., Ding, Q.Z., (2012). Dissolution Characteristics of Inorganic Elements Existing in Biomass during the Supercritical Water Gasification Process. *Energy Sources, Part A: Recovery, Utilization, and Environmental Effects* 34, 1893–1900. <https://doi.org/10.1080/15567036.2011.592913>

Zhiyong, Y., Xiuyi, T., (2015). Hydrogen generation from oily wastewater via supercritical water gasification (SCWG). *Journal of Industrial and Engineering Chemistry* 23, 44–49. <https://doi.org/10.1016/j.jiec.2014.07.040>

Zhu, W., Xu, Z.R., Li, L., He, C., (2011). The behavior of phosphorus in sub- and super-critical water gasification of sewage sludge. *Chemical Engineering Journal* 171, 190–196. <https://doi.org/10.1016/j.cej.2011.03.090>

Ziemiński, K., Romanowska, I., Kowalska, M., (2012). Enzymatic pretreatment of lignocellulosic wastes to improve biogas production. *Waste Management* 32, 1131–1137. <https://doi.org/10.1016/j.wasman.2012.01.016>

Zodi, S., Louvet, J., Michon, C., Potier, O., Pons, M., Lapicque, F., Leclerc, J., (2011). Electrocoagulation as a tertiary treatment for paper mill wastewater: Removal of nonbiodegradable organic pollution and arsenic. *Separation and Purification Technology* 81(1), 62–68. <https://doi.org/10.1016/j.seppur.2011.07.002>.

Zöhrer, H., De Boni, E., Vogel, F., (2014). Hydrothermal processing of fermentation residues in a continuous multistage rig – Operational challenges for liquefaction, salt separation, and catalytic gasification. *Biomass and Bioenergy* 65, 51–63. <https://doi.org/10.1016/j.biombioe.2014.03.023>



## 4 FAST PYROLYSIS (FP) BASED TECHNOLOGY PATHWAY

In this section, the overall process chain for technology pathway 2 will be defined and an initial screening of technologies will be performed. TP2 comprises bio-oil production via fast pyrolysis (Section 4.1 ), MILD-combustion (Section 4.2 ), bio-oil upgrading, bio-oil decontamination and reuse options for bio-char (Section 4.3 (CNR and CERTH)). An extensive literature and market survey for the selection of the appropriate technology for bio-oil production will be performed, taking into account the presence of contamination in the feedstock. Key influential parameters for process performance will be identified for every technology, while considering the destruction of organic contaminants and separation/fixation of inorganics. As for TP1, the results will be summarized in the biomass technology matrix, displaying all technologies and influential parameters (Section 5 ).

### 4.1 Fast pyrolysis (FP)

---

In this section, an overview of the pyrolysis fundamentals is presented first aimed at identifying the most relevant operating variables that affect the yields and the properties of the process products. Then, a brief description of the reactors configurations typically adopted for the fast pyrolysis process will be introduced in order to highlight the criteria under the choice of the auger reactor as the optimal configuration in relation to the CERESiS scope.

#### 4.1.1 Pyrolysis fundamentals and influential parameters of FP

Pyrolysis is a thermochemical conversion process conducted in absence of molecular oxygen through which biomass is decomposed to form a vapor phase consisting in condensable and incondensable compounds, typically known as bio-oil and pyrolysis gas. The remaining solid carbonaceous residue is known as char or bio-char. The yields and characteristics of the pyrolysis products are influenced by the following operating variables: temperature, heating rate, pressure and gas residence time, feedstock composition and size. Optimal ranges of temperature, heating rate and gas residence time have been defined for the maximization of condensable fraction yields, thus leading to the identification of fast pyrolysis as the most suitable processes for the maximization of the bio-oil. Fast pyrolysis is characterized by high heating rate (~100-1000 °C/s), very short residence time of hot vapors (~1 s) and temperatures between 400 and 550 °C.

##### Temperature

In the pyrolysis process, as the temperature increases, the primary degradation of biomass causes the formation of condensable volatiles, while the formation of gas (mainly CO, CO<sub>2</sub>, CH<sub>4</sub>) is limited; the condensable fraction yield increases with temperature up to about 500°C. At this temperature, most of the volatile species have been released and can undergo secondary degradation reactions that produce gas (mostly CO, CO<sub>2</sub>, CH<sub>4</sub> and H<sub>2</sub>)

and low molecular weight (LMW) condensable species. In conditions where the secondary reactions are relevant (prolonged vapors residence time in the high temperature environment), the condensable fraction yield reaches a maximum, while the gas yield increases significantly. In the meantime, the solid residue, whose structure and chemistry have been greatly altered by the thermal treatment, evolves towards a porous carbonaceous structure with a reduced oxygen content (primary char). The vapors still entrapped into the porous char matrix, depending on the temperature and the residence time, can undergo polymerization reactions producing a solid product called secondary char whose structure and chemical composition is much more similar to that of carbon coke than that of primary char (Zhang et al., 2006).

Figure 4-1 represents qualitatively the evolution of the pyrolysis products as the severity of heat treatment increases (Giudicianni et al., 2021).

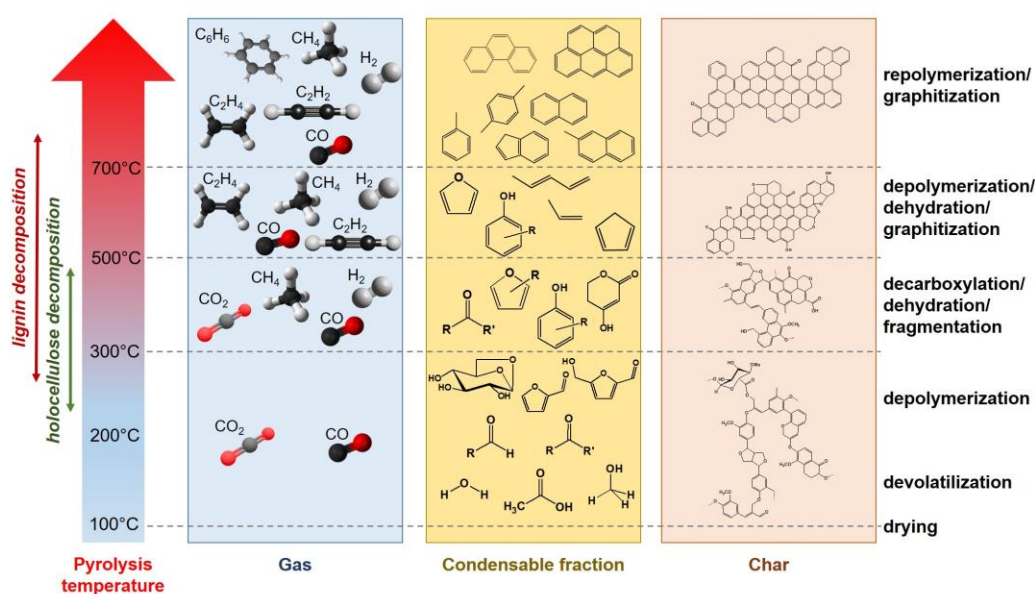


**Figure 4-1: Schematic representation of the evolution of the pyrolysis products as the severity of heat treatment increases (Giudicianni et al., 2021).**

### Heating rate

At low heating rate, woody biomass typically exhibits char yield decreasing from about 40 to 20 wt.% as temperature increases from 400 to 700 °C, whereas the decay curve is shifted to higher values for biomass characterized by a high ash content such as herbaceous biomass and agricultural residues, sludges (Fytli and Zabaniotou, 2008) and macroalgae (Lee et al., 2020). Microalgae are targeted as a source of lipids for algal oil including the production of biofuels (Chisti, 2007), therefore their use in pyrolysis is less attractive.

At high heating rate char yields decrease in favor of gas and condensable fraction. For temperature lower than 500°C, high heating rates correspond, on average, to higher temperature at which primary decomposition occurs. In these conditions, devolatilization is promoted at the expense of char forming reactions (Di Blasi, 2008). If a high heating rate

is applied at temperature exceeding 500°C, the activity of secondary reactions is enhanced thus promoting gas production and even secondary char formation if the temperature is sufficiently high (Di Blasi, 2009). Two opposing driving forces concur in determining the formation of secondary char in these conditions: higher average temperatures inside the particles enhance the activity of the repolymerization reactions promoting the production of secondary chars; conversely, the disruptive devolatilization induced by the higher heating rate creates a more open char structure that favors an easier escape of volatiles and reducing the extent of reactions forming secondary char given the reduced residence time of the volatiles inside the char pores (Cetin et al., 2004).

#### Pressure and gas residence time

Pressure affects indirectly the progress of the secondary reactions by changing the vapors residence time. Limited data are presented in the literature on the effect of pressure on char yield (Antal et al., 2000; Antal et al., 1996; Blackadder et al., 1995; Mahinpey et al., 2009; Mok and Antal, 1983; Pindoria et al., 1998). Previous studies on cellulose pyrolysis have demonstrated that an increase in pressure, if associated to high gas residence time in the reaction environment, generates higher char yields and produces lighter volatiles (Antal et al., 2000). High pressure accompanied by low gas flow rate (which imply high residence time) limits the mass transport favoring the decomposition to lighter volatiles (Mok and Antal, 1983) and further polymerization of primary pyrolysis products rather than their evaporation, thus promoting secondary char production. Conversely, low pressure and high gas flow rate reduce the char yield as observed for cellulose (Mok and Antal, 1983). The mechanisms observed for cellulose pyrolysis can be somewhat extended to the other biomass components and to the biomass itself.

#### Carrier gas flow rate and feedstock size

Carrier gas flow rate and feedstock size affect indirectly gas residence time and heating rate, respectively. However, they play an additional role when contaminated biomass is considered. In presence of contaminants, FP experiments should be properly designed taking into account different needs:

- To limit the transfer of heavy metals in the vapor phase forming bio-oil;
- To concentrate the contaminants and reduce their mobility in the solid residue;
- To avoid the production of contaminated streams hard to be managed.

In order to reach this goal it is pivotal to elucidate the mechanisms of transfer of heavy metals from the feedstock to bio-oil during FP. Leijenhurst et al. (2016) reviewed the mechanisms involved in the transfer of inorganic elements during pyrolysis by critically analysing the wide literature on the thermal behaviour of alkali and earth alkali metals in biomass pyrolysis. However, Leijenhurst et al. (2016) pointed out that heavy metals also follow similar mechanisms.

Concerning heavy metals, it was demonstrated that due to the low temperature reached during fast pyrolysis, heavy metals contained in biomass used for phytoextraction are almost totally retained in the chars and that most of them are in a water leachable forms

(Grottola et al., 2018). Biomasses contaminated with Cd, Pb, Cu and Zn were investigated (Lievens et al., 2008, 2009; Stals et al., 2010a) and Cd was found to be the most volatile, both under fast and flash pyrolysis conditions. However, some discrepancies exist on the threshold temperatures over which the devolatilization of Cd occurs because of the effect of the specific reactor used for the tests (type of fluidization medium, reactor material, presence of hot filters). Transition metals (Fe, Cu, Ni, Cd, Cr, Co, Mn, Zn) and post transition metals (Al, Pb) remain largely on the solid char by-product in the typical fast pyrolysis temperature range (400-550 °C) (Leijenhorst et al., 2016). Incomplete solid separation from the gaseous stream prior to condensation is then the main route for their transfer to the pyrolysis oil.

Small particle size and high carrier gas flowrate could favour char elutriation phenomena and pelletization could be applied for reducing the presence of fines that can be easily transferred to the vapor phase and then to the bio-oil. Pelletization could be detrimental for the heating rate by shifting the pyrolysis conditions from fast to intermediate, thus penalizing the bio-oil yield. However, in presence of heavy metals it might be appropriate to find a compromise between maximizing bio-oil yield and minimizing elutriation phenomena.

### Biomass composition

The feasibility of a pyrolysis-based bio-refinery is strictly dependent on its capability of being flexible with respect to the biomass source. Depending on the geographical context and the territorial development, biomass species may have very different chemical and physical characteristics. A fundamental description of biomass composition is given in section 2.1

The elemental, the proximate and the ash analyses provide only bulk properties that are not sufficient to describe adequately the impact of biomass heterogeneity on pyrolysis products quality and plant performance. A more reliable approach is to describe biomass in as a composite made up of many components constituting the plant cell wall. Organic components and inorganic elements evolve differently during the thermal treatment and they can interact with each other producing a not linear combination of effects that determine the properties and yields of the pyrolysis products (Ferreiro et al., 2017; Ferreiro et al., 2018).

The role of inherent (or intrinsic) inorganic elements (Vassilev et al., 2010), received a great attention since they showed a catalytic activity in promoting some decomposition pathways. Among the inorganics elements, alkali and alkaline earth metals (AAEMs) were the most studied given their abundance in the lignocellulosic biomass (Vassilev et al., 2012). Their presence affects significantly the chemical composition and the physical properties of the pyrolysis products, sometimes compromising their further utilization (Lehto et al., 2014, Weber and Quicker, 2018) or upgrading (Kalogiannis et al., 2019). There are specific cases in which the presence of other inorganic elements may also play a role. This is the case, for example, of some agricultural residues such as cereal straw and rice husks rich in Si (Raveendran et al., 1995) or hyperaccumulator plants grown on contaminated soils

enriched with heavy metals (HMs). HMs, which are usually neglected due to their overall low level of concentration, exhibited a clear role in catalytic upgrading of biomass pyrolysis assisted by zeolite-based catalysts (Iliopoulou et al., 2019) but also raised environmental issues due to their transfer in the condensable fraction or their retention in the char (Leijenhorst et al., 2016, Liu et al., 2020).

To sum up, the different nature of organic components strongly affect the pyrolysis products yields and composition as well as the presence of inorganic elements catalyzing their decomposition pathways (Giudicianni et al., 2021). Moreover, according to the recent literature data, the inorganic elements also interact with heavy metals in the contaminated biomass promoting or reducing their retention in the char. For example, some metals form complexes with P, Ca, Fe or Si during pyrolysis and they are thermally stable at high temperatures (Han et al., 2016). However, the mechanisms involved in the chemical transformation of PTEs in presence of these elements still need to be elucidated since they are strictly dependent on the pyrolysis conditions (mainly temperature and heating rate) and on the PTEs chemical form in the raw biomass.

Among the described parameters, temperature, carrier gas flow rate, feedstock size and composition will be investigated in the experimental campaign within the CERESiS process.

#### 4.1.2 FP reactor

Numerous reactor solutions have been used for years to carry out biomass pyrolysis in a variety of operating conditions. Reactors for pyrolysis, in which the two dominant mechanisms of heat transport are convective and conductive, can be classified, according to the pathway of the gas and solid phases, in:

- Plug flow: unidirectional motion for gas and solid.
- Partial back mixed: unidirectional motion for the gas but not for the solid, which is subject to back mixing phenomena.
- Tumbling: the solid is subjected to continuous rotations and tumbling inside a rotating chamber inside a cylindrical tunnel.
- Entrained: the solid is transported by the gas.

In addition, the different pyrolysis technologies are generally classified into two main categories, based on the heating mode:

- directly heated reactors;
- indirectly heated reactors.

In the former, the biomass is heated by direct contact with the pyrolysis medium, which may consist of hot gases, heated solids, superheated steam or electromagnetic radiation. In the latter, the biomass is heated through the reactor walls.

The typical reactors used to realize fast pyrolysis conditions are fluidized bed reactors, circulating fluidized bed reactors, entrained flow reactor, ablative pyrolyzer, rotating cone reactors, and screw reactors.

The following is a brief description of the different reactor types:

- **Fluidized Bed Reactor:** A stream of inert gas is blown through a solid granular bed, which behaves as a fluid and acts as a heat transfer medium. These hot particles, vigorously mixed, heat up very quickly the biomass particles fed to the reactor, which undergo pyrolysis in a state of optimal mixing with uniform temperature distribution. This justifies one of the main advantages of such a configuration, i.e. the uniform quality of the product, which is difficult to achieve in other reactor configuration. The separation of solid heat transfer particles from the solid pyrolysis residue obtained represents, instead, one of the main limitations of this technology.
- **Circulating fluidized bed reactor:** Unlike the fluidized bed reactor, the solid heat transfer medium is dragged outside the reactor together with the char, and sent to a combustion chamber, where the char burns. The advantage is related to the direct heat input by recirculating hot sand from the char combustion chamber to the pyrolysis one.
- **Entrained flow reactor:** Biomass particles are entrained in high-velocity jets of hot gas. The main features of such a reactor are the high heat and mass transfer and the absence of moving mechanical parts. Char exits the pyrolysis reactor and is then separated through cyclones before the condensation of the pyrolysis vapors.
- **Ablative pyrolyzer:** Heat transfer occurs from the heated reactor walls to the biomass particles in contact with them under pressure generated either by centrifugal force or mechanically. The pyrolysis front moves unidirectionally along the radius of the particle. When a particle is mechanically moved from one part of the reactor to another, the residual oil film partly provides the necessary lubrication to the subsequent biomass particles that contact the wall and partly evaporates and then collected and condensed to form bio-oil. The reaction rate is strongly influenced by the pressure, the relative velocity of the biomass on the reactor walls, and the temperatures of the reactor walls. Inert gas flow is not required. In addition, the process is limited by the rate at which heat is delivered to the reactor walls, rather than the rate at which heat is absorbed by the biomass, and for this reason, even quite large particles can be processed.
- **Rotating Cone:** A rapid heat transfer occurs from the solid surface of a rotating cone to small biomass particles that are mixed with hot sand to make the heat exchange more efficient. Such a reactor features two fluid beds: one inside the cone, which allows for multi-pass conversion for the biomass particles, and a second fluid bed around the cone, which contains sand and char. Between the two fluid beds there is a connection via orifices. The carbon particles left in the second bed are burned and the energy is used to heat the reactor. The transport of the hot sand to the inside of the cone is done by a small lifting system. The advantage of this system is that no inert gas flow is required. The disadvantage is the need for small particle sizes.
- **Screw (auger) Reactor:** It consists of a fixed cylindrical reactor in which a screw mounted on a rotating shaft transports the biomass from the inlet to the outlet of the reactor with variable speed depending on the rotational speed of the drive

shaft. Biomass can be heated directly, by flowing an inert hot gas into the reactor or by inserting previously heated sand or steel balls, and/or indirectly, by heat transfer through the walls. The reactor walls can be heated by external furnaces or by heat exchange with a heated fluid flowing in a shell (or annulus) outside the reactor. The screw, in addition to mechanically transporting the material, also promotes heat exchange between the material and the reactor walls and/or carrier gas.

### Choice of the CERESiS FP reactor

Within the CERESiS project, it is important to take into account that reactor flexibility in terms of pyrolysis temperature, vapor and solid residence time, feedstock size and carrier gas flow rate is even more important since the minimization of transfer of heavy metals from the feedstock to the bio-oil should be achieved other than the production of high bio-oil yields. The auger reactor, as shown in Table 4-1, has a great flexibility with regard to the operating conditions in which it can be used to carry out the pyrolysis of biomass.

Moreover, since within the CERESiS project both the liquid and the solid products need to be produced, the auger reactor was preferred to other configurations since they would have required a complex gas/solid separation train to limit the transfer of solid fines inside the condensation unit and finally into the bio-oil.

The auger reactor configuration guarantees an appropriate mixing efficiency of the biomass inside the reaction chamber and, therefore, homogeneity of heating. The advantages of using an auger reactor are summarized as follows:

- Proven technology: the first report on the use of the screw reactor was described by Laucks in 1927. He found quite a few problems, arising from the temperature difference between the hot walls and the cold crankshaft, which caused tar deposit. Laucks suggested to transfer heat by providing a hollow crankshaft. From 1950 onward, numerous studies have been performed on biomass pyrolysis in screw reactors.
- Wide range of particle sizes that can be processed: particles that are too small, on the other hand, may be subject to entrainment in the carrier gas stream, while particles that are too large may obstruct the reactor aperture and, depending on the auger pitch, not provide the mixing necessary for efficient heat transfer
- Good control of residence time and temperature: the biomass feed rate, reactor size, and auger speed combine to determine the residence time in the reactor, which must ensure complete thermal degradation of the biomass but can be easily varied to achieve different pyrolysis product properties
- Good mixing characteristics.

**Table 4-1: Operating conditions and characteristics of the biomass pyrolysis process in screw reactors.**

	Liaw et al., (2011)	Pittman et al., (2012)	Ingram et al., (2008)	Yang et al., (2013)	Puy et al., (2011)
Feedstock type and size	Douglas Fir < 2mm	Cornstalk 0.5-5 mm	Oak and pine 2-4 mm	Citron wood, pine, willow, bamboo canes 1-5 mm	Pine 20 mm
Flow rate [g/min]	10 - 12	16.67 - 33.3	16.67	4.3 - 4.5	65 - 115
Carrier gas	N <sub>2</sub> 20 L/min	N <sub>2</sub> 34 L/min	none	N <sub>2</sub> 2 L/min	N <sub>2</sub> 5 NL/min
Reactor size	L=58.5 cm D=10 cm	L=101.6 cm D=7.62 cm	L=102 cm D=7.6 cm	L=15 cm D=5 cm	n.a.
Screw rate [rpm]	13	12	12	variable	
Temperature [°C]	200-600	400-450	450	500-550	500-800
Gas residence time [s]	8	1 - 2	n.a.	n.a.	n.a.
Solid residence time [s]	60	30	30	47 - 470	90 – 300

In contrast, the main disadvantages are:

- High cost of maintenance due to the presence of moving parts in the hot environment.
- Scalability is limited because the ratio of screw surface area to reactor volume decreases for larger reactors. Some sources mention that scaling up is reasonable up to 40 cm of the inner diameter of the reactor (Batidzirai et al., 2013).
- Tar condensation on the shaft for auger reactors heated only indirectly through the external wall.

### 4.1.3 Pyrolysis vapors cleaning and condensation

Even though it is possible to tune properly the operating variables of the pyrolysis reactor (feedstock size and moisture, temperature, carrier gas flow rate) for limiting both the water content and the transfer of heavy metals into the vapor phase, it is pivotal to design properly the cleaning of the vapor phase before its condensation and optimize the condensation train.



It is inevitable that a fine fraction of char will be elutriated and dragged by the vapor phase exiting the screw reactor. In order to remove this fraction different gas/solid separation systems can be considered, namely cyclones, hot filters and electrostatic precipitators. In Figure 4-2, the separation efficiency of these systems as function of the solid particle size is shown.

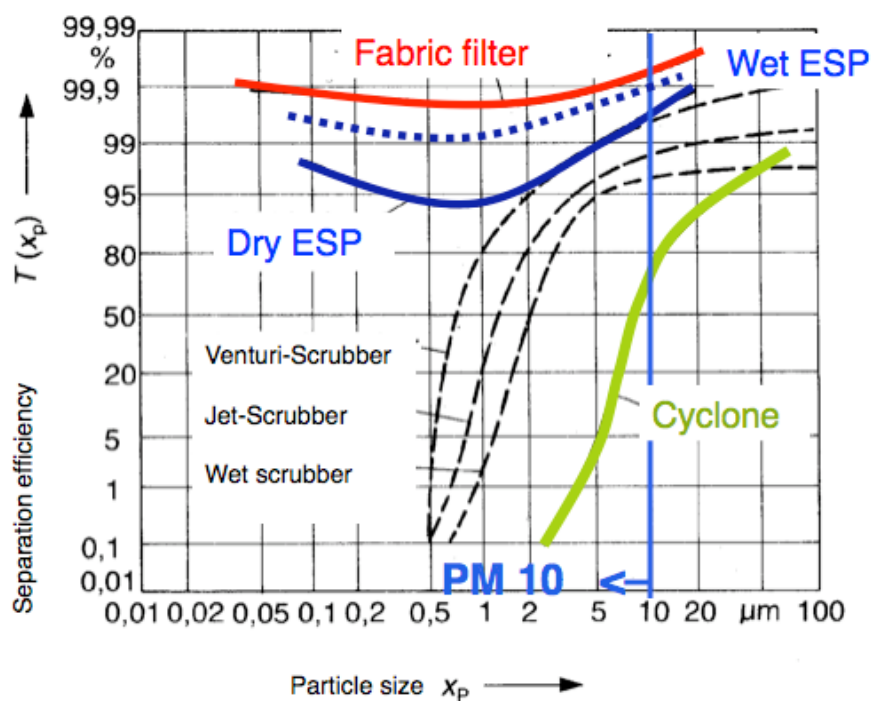


**Figure 4-2: Separation efficiency of gas/solid separation systems as function of the solid particle size.**

Based on the separation efficiency reported in Figure 4-2, it has been decided to include a cyclone at the exit of the pyrolysis reactor before the condensation train. This gas/solid separation system will prevent the transfer of the bigger particles. This is the reason why a further off-line filtering treatment is required for the condensed bio-oil. Given the low efficiency of the cyclone for particles size  $< 10 \mu\text{m}$ , a dry electrostatic precipitator (ESP) will be placed at the end of the condensation train with the aim of capturing the finer particles that escape the condensation train.

The produced bio-oil will undergo to off-line filtering treatment. To obtain high microfiltration performances bio-oil is required to have a proper water content and viscosity.

The bio-oil water content will be tuned, according to the requirements of the off-line microfiltration treatment, with a two stage condensation train that consists in two heat exchanger in series, a gas-diathermic oil followed by a gas-water heat exchanger both of them equipped with a temperature control for the cold fluid temperature. This condensation system will allow to condense the excess water in the first stage and recover the proper bio-oil-water solution/emulsion in the second stage.

#### 4.1.4 Market survey

A market survey was conducted to evaluate the best offer for the realization of the plant on the basis of the aims of the project.

In particular, the object of the request was the design and construction of a pilot pyrolysis plant for biomass based on a screw reactor. Specifically, the plant must meet the following characteristics:

- Be able to process a nominal flow rate of 2 kg/h of biomass.
- Be able to reach temperatures between 450 and 600 °C
- To achieve fast pyrolysis conditions.
- To avoid tar condensation of the reactor shaft.
- To guarantee the possibility to collect condensable products with high efficiency.
- To guarantee the possibility to operate a fractional condensation.
- Ensure the abatement of particulate matter leaving the reactor and its separation from condensable products.

The entire plant must be provided with appropriate locations for thermocouples and pressure transducers and access points for sampling the gaseous stream. In addition, temperature control and regulation systems and biomass handling and feeding must be provided. In order to limit tar condensation on the reactor shaft, it is required that the shaft is heated through an induction heating system, whereas the external walls should be made of ceramic material.

Most of the contacted companies could only provide a standard product that could not be adapted to the project needs:

- Norris Thermal Technologies, Inc. (<https://www.norristhermal.com/>)
- Kansai Corporation (<http://www.kansai-sangyo.co.jp/e-index.html>)
- ICM, Inc. (<https://icm-inc.com/>)
- HEAT Systems (<http://heatsystems.ie/index.html>)
- Biogreen (ETIA SAS) (<http://www.biogreen-energy.com/etia-ecotechnologies/>)
- ABRI-Tech inc. (<https://abritechinc.com/en/home/>)
- PYREG GmbH (<https://www.pyreg.de/>)

Ansaldo CCA was the only company able to design the plant as requested by the customer at a cost reasonably lower than that proposed by the other companies. In Figure 4-3 a schematic diagram of the FP plant is shown, whereas in Figure 4-4 and Figure 4-5, the executive drawings of the pyrolysis reactor and of the whole plant are sketched.

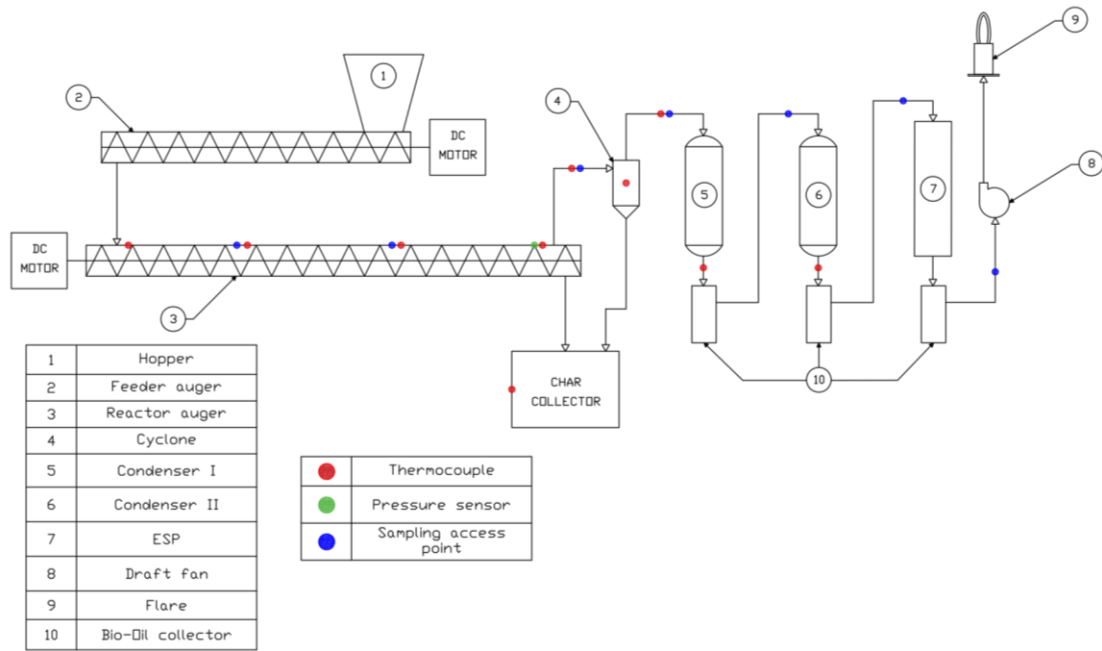


Figure 4-3: Schematic diagram of the FP plant.

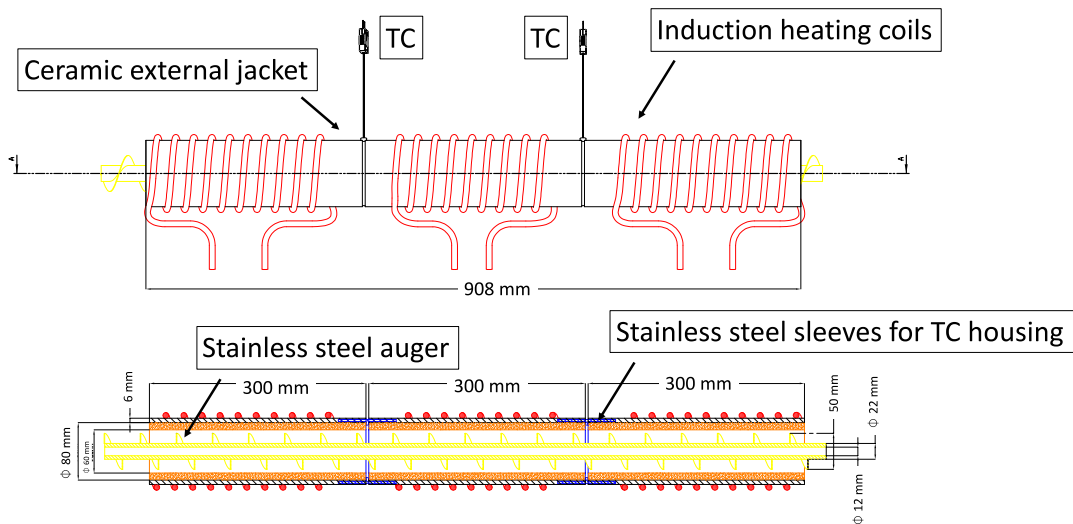


Figure 4-4: Executive drawings of the pyrolysis reactor.

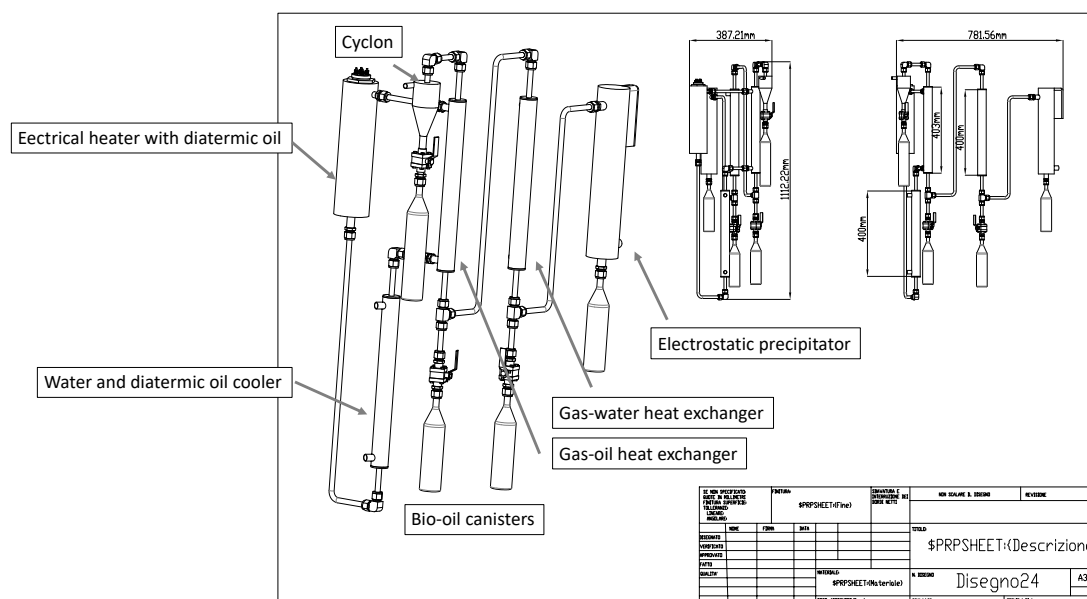


Figure 4-5: Executive drawings of the pyrolysis plant.

## 4.2 MILD combustion

Within the CERESiS project, the gas-phase from biomass thermal treatments as pyrolysis processes consists of a mixture of gases composed by CO, CO<sub>2</sub>, H<sub>2</sub>, CH<sub>4</sub>, Hydrocarbons C<sub>2</sub>-C<sub>4</sub>, other (balance) in the typical range reported in the Table 4-2.

Table 4-2: Typical concentration ranges of permanent gases under FP conditions. (Di Blasi et al., 2009)

Species	Concentration range FP @ 400-600 °C, wt.%
CO <sub>2</sub>	10-60
CO	20-60
CH <sub>4</sub>	0-20
C <sub>2</sub> H <sub>4</sub>	0.5-1
C <sub>2</sub> H <sub>6</sub>	0.5-1
H <sub>2</sub>	0.5-2

Given the high concentration of CO<sub>2</sub>, these mixtures are characterized by a low LHV (Lower Heating Value). The necessity to recover heat/energy from the pyrolysis gases requires the use of combustion processes not based on traditional heat-feedback mechanisms typical of conventional premixed or diffusive flame structures, as the adiabatic flame temperature may be not high enough to guarantee the stabilization of the combustion process. In addition, the characteristic kinetic time (ignition/oxidation) may be not compatible with

traditional flame-based system characteristic residence times, with drastic effect on fuel conversion and pollutant formation/emissions

A challenging process to simultaneously meet thermal efficiency and pollutant emission restrictions is the Moderate or Intense Low-oxygen Dilution (MILD) combustion (Cavaliere and de Joannon, 2004; Dally et al., 2004), alternatively known as FLOX (Wünning and Wünning, 1977; Milani and Wünning, 2007), High-Temperature Air Combustion (HiTAC) (Katsuki and Hasegawa, 1998), or Low Temperature Combustion (LTC) in engine applications (Saxena and Bedoya, 2013). MILD combustion relies on a strong recirculation of mass and sensible enthalpy by recycling the exhausted gases to dilute and simultaneously preheat fresh reactants, up to autoignition conditions. Because of the stability of the oxidation process does not relies on heat feedback mechanisms from the flame front, as in conventional diffusion/deflagrative flames, but on recycled sensible heat, the process is intrinsically highly flexible with respect to fuels chemical/physical properties and quality. This condition is guaranteed when the mixture temperature, after the mixing process between fresh reactants and recirculated gas, is higher than the mixture auto-ignition one.

Characteristic working temperatures are modest and below critical values for the production of pollutants (i.e. NO<sub>x</sub>, particulate matter) while complete fuel conversion, high thermal efficiencies and process stability are ensured by the high recirculated sensible enthalpy

MILD combustion has been successfully employed in furnaces and boilers, gas turbines, bio-gas burners, burners for hydrogen reformers or for CHP units and engines (Khalil and Gupta, 2011; Li et al., 2011).

Commercially, there are different MILD combustion based burners that could be used and have been successfully applied for biogases oxidation. In particular, FLOX@ auto-generative burners (Milani and Wünning, 2007; Lückerath et al., 2008) have been demonstrated to be particular efficient. Exhausted gases are internally recirculated back towards the reaction zone to locally dilute fresh reactants, while exiting through an annular SiC chamber integrated with the burner itself for heat recovery purposes, used for fresh-reactants pre-heating, with an overall heat-recovery efficiency of ~ 75-85%.

Within the CERESiS project, the oxidation performance of pyrolysis gases will be investigated in a Lab Unit Cyclonic burner (LUCY) available at the STEMS-CNR, Naples (de Joannon et al., 2017; Sorrentino et al., 2019; Sabia et al., 2019; Ariemma et al., 2021). The core of the facility is a prismatic chamber (20x20x5 cm<sup>3</sup>), schematically reported in Figure 4-6. Reactants are fed to the reactor by means of two couples of straight ducts located in the two opposed corners of the combustion chamber, thus producing a cyclonic flow field within the combustion chamber. The establishment of a cyclonic flow field ensures a strong internal recirculation of mass/sensible enthalpy, diluting the fresh reactants and increasing the temperature above the autoignition one. The resulting formation of hot gases/fresh reactants mixtures with local conditions of high dilution and preheating allow to achieve MILD combustion conditions. Fuel and oxidant can be fed together or

separately, thus realizing respectively the “premixed” or the “non-premixed” configuration.

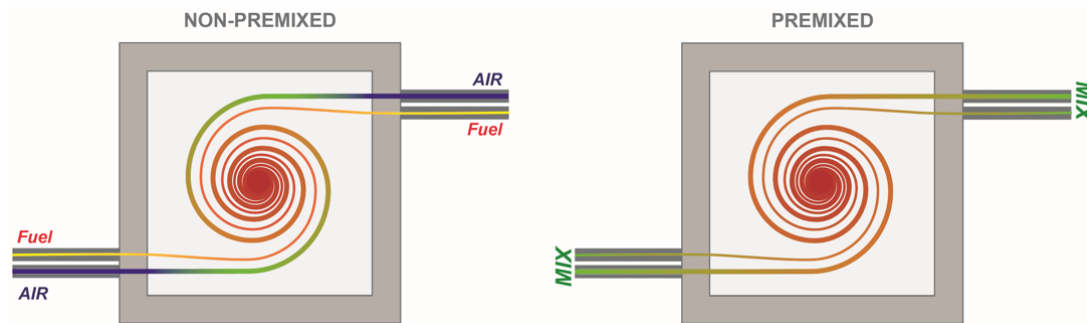


**Figure 4-6: Experimental facility and gas feeding configuration.**

The reactor is equipped with two N-type thermocouples located within the reactor to monitor the temperature during the experimental campaigns. A third N-type thermocouple is located at the center of the outflow section of the reactor, flushed to the internal wall, to detect the characteristic temperature of gases when they exit from the reactor.

Exhausts are sampled using a water-cooled probe installed at the chamber outlet, aligned with the external chamber wall for the gas sampling. A condenser is used to separate the water from the gas stream before injecting it in an Agilent micro-GC analyzer. The micro-GC allows to measure CO, CO<sub>2</sub>, O<sub>2</sub> and N<sub>2</sub> concentrations, while an online gas analyzer (TESTO 350) can be used to monitor continuously NO and NO<sub>2</sub> emissions.

With respect to FLOX@ burners, LUCY offers several advantages:

- The internal recirculation of exhausted gases, without heat exchanger modules, implies a complete heat-recovery. Given this condition, the stabilization of the oxidation process of low LHV gases is more likely to occur, thus implying an extension of exploitable-stable system operating conditions;
- The heat recovery process does not requires expensive (SiC heat exchangers-SiC burners) solutions;
- FLOX@ burners are designed ad-hoc for a defined gas composition. The combustion chamber geometry and the internal recirculation fluid-dynamic pattern are properly designed for specific gas properties, thus they are not promptly versatile with respect to a plausible change of pyrolysis gases composition, given the different range of exploitable biomasses to treat and the different modulable pyrolysis conditions. In contrast, the operating conditions of LUCY can be easily parametrically adjustable with respect to all the external parameters (mixture composition, mixture residence time, thermal power) in order to identify the optimal operating conditions in terms of combustion efficiency and pollutant emissions;
- The possibility to easily shift from the non-premixed to the premixed condition is a concrete efficient way to exploit the most performing strategy to optimize the combustion performances. From the previous analyses (Li et al., 2011; de Joannon

et al., 2017; Sorrentino et al., 2019; Sabia et al., 2019; Ariemma et al., 2021), it has resulted that for very low LHV fuels, the pre-mixed condition may consist in a more efficient strategy to stabilize the oxidation process, as the initial premixed conditions allows to promote the ignition of mixtures locally less diluted.

- The level of internal mixing between hot exhausted gases and fresh reactants is easily controllable by simply change reactant mass flow rates (thus the thermal power). This paves the way to control the local dilution level and exploit conditions more prone to auto-ignition.

## Key influential parameters

### Equivalence ratio

The mixture equivalence ratio is a key influential parameter both in terms of oxidation process stability and pollutant emissions. The auto-ignition delay time is governed by the mixture stoichiometry at local scales, thus it is of paramount importance to investigate the mixture equivalence ratios to identify the operational range that allows to minimize auto-ignition/oxidation times to match with mixture residence times. In addition, for carbon-based fuels, the minimization of pollutants as CO occurs for fuel-lean mixtures, thus experimental tests will be devoted to the identification of mixture equivalence ratios that allow to minimize CO emissions, while guaranteeing NO<sub>x</sub> emissions to levels compatible with regulations.

### Thermal power

The other parameter to consider is the system thermal power (P). The higher the P, the higher the system temperature is, thus the stabilization of the oxidation process is more prone to occur. From the other point of view, the higher the P, the lower are the mixture residence times, thus implying the characteristic auto-ignition/oxidation times have to be compatible with the mixture residence times, under the penalty to increase CO/Unburned Hydrocarbons (UH) emissions. In addition, the thermal power has to be high enough to establish a fluid-dynamic patten within the burner that allows the stabilization of a cyclonic motion, necessary to establish MILD combustion conditions. As a further consideration, the variation of the system thermal power (P) implies also a change of heat exchange mechanisms from the burner to the surroundings, thus governing the balance between heat released from the oxidation process and heat loss to the surroundings. Thus, the thermal power (P) has to be carefully investigated as a key-parameter to guarantee the stabilization of the oxidation process itself.

The optimal P will be identified as the thermal power that guarantees the full fuel conversion under process stable conditions, while minimizing pollutant emissions.

In Table 4-3, the experimental conditions that will be tested in the MILD burner are summarized.

**Table 4-3: Experimental conditions of the combustion experiments in the MILD burner.**

Parameter	
Fuel	Gas
Equivalence ratio	0.4 - 1.3
Nominal Thermal Power (P), kW	2 - 8
Reactant feeding mode	Premixed, non-premixed

## 4.3 Bio-oil decontamination (microfiltration) and reuse options

---

### 4.3.1 Microfiltration

The microfiltration (MF) membrane separation process is the method selected for the removal of the undesirable HM-laden char particles (less than 10  $\mu\text{m}$  in size) from the bio-oil. More details on the selection procedure and analysis of the advantages and challenging aspects of the method have been presented in D1.2. The main challenges in this investigation will be a) to understand, quantify and reduce membrane fouling and b) to deal with highly viscous liquid streams.

#### Experimental setup

A fully automated laboratory pilot MF unit, designed and constructed in-house at CERTH, will be used, testing different commercially available tubular ceramic membranes of nominal pore sizes (e.g., 0.5 to 1  $\mu\text{m}$ ) that are stable in a hot, pressurized bio-oil feed. A schematic diagram and images of the pilot unit are included in Figure 4-7-a and b-d, respectively. The system is comprised of the following main components: the MF membrane module (Figure 4-7-c), the feed pump (Figure 4-7-d), the feed tank (Figure 4-7-d), the balance for measuring permeate flow, as well as the measuring/recording and



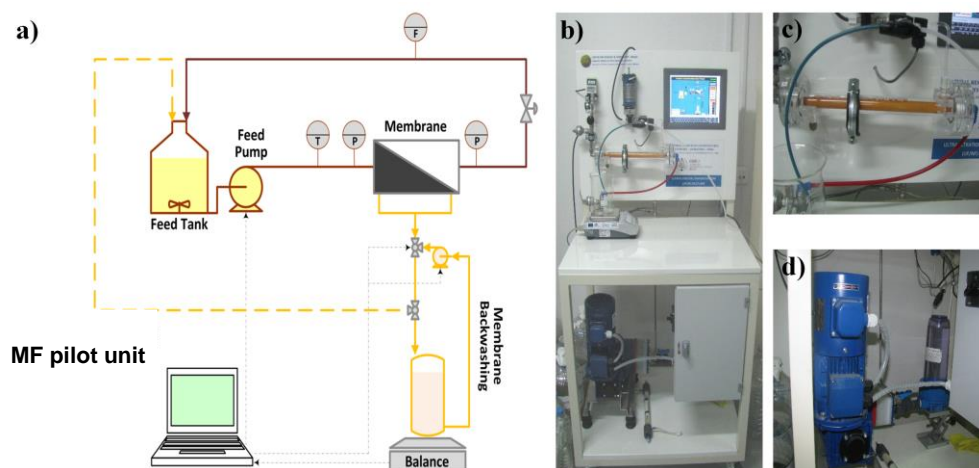


**Figure 4-7: (a) Schematic diagram of the experimental set-up, (b) front view of the MF pilot scale system, (c) membrane module and (d) feed pump and feed/recirculation tank.**

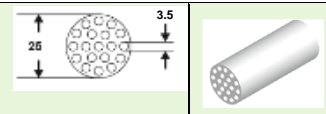
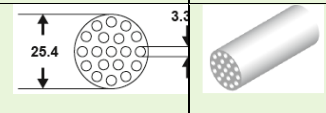
### Membranes

Different tubular ceramic membranes will be examined for the scope of the project. These composite membranes consist of a highly porous support material made of chemical-grade  $\alpha$ -aluminum oxide ( $\text{Al}_2\text{O}_3$ ) onto which a ceramic film is deposited (made of  $\text{Al}_2\text{O}_3$ ,  $\text{TiO}_2$  or  $\text{ZrO}_2$ ) - the actual membrane layer. The technical data of the selected membranes are summarized in Table 4-4 and their characteristic are as follows:

- High thermal resistance (up to 80-90 °C)
- Resistance to chemical agents
- High mechanical resistance (pressure surges, up to 10 bar operating pressure)
- Easy backpulsing
- Easy and fast cleaning
- High filtrate yield
- Regenerable, e.g. by pyrolysis
- Low operating cost due to long life

**Table 4-4: Technical data of the ceramic membranes selected for the MF of the produced bio-oil.**

Membrane material (active layer)	Mean pore diameter / Cut-off ( $\mu\text{m}$ )	Amount of channels	Length (mm)	Length-specific membrane area ( $\text{m}^2/\text{m}$ )	Design	Illustration
$\text{Al}_2\text{O}_3$	0.8	1	500	0.05		
$\text{Al}_2\text{O}_3$	0.2	1	500	0.05		
$\text{Al}_2\text{O}_3$	0.8	7	500	0.13		
$\text{Al}_2\text{O}_3$	0.2	7	500	0.13		

ZrO <sub>2</sub>	0.05	19	500	0.10	
ZrO <sub>2</sub>	0.02	19	500	0.10	
TiO <sub>2</sub>	0.8	19	500	0.20	
TiO <sub>2</sub>	0.01	19	500	0.10	

Considering the importance of the membrane hydrophobicity on the effective blockage of the water phase from the bio-oil, efforts will be made to modify the hydrophobic property of the best performing membrane (in terms of higher particle separation and lower fouling tendency). The review of the different methods applied in literature for the production of superhydrophobic ceramic based-membranes showed that the immersion technique is the most widely used due to its simplicity, while the chemical vapor deposition (CVD) technique is a promising potential alternative which has not been widely assessed in the literature (Koonaphapdeelert and Li, 2007; Hubadillah et al., 2019). In both techniques, grafting occurs through surface reactions between the hydroxyl groups found in the membrane and the Si–O–alkyl groups of the silane. Considering the attributes of these techniques, CERTH developed recently a silane grafting method through immersion and CVD for the hydrophobic modification of tubular ceramic membranes. The hexyltrimethoxysilane (C<sub>9</sub>H<sub>22</sub>O<sub>3</sub>Si) was proposed as a potential economic alternative (about an order of magnitude lower cost), with similar properties, to 1H,1H,2H,2H-perfluorodecyltriethoxysilane, which is considered the “gold standard” in the literature. The grafting procedure included an initial membrane preparation stage (same for both methods), where the ceramic membranes were cleaned by distilled water and ethanol and then dried overnight at 110°C. Grafting solutions (0.1 M) for the immersion method were prepared by dissolving an appropriate amount of silane in chloroform (stabilized by 1% ethanol). The membranes were placed in a sealed volumetric cylinder filled with the grafting solution for 6h and then dried overnight at 110°C. On the other hand, the membranes were placed in a sealed membrane cell and the silane (stabilized by 1% ethanol) was placed in a bubbler, for the CVD method. Bubbler and membrane cell temperature was set at 60 °C and N<sub>2</sub> was used as carrier gas to transfer silane vapors to the membrane for 6h. Then the membrane was dried at 110°C under N<sub>2</sub> for 6h. The efficacy of both methods was evaluated by water contact angle measurements and confirmed by monitoring the gas pressure needed for bubbles formation in the water, in a gas-liquid membrane contactor setup.

### Design of experiments

Experiments will be conducted in the cross-flow mode at different temperatures ranges (based on the FP and the primary water recovery process, i.e., 35-45 °C) and at different trans-membrane pressures (e.g., varying from 0.5-2 bars). The concentrate of the membrane filtration is recycled back to the feed tank, whereas the membrane permeate is collected in a beaker (permeate tank) through a manual three-way valve. The permeate volumetric flow rate is determined by measuring the mass flow with the electronic balance, connected to a PC (by means of GeniDAQ software). Microscopic (membrane autopsy), ICP

(HM determination) and ash content analysis of the feed and permeate streams will be conducted to determine the efficacy of the process. Special attention will be given to fouling analysis from longer runs of bio-oil through the membranes to determine the predominant fouling mechanisms. This will help propose measures for fouling mitigation and overall process optimization.

In order to define the threshold values of bio-oil water content and viscosity for microfiltration experiments, one or more blends reproducing viscosity and water content of a real bio-oil will be used, since, according to the Gantt chart of WP3, the first sample of bio-oil will be available at the end of 2021. The liquid blends will be mixed with a proper amount of char particles (with a size distribution to be defined) already available at CNR. A literature survey has been conducted for the identification of the proper surrogate. In Table 4-5, the typical properties of bio-oils from fast pyrolysis are reported (Letho et al., 2014).

**Table 4-5: Physical properties of wood fast pyrolysis bio-oils (Letho et al., 2014).**

Analysis	Typical bio-oil
Water, wt%	20-30
Water and sediment, vol%	
Solids, wt%	Below 0.5
Ash, wt%	0.01-0.1
Nitrogen, wt%	Below 0.4
Sulphur, wt%	Below 0.05
Stability	Unstable
Viscosity (40 °C), cSt	15-35
Density (15 °C), kg/dm <sup>3</sup>	1.10-1.30
Flash point, °C	40-110
Pour point, °C	-9-36
LHV, MJ/kg	13-18
pH	2-3
Distillability	Non-distillable

Preliminary experiments will be carried out with the aid of synthetic mixtures emulating the relevant bio-oil properties. Specifically, the simulation of the bio-oil viscosity will be based on proper solutions of water glycerol. As an example, in Table 4-6 the viscosity of an aqueous solution of glycerol at 83.4 wt.% is reported. It reproduces quite well the viscosity of a typical bio-oil containing 20-25 wt.% water at 40 °C (see Table 4-6 and Figure 4-8).

**Table 4-6: Viscosity of an aqueous solution of glycerol at 83.4 wt.% and of 4 different bio-oils.**

T (°C)	Glycerol aqueous solution 83.4 wt.%			Bio-oil kinematic viscosity (cSt)				
	Dynamic viscosity (cP)	Density, $\rho$ (g/cm <sup>3</sup> )	Kinematic viscosity (cSt)	Bio-oil 1 (water 18.9 wt.%)	Bio-oil 3 (water 25.3 wt.%)	Bio-oil 4 (water 23.4 wt.%)	Bio-oil 5 (water 19.8 wt.%)	Bio-oil 6 (water 24.1 wt.%)
20	91.45	1.22	75.0		148	341	91	153
25	66.65	1.21	55.1	66.7				
30	49.69	1.21	41.1					
35	37.83	1.21	31.3					
40	29.35	1.21	24.3	25.0	36	75	28	39
45	23.16	1.2	19.3					
50	18.56	1.2	15.5					
55	15.1	1.2	12.6	15.4				
60	12.44	1.19	10.5		13	24	10	14
65	10.38	1.19	8.7					
70	8.75	1.19	7.4	8.3				
75	6.42	1.18	5.4		6	10	5	6
80	5.57	1.18	4.7					

As for the liquid blend reproducing the water content of a typical bio-oil it has been decided to use a bio-oil representing the worst case for risk of phase separation, namely a bio-oil produced under slow pyrolysis conditions. The bio-oil amount and the time scheduling for the delivery will be discussed between CERTH and CNR. As for the solid content, the liquid blends will be mixed with a proper amount of solid particles; e.g., activated carbon with a pre-defined/well-known particle size distribution.

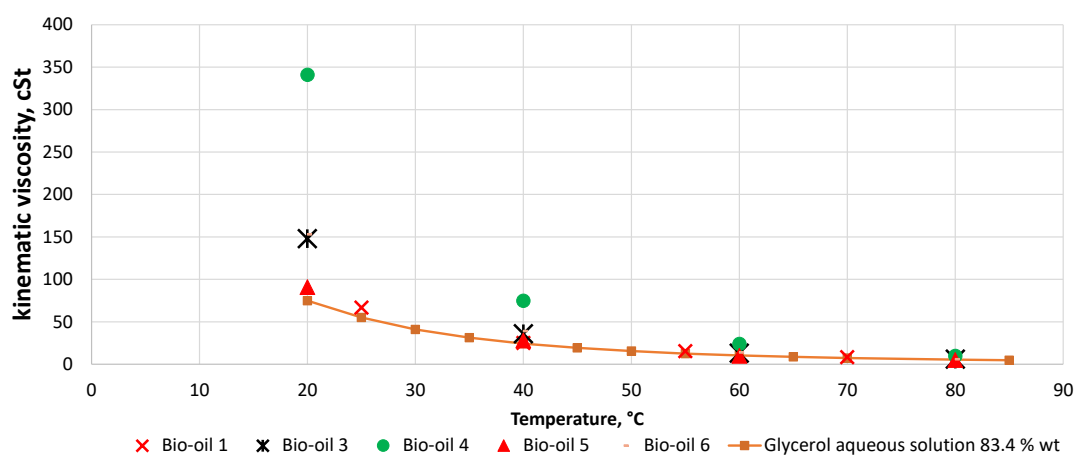


**Figure 4-8: Change of the kinematic viscosity of five bio-oil samples and a glycerol aqueous solution of 83.4 wt.% with temperature.**

### Operating parameters

The operating parameters will be chosen according to the medium to be filtered. The following operating parameters will be used as a basis:

*Velocity inside membrane ducts (c)*

$$c = \frac{V}{A} \quad (4.1)$$

where c is the velocity (m/s), V the feed volume flow (m<sup>3</sup>/s) and A the surface of ducts flown past (m<sup>2</sup>). The membrane manufacturer recommends c values approx. 4-6 m/s.

*Trans-membrane pressure ( $\Delta p$ )*

$$\Delta p = \frac{P_1 + P_2}{2} - P_p \quad (4.2)$$

where  $\Delta p$  is the trans-membrane pressure (bar), P<sub>1</sub> the pressure at entry of module (bar), P<sub>2</sub> the pressure at exit of module and P<sub>p</sub> the pressure of permeate (atmospheric). The membrane manufacturer recommends  $\Delta p$  values approx. 1.5-3 bar.

### MF concentrate treatment and reuse options

As mentioned earlier, the application of the MF process for the upgrade of the FP bio-oil is a new concept and therefore, no previous knowledge is available on the amount and composition of the final concentrate stream produced. Although the primary focus of this work is the implementation of the MF process to determine its efficacy in removing undesirable HM-laden char particles (less than 10  $\mu\text{m}$  in size) from the bio-oil, while minimizing fouling, special attention will be also given to detailed characterization of the concentrate (ash, HM, water, oil, other), in an effort to assess its potential application or reuse back to the FP process (see Section 4.3.2).

#### **4.3.2 Char reuse options**

Char valorization is a key point for the feasibility of the whole phytoremediation process. Char can be considered as a multiphase system composed of a carbon network and a mineral phase. Low temperature char can contain condensed vapors occluding partly the porosity of the solid matrix. The addition of organic vegetable matter to poorly productive soils in order to improve their physical-chemical characteristics was a well-known practice in ancient times (Glaser et al., 2001). Nowadays, the deep knowledge of the chemical and physical characteristics of the char is leading to the exploration of many routes for valorizing char potential for diverse applications (Cha et al., 2013).

The relative contents of organic and mineral phases and their composition varies with the process operating variables, namely temperature, heating rate, pressure, and gas and solid residence times. A detailed description of the effects of these variables on the char characteristics is available in (Weber and Quicker, 2018). Pyrolysis temperature affects more than the other variables the chemical and physical characteristics of the char. The C and O contents of biomass typically range between 50 wt.% and 40 wt.% on dry ash free

basis, whereas the H content varies between 5 and 7 wt.%. The most significant changes during char production occur in the temperature range of 200–400 °C, where C and O contents are in the range 70-80 wt.% and 10-30 wt.%, respectively (Weber and Quicker, 2018). The char produced at temperatures lower than 300 °C is the result of dehydration and depolymerization reactions of hemicellulose and the cleavage of the glycosidic linkages between the sugars of cellulose; therefore, it is mainly composed of oligosaccharides in an amorphous phase with high concentration of free radicals as result of the competition between the mechanism of devolatilization and the reactions of dehydration. The removal of acid groups as temperature increases determines a strong increase of pH from mild acid to basic values in the temperature range between 200 °C and 400 °C. Hydroxyl groups are at first concentrated and then released determining the non-monotonous trend of the cation exchange capacity (CEC) (Harvey et al., 2011). Carboxyl, carbonyl and methoxyl groups decrease up to the complete falling off at temperatures in the range 600 °C–700 °C. Above 600 °C, typical pH values are in the range 8-10. At temperatures higher than about 700 °C, charring reactions occur, determining the growth of graphene layers and the removal of heteroatoms, thus increasing the char aromaticity. At these temperatures, chars may reach C and O contents of higher than 95% and lower than 5%, respectively, whereas the H content decreases to less than 2% or even below 1% for very high treatment temperatures. Data collected in Weber and Quicker (2018) show a not clear correlation between the pyrolysis temperature and the N content of the char.

The mineral phase is very stable, except for some inorganic elements in volatile compounds. As a consequence of this thermal stability, the ash yield is almost independent on the temperature, while its content increases almost linearly due to the devolatilization of the organic fraction (Lua et al., 2004). The increase of pH char towards alkaline values with the temperature is mainly due to the concentration of inorganic elements in the alkaline form.

The textural characteristics of the char evolve as the pyrolysis temperature increases changing the relative weight of the micro-, meso- and macro-porosity (Gargiulo et al., 2018), including pores with diameter smaller than 2 nm, between 2 and 50 nm and greater than 50 nm, respectively. Devolatilization, repolymerization of entrapped condensable species, graphitization and ash sintering phenomena occur and thus resulting in a non-monotonous trend of the char specific surface area with temperature. A maximum in the range 300-500 m<sup>2</sup>/g at temperature varying between 500 and 700 °C was observed depending on the original biomass type and the heating rate (Weber and Quicker, 2018).

Literature review suggests many possibilities for valorizing char potential for diverse applications such as fertilizer and carbon sink (Lehmann, 2009; Kambo et al., 2015; Qian et al., 2015; Amin et al., 2016), contaminants adsorbent in wastewater and soil (Downie et al., 2009; Keiluweit et al., 2010; Kambo et al., 2015; Beesley et al., 2011; Tan et al., 2015; Qian et al., 2015), adsorbent or catalyst for gas cleaning (Shen, 2015; Qian et al., 2015), catalyst for syngas conversion to liquid hydrocarbons and biodiesel production (Qian et al., 2015), raw material for supercapacitors (Qian et al., 2015) and filler in wood and polymer composites (Das et al., 2015a).

## Adsorbent

Different mechanisms are involved in inorganic anion, cation, and organic compound adsorption. Usually, the different mechanisms interfere with each other, further complicating adsorption phenomena.

The characteristics of the char porous structure, namely surface area, pore volume, and pore size distribution, are fundamental in adsorption processes and depend both on the original structure of the pyrolyzed biomass and its thermal history. The pore size distribution is a very important aspect since it is related to the mass transfer phenomena occurring during the adsorption process. A proper distribution of micro-, meso- and macropores is needed to provide a sufficient adsorption surface and to facilitate mass transfer into the smaller pores, in relation to the specific adsorbate.

Surface functional groups, aromaticity, and inorganic content and speciation determine the adsorption efficiency and selectivity of char with respect to different types of molecules or ions.

Adsorption in the pores and partition are both based on diffusion-organic molecules can diffuse and be adsorbed both inside the pores of the char and on the surface of the matrix not completely carbonized according to a mechanism called char 'partition'. According to Han et al (2014), the adsorption in the pores is closely related to the total volume of micropores and mesopores. It is often difficult to draw a clear boundary between the two adsorption mechanisms, although in general, a higher pyrolysis temperature leads to the formation of char with a higher carbonized fraction, making adsorption in the pores predominant compared to 'partition' (Devi and Saroha, 2015). Depending on the other characteristics of char, these adsorption mechanisms may involve organic compounds of different nature and may occur in conjunction with other mechanisms.

Hydrophobic species tend, due to their nature, to minimize the contact surface with water by approaching each other and creating agglomerates. Char can have a hydrophobic or hydrophilic character according to its chemical composition, in particular according to the O/C ratio—the lower the ratio, the more hydrophobic the char.

Adsorption through the formation of hydrogen bonds occurs when the adsorbate presents some acceptor groups; the hydrogen atom that participates in the binding may be present on the char or in some surface functional group or in a water molecule bound to the surface of the char. This adsorption mechanism is influenced by the pH of the solution.

Another mechanism involved in char adsorption is the so-called electron donor acceptor (EDA). The electrons that are shared during the formation of this bond belong to an orbital  $\pi$ . Therefore, the groups that mainly contribute to this adsorption mechanism are the aromatic rings, which can behave both as acceptors and donors. The higher the degree of graphitization of char, the higher the role of this mechanism in the adsorption (Xie et al., 2014).

Surface complexation is an adsorption mechanism that involves the formation of complex structures, usually due to interactions between a metal ion and a ligand (Carbtree, 2005a and b). Therefore, this mechanism is mainly involved in the adsorption of heavy metal species, but it can also involve organic species that can interact with the metals contained in char. Metals can also be adsorbed through a cation exchange with the char surface.

Char has a non-zero net charge distributed on its surface and this characteristic is involved in two possible mechanisms of adsorption, namely ion exchange and electrostatic interaction. The presence of oxygenated functional groups is positively correlated with the cation exchange capacity of char and this mechanism is involved in heavy metals adsorption (Tan et al., 2015). Typically, char has a negative charge, making possible the adsorption by electrostatic attraction of positively charged compounds (Ahmad et al., 2014). Some authors report that the presence of acidic functional groups such as phenolic and carboxylic groups on the surface promotes ammonium adsorption (Gao et al., 2015). However, it is possible, through proper modifications, to obtain a char suitable for the adsorption of anionic species such as nitrates and phosphorus (Micháleková-Richveisová et al., 2017). The electrostatic interaction is particularly affected by the pH of the solution, which is closely related to the surface charge of the char. Electrostatic attraction is one of the most common mechanisms in the adsorption of organic compounds as they often have a certain polarity (i.e. a charge accumulation) which allows the interaction with char.

Heavy metals and antibiotics represent typical water contaminants. Concerning heavy metals, it was demonstrated by many authors that the chemical properties of char were more important factors in the adsorption of heavy metals than specific surface area. More specifically, oxygen-functional groups and mineral compounds, such as  $\text{CO}_3^{2-}$  and  $\text{PO}_4^{3-}$ , play important roles in the sorption of heavy metals on char (Möller and Müller, 2012). The main mechanisms for the removal of aqueous Cd were sorption due to large specific surface area of char and precipitation due to the high pH (Kim et al., 2013). Copper removal by char is dominated by ion exchange rather than by adsorption (Cho et al., 2013). As for organic contaminants, many studies applied char to the adsorption of tetracycline (TC), which is used as antibiotic for animals and plants. In this case the organic matter adsorption on char is correlated closely with aromaticity index (H/C), polarity index (O/C and (O + N)/C), and porosity (Zhu et al., 2014; Mubarik et al., 2016). Also, the carboxylic groups affect positively the adsorption of TC.

Char was tested also for the adsorption of gaseous toxic compounds such as formaldehyde and carbon dioxide. The basicity due to metal species and oxygen and nitrogen functional groups are important factors that improve the formaldehyde adsorption capacity of the char (Lee et al., 2011). Physio-sorption is found to be the main mechanism involved in  $\text{CO}_2$  adsorption. When the char specific surface area was sufficiently large, however, the quantity of nitrogenous groups played a more important role in the adsorption of  $\text{CO}_2$  on the char surface (Creamer et al., 2014).

### Catalysts

Char was studied as support material for catalysts in different processes such as:



1) Tar catalytic reforming in syngas: char was found to be very effective in naphthalene conversion (Abu El-Rub et al., 2008) and in lignin derived tar conversion (Qian et al., 2015). Some authors reported that the type of char had little effects on tar reduction, whereas the tar reduction efficiency decreased as the specific surface area decreases (Chen et al., 2019).

2) Trans-esterification reactions in biodiesel production: it was demonstrated that a large specific surface area and high acid density led to a high biodiesel production yield, whereas high transesterification activity was accompanied by a high specific surface area when the acid density was similar (Dehkhoda et al., 2010)

3) Selective catalytic reduction of NO<sub>x</sub>: the chemical properties, such as oxygen functional groups and NH<sub>3</sub> adsorption sites, were more important factors for NO<sub>x</sub> removal than the physical properties, such as specific surface area and pore size (Jo et al., 2011).

### Soil amendment

Application of char in the soil has several advantages other than the storage of the organic carbon due to its recalcitrance. Spokas et al. (2009) reported that the amendment of soil using char suppressed the decomposition activity of microorganisms, reduced N<sub>2</sub>O emission by 60%, and reduced CH<sub>4</sub> oxidation. They also reported that the application of 5% (w/w) of char to soil enhanced the sorption of pesticides and reduced the dissipation rate of herbicides. In addition, the phenolic, carboxyl and hydroxyl functional groups as well as silicates, carbonates and bicarbonates in char can combine with H<sup>+</sup>, controlling the pH of acidic soils. Moreover, the basic cations in the char can be discharged in the soil thus increasing its CEC. Char contains high concentrations of N, P, Ca, and K, which may provide soil with nutrients directly or may be used as nutrients of microorganisms. When char is used as a soil amendment, the pore fraction of soil is increased by char. Each pore provides the space in which the microorganisms can grow and increases the quantity of air and moisture and the residence time of nutrients, resulting in the enhanced activity of microorganisms and increased growth rate of plants in that soil.

### Filler in composite materials

Many applications of char as a filler in building materials and polymeric composites benefit from certain char properties, such as low density, low thermal conductivity, thermal stability, electrical conductivity, and intrinsic mechanical properties (hardness and elastic modulus). These are greatly affected by some chemical and structural char characteristics, such as elemental composition, volatiles, fixed carbon and ash content, aromatization degree, and porosity.

- Density and thermal conductivity: the bulk density and thermal conductivity depend on the conversion of the low- density disordered carbon into high-density graphene sheets and on the arrangement of the graphene sheets in turbostratic crystallites. This means that they can be negatively correlated to the porosity caused by devolatilization and char shrinkage and to the H/C content as a measure of the advancement of the graphitization process (Kercher and Nagle, 2003;

Yargicoglu et al., 2015). Ash should also be taken into account since they contribute to an increase in bulk density.

- **Thermal stability:** the extent of aromatization and graphitization affect the thermal stability of char positively. The reactivity of char toward oxidation is depressed by the change in the char carbon structure induced by thermal annealing (Sun et al., 2014). However, the content of inorganics, such as alkali metals, that are in such a form as to be catalytically active for oxidation are relevant in the determination of char reactivity (Zhang et al., 2018). The content of volatiles promotes the flammability of char, whereas the content and the chemical form of inorganics can act as a flame promoter or retardant (Di Blasi et al., 2009).
- **Electrical conductivity:** the process of electronic conduction within a carbon matrix is strongly dependent on the presence of sp<sup>2</sup> hybridized orbitals of the carbon atom associated with an electron delocalized in a p orbital perpendicular to the sp<sup>2</sup> orbitals' plane. It follows that the processes of aromatization and graphitization that occur at a molecular level in a biomass subjected to pyrolysis play a fundamental role in determining the electrical conductivity of char. Graphite represents a sort of asymptote towards which char tends as the process of aromatization progresses. Its crystallographic structure, organized in parallel layers, has electrons delocalized on the whole plane, thus determining an anisotropic electrical conductivity with the maximum in the  $\sigma_{-1}$  plane direction equal to  $0.33 \times 10^5$  S m. The electrical conductivity of complex micro-structured carbon materials has been explained through the two-phase composite model going through a percolation transition (McLachlan et al., 2001). Kercher and Nagle (2003), based on XRD spectra of carbonized monolithic fiberboards, adopted the so-called quasi-percolation model to explain the microstructural evolution of woody material during carbonization and showed that the model is able to account for most of the changes to char's physical properties, such as electric conductivity. The presence of defects such as pores and inorganic elements is typically detrimental for the electrical conductivity and should be taken into account for interpreting some phenomena that occur in carbonaceous materials (Rhim et al., 2010, Emmerich et al., 1987). Moreover, when the char structure has a low degree of aromatization, the polar functionalities on its surface play a pivotal role in the determination of the electrical conductivity (Rhim et al., 2010).
- **Hardness and elastic modulus:** char chemistry exhibits a strong correlation with the mechanical properties. More specifically, the hardness/elastic modulus is positively correlated with the carbon content and the occurrence of covalent bonds between carbon atoms in aromatic structures associated with the loss of oxygenated functional groups. The evolution of charred material towards a turbostratic structure is also beneficial for the hardness/elastic modulus (Das et al., 2016). On the other hand, in some biomass, sources such as sludge and poultry litter the order and crystallinity of the char structure is mostly contributed by the high amount of impurities present in form of crystal phases. In this case, char crystallinity cannot be correlated with its respective hardness/ elastic modulus (Das et al., 2015). This means that in some cases the ash content and chemical form could also affect the char's mechanical properties.

## Other applications

Among the other applications the ones exploiting char electrical properties are worth to be mentioned such as:

- Carbon source in phosphoric acid fuel cell and direct carbon fuel cell: despite the high ash content that negatively affect the char power density, the porous characteristics of biomass char and the functional groups on the char surface promote the electrochemical reactions in the low current density region (Ahn et al., 2013).
- Electrode for supercapacitors: capacitive performance of char electrode was influenced by surface functional groups, electric conductivity, and pore structure and distribution as well as the specific surface area (Inal et al., 2015).

Zhang et al. (2019) reported a list of pros and cons in different char applications (Table 4-7). In presence of organic or inorganic contamination, the risk of introducing heavy metals or organic contaminants into soil should be investigated. To this aim, in the CERESiS project a detailed characterization of char will be provided to assess its suitability to be used for agronomic purposes. Only the procedures required by the European Standard Certificate will be taken into account for the char characterization. For chars that do not fulfill the above mentioned criteria additional characterizations will be performed by traditional and advanced diagnostics (FTIR spectroscopy, total OH functional groups through Bohem titration, porosimetry, FESEM-EDX spectroscopy) to assess other possible uses among the ones reviewed in. To evaluate the leaching potential of the derived chars, toxicity characteristic leaching procedure (TCLP) will be performed.

**Table 4-7: Primary advantages and disadvantages of various char applications (Zhang et al., 2019).**

Application	Purpose	Advantages	Disadvantages
Adsorbents	Adsorption of organic contaminants and heavy metals present in soil and water	Low cost, abundant and sustainable resource, and oxygenated groups on biochar surface facilitate adsorption	Effectiveness of organic/inorganic contaminants remediation is still uncertain, and persistence of heavy metals
Precursor of catalysts	Catalyst support and carbon-based materials act as direct catalysts	Easy to recycle supported metal, large surface area, abundant functional groups, co-catalyst, low cost	Relative low efficiency and low abrasive resistance compared with commercial catalyst
Soil amendment	Carbon sequestration, soil quality improvement	Low cost, sustainable resource, retain water and nutrient, reduce fertilizer consumption, reduce greenhouse gas emission and nutrient losses	Possible heavy metal and PAHs contaminant
Additives for anaerobic digestion/composting	Enhancing carbon mineralization, and changing the microbial community structure	Large specific surface area, porosity, and a large amount of functional groups, reducing the emission of GHG and total nitrogen loss, high nitrogen retention and good heavy metals stabilization	The risk of introducing heavy metals and organic contaminants into soil
Electrochemical energy storage	Used as electrodes material or template	Low cost, renewable feedstock, high surface areas, rich porosity, intriguing structures of biomass (such as hierarchical organization, periodic pattern or some special nanoarchitectures),	Possible low performance

## 4.4 List of References

---

Abu El-Rub, Z. A.; Bramer, E. A.; Brem, G. (2008). 'Experimental comparison of biomass chars with other catalysts for tar reduction', *Fuel*, 87, p2243.

Ahmad, A.; Rajapaksha, A.U.; Lim, J. E.; Zhang, M.; Bolan, N.; Mohan, D.; Vithanage, M.; Lee, S. S.; Ok, Y. S. (2014). 'Biochar as a sorbent for contaminant management in soil and water: a review', *Chemosphere*, 99, p19–33.

Ahn, S.Y.; Eom, S.Y.; Rhie, Y.H.; Sung, Y.M.; Moon, C.E.; Choi, G.M.; Kim, D.J. (2013). 'Utilization of wood biomass char in a direct carbon fuel cell (DCFC) system', *Applied Energy*, 105, p207.

Amin, F.R.; Huang, Y.; He, Y.; Zhang, R.; Liu, G.; Chen, C. (2016). 'Biochar applications and modern techniques for characterization'. *Clean Technology and Environmental Policy*, 18, p1457-1473.

Antal, M. J.; Allen, S. G.; Dai, X.; Shimizu, B.; Tam, M. S.; Grønli, M. G. (2000). 'Attainment of the theoretical yield of carbon from biomass'. *Industrial and Engineering Chemistry Research*, 39, p4024–4031.

Antal, M. J.; Croiset, E.; Dai, X. F.; De Almeida, C.; Mok, W. S. L.; Norberg, N.; Richard, J-R.; Al Majthoub, M. (1996). 'High yield biomass charcoal'. *Energy and Fuel*, 10, p652–658.

Ariemma, G. B.; Bozza, P.; de Joannon, M.; Sabia, P.; Sorrentino, G.; Ragucci, R. (2021). 'Alcohols as Energy Carriers in MILD Combustion'. *Energy and Fuels*, 35(9), p7253-7264.

Arnon, D. I.; Stout, P. R. (1939). 'The essentiality of certain elements in minute quantity for plants with special reference to copper'. *Plant Physiology*, 14, p371.

Beesley, L.; Moreno-Jiménez, E.; Gomez-Eyles, J.L.; Harris, E.; Robinson, B.; Sizmur, T. (2011). 'A review of biochars' potential role in the remediation, revegetation and restoration of contaminated soils'. *Environmental Pollution*, 159, p3269-3282.

Blackadder, W.; Rensfelt, E. A. A (1985). 'Pressurized Thermo Balance for Pyrolysis and gasification studies of biomass, wood and peat'. *Fundamentals of Thermochemical Biomass Conversion*, Overend, R. P., AT Milne, A. T., Mudge, K. L., Eds.; London, p747-759.

Batidzirai, B.; Mignot, A. P. R. W.; Schakel, B.; Junginger, H. M.; Faaij, A. P. C. (2013). 'Biomass torrefaction technology: Techno-economic status and future prospects'. *Energy*, 62, p196–214.

Cavaliere, A.; de Joannon, M. (2004). 'Mild Combustion'. *Progress in Energy and Combustion Science*, 30, p329-366.

Cetin, E.; Moghtaderi, B.; Gupta, R.; Wall, T. F (2004). 'Influence of pyrolysis conditions on the structure and gasification reactivity of biomass chars'. *Fuel*, 83, p2139-2150.

Cha, J. S.; Park, S. H.; Jung, S. C.; Ryu, C.; Jeon, J. K.; Shin, M. C.; Park, Y. K. (2016). 'Production and utilization of biochar: A review'. *Journal of Industrial Engineering and Chemistry*, 40, p1-15.

Characterization', *International Journal of Refractory Metals and Hard Materials*, 19, p437–45.

Chen, Y.; Luo, Y. H.; Wu, W.G.; Su, Y. (2009). 'Experimental Investigation on Tar Formation and Destruction in a Lab-Scale Two-Stage Reactor'. *Energy and Fuels*, 23, p4659.

Chisti, Y. (2007). 'Biodiesel from microalgae'. *Biotechnology Advancements*, 25, p294-360.

Cho, H. J.; Baek, K. T.; Jeon, J. K.; Park, S. H.; Suh, D. J.; Park, Y. K. (2013). 'Removal characteristics of copper by marine macro-algae-derived chars'. *Chemical Engineering Journal*, 217, p205.

Crabtree, R. H. (2005a). 'Complexes of  $\pi$ -bound ligands'. *The Organometallic Chemistry of the Transition Metals*, New York: Wiley, p125–58.

Crabtree, R. H. (2005b). 'Metal–ligand multiple bonds'. *The Organometallic Chemistry of the Transition Metals*, New York: Wiley, p309–41.

- Creamer, A. E.; Gao, B.; Zhang, M. (2014). 'Carbon dioxide capture using biochar produced from sugarcane bagasse and hickory wood'. *Chemical Engineering Journal*, 249, p174.
- Dally, B.B.; Riesmeier, E.; Peters, N. (2004). 'Effect of fuel mixture on moderate and intense low oxygen dilution combustion'. *Combustion and Flame*, 137(4), p418-431.
- Das O.; Sarmah, A.K.; Bhattacharyya, D. (2015). 'Structure–mechanics property relationship of waste derived biochars', *Science of Total Environment*, 538, p611–20.
- Das, O., Sarmah, A.K., Bhattacharyya, D. (2015). 'A novel approach in organic waste utilization through biochar addition in wood/polypropylene composites'. *Waste Management*, 38, p132–140.
- Das, O.; Sarmah, A. K.; Bhattacharyya, D. (2016). 'Nanoindentation assisted analysis of biochar added biocomposites', *Composites B*, 91, p219–27.
- De Joannon, M.; Sabia, P.; Sorrentino, G.; Bozza, P.; Ragucci, R. (2017). 'Small Size Burner Combustion Stabilization by Means of Strong Cyclonic Recirculation'. *Proceedings of the Combustion Institute*, 36 (3), p3361–3369.
- Debiagi, P. E. A.; Pecchi C.; Gentile, G.; Frassoldati, A.; Cuoci, A.; Faravelli, T.; Ranzi, E. (2015). 'Extractives extend the applicability of multistep kinetic scheme of biomass pyrolysis'. *Energy and Fuel*, 29, p6544-6555.
- Dehkhoda, A. M.; West, A. H.; Ellis, N. (2010). 'Biochar based solid acid catalyst for biodiesel production', *Applied Catalysis A: General*, 382, p197.
- Devi, P.; Saroha, A. K. (2015). 'Effect of pyrolysis temperature on polycyclic aromatic hydrocarbons toxicity and sorption behaviour of biochars prepared by pyrolysis of paper mill effluent treatment plant sludge'. *Bioresource Technology*, 192, p312–20.
- Di Blasi C. (2008). 'Modeling chemical and physical processes of wood and biomass pyrolysis'. *Progress in Energy Combustion Science*, 34, p47-90.
- Di Blasi, C. (2009). 'Combustion and gasification rates of lignocellulosic chars'. *Progress in Energy Combustion Science*, 35, 121-140.
- Di Blasi, C.; Galgano, A.; Branca, C. (2009). 'Influences of the chemical state of alkaline compounds and the nature of alkali metal on wood pyrolysis', *Industrial Engineering and Chemistry Research*, 48, p3359–69.
- Downie, A., Crosky, A., Munroe, P. (2009). 'Physical properties of biochar' in: Lehmann, J., Joseph, S. *Biochar for Environmental Management Science and Technology*. Earthscan Publishing, London, p13-32.
- Emmerich; F. G.; De Sousa, J. C.; Torriani, I. L.; Luengo, C. A. (1987). 'Applications of a granular model and percolation theory to the electrical resistivity of heat treated endocarp of babassu nut', *Carbon*, 25, p417–24.
- Ferreiro, A. I.; Giudicianni, P.; Grottola, C. M.; Rabaçal, M.; Costa, M.; Ragucci, R. (2017) 'Unresolved Issues on the Kinetic Modeling of Pyrolysis of Woody and Nonwoody Biomass Fuels'. *Energy and Fuel*, 31, p4035–4044.
- Ferreiro, A. I.; Rabaçal, M.; Costa, M.; Giudicianni, P.; Grottola, C. M.; Ragucci R. (2018). 'Modeling the impact of the presence of KCl on the slow pyrolysis of cellulose'. *Fuel*, 215, p57-65.
- Fytli, D.; Zabaniotou, A. (2008). 'Utilization of sewage sludge in EU application of old and new methods—a review'. *Renewable Sustainable Energy Reviews*, 12, p116-140.
- Gargiulo, V.; Gomis-Berenguer, A.; Giudicianni, P.; Ania, C. O.; Ragucci, R.; Alfè, M. (2018) 'Assessing the potential of biochars prepared by steam-assisted slow pyrolysis for CO<sub>2</sub> adsorption and separation'. *Energy and Fuel*, 32, p10218-10227.
- Giudicianni, P., Gargiulo, V., Grottola, C. M., Alfè, M., Ferreiro, A. I., Mendes, M. A. A., Ferreiro, A. I., Ragucci, R. (2021). 'Inherent metal elements in biomass pyrolysis: A review', *Energy & Fuels*, 35(7), p5407-5478.
- Glaser, B.; Haumaier, L.; Guggenberger, G.; Zech, W. (2001). 'The 'Terra Preta' phenomenon: a model for sustainable agriculture in the humid tropics'. *The Science of Nature*, 88, p37-41.

- Grottola, C. M.; Giudicianni, P.; Michel, J. B.; Ragucci, R. (2018). 'Torrefaction of woody waste for use as biofuel'. *Energy and Fuel*, 32, p10266-10271.
- Han, H.; Hu, S.; Lu, C.; Wang, Y.; Jiang, L.; Xiang, J.; Su, S. (2016). 'Inhibitory effects of CaO/Fe<sub>2</sub>O<sub>3</sub> on arsenic emission during sewage sludge pyrolysis'. *Bioresource Technology*, 218, p134–139.
- Han, L.; Sun, K.; Jin, J.; Wei, X.; Xia, X.; Wu, F.; Gao, B.; Xing, B. (2014) 'Role of structure and microporosity in phenanthrene sorption by natural and engineered organic matter'. *Environmental Science and Technology*, 48, p11227–34.
- Harvey, O. R.; Herbert, B. E.; Rhue, R. D.; Kuo, L. J. (2011). 'Metal interactions at the biochar– water interface: energetics and structure–sorption relationships elucidated by flow adsorption microcalorimetry'. *Environmental Science and Technology*, 45, p5550–56.
- Ho, R. J.; Kumaran, P.; Yusoff, M. Z. (2016). 'Development of High Efficiency and Low Emission Low Temperature Combustion Diesel Engine with Direct EGR Injection', *IOP Conf. Series: Earth and Environmental Science*, 32, p012016.
- Hubadillah, S.K.; Tai, Z.S.; Othman, M.H.D.; Harun, Z.; Jamalludin, M.R.; Rahman, M.A.; Jaafar, J.; Ismail, A.F. (2019) Hydrophobic ceramic membrane for membrane distillation: A mini review on preparation, characterization, and applications, *Separation and Purification Technology*, 217, 71–84.
- Iliopoulou, E. F.; Triantafyllidis, K. S.; Lappas, A. A. (2019). 'Overview of catalytic upgrading of biomass pyrolysis vapors toward the production of fuels and high-value chemicals'. *WIREs Energy Environment*, 8 (1), pe322.
- Inal, I. I. G.; Holmes, S. M.; Banford, A.; Aktas, Z. (2015). 'The performance of supercapacitor electrodes developed from chemically activated carbon produced from waste tea', *Applied Surface Science*, 357, p696.
- Ingram, L.; Mohan, D.; Bricka, M.; Steele, P.; Strobel, D.; Crocker, D.; Mitchell, B.; Mohammad, J.; Cantrell, K.; Pittman Jr, C. U. (2008). 'Pyrolysis of wood and bark in an auger reactor: physical properties and chemical analysis of the produced bio-oils'. *Energy and Fuels*, 22(1), p614-625.
- Jo, Y. B.; Cha, J. S. ; Ko, J. H. ; Shin, M. C.; Park, S. H.; Jeon, J. K.; Kim, S. S.; Park, Y. K. (2011). 'NH<sub>3</sub> selective catalytic reduction (SCR) of nitrogen oxides (NO<sub>x</sub>) over activated sewage sludge char', *Korean Journal of Chemical Engineering*, 28, p106.
- Kalogiannis, K. G.; Stefanidis, S. D.; Lappas, A. A. (2019). 'Catalyst deactivation, ash accumulation and bio-oil deoxygenation during ex situ catalytic fast pyrolysis of biomass in a cascade thermal-catalytic reactor system'. *Fuel Processing Technology*, 186, p99-109.
- Kambo, H.S., Dutta, A. (2015). 'A comparative review of biochar and hydrochar in terms of production, physico-chemical properties and applications'. *Renewable and Sustainable Energy Reviews*, 45, p359-378.
- Katsuki, M.; Hasegawa, T. (1998). 'The science and technology of combustion in highly preheated air'. *Proceedings of the Combustion Institute*, 27(2), p3135-3146.
- Keiluweit, M., Nico, P.S., Johnson, M.G., Kleber, M. (2010). 'Dynamic molecular structure of plant biomass-derived black carbon (biochar)'. *Environmental Science and Technology*, 44, p1247–1253.
- Kercher, A. K.; Nagle, D. C. (2003). 'Microstructural evolution during charcoal carbonization by x-ray diffraction analysis', *Carbon*, 41, p15–27.
- Khalil A. E. E.; Gupta A. K. (2011). 'Distributed swirl combustion for gas turbine application'. *Applied Energy*, 88 (12), p 4898-4907.
- Kim, W. K.; Shim, T. Y.; Kim, Y. S.; Hyun, S.; Ryu, C.; Park, Y. K.; Jung, J. (2013). 'Characterization of cadmium removal from aqueous solution by biochar produced from a giant Miscanthus at different pyrolytic temperatures' *Bioresource Technology*, 138, p266.
- Kirkbey, E. (2012). 'Introduction, definition and classification of nutrients'. In *Marschner's mineral nutrition of higher plants*, Academic Press, p3-5.

- Koonaphapdeelert, S.; Li, K. (2007). Preparation and characterization of hydrophobic ceramic hollow fibre membrane, *Journal of Membrane Science*, 291, 70–76.
- Lee, J. Y.; Park, S. H.; Jeon, J. K.; Yoo, K. S.; Kim, S. S.; Park, Y. K. (2011). 'The removal of low concentration formaldehyde over sewage sludge char treated using various methods'. *Korean Journal of Chemical Engineering*, 28, p1556.
- Lee, X. J.; Ong, H. C.; Gan, Y. Y.; Chen, W. H.; Mahlia, T. M. I. (2020). 'State of art review on conventional and advanced pyrolysis of macroalgae and microalgae for biochar, bio-oil and bio-syngas production'. *Energy Conversion Management*, 210, 112707.
- Lehmann, J., Joseph S. (2009). 'Biochar for environmental management'. Earthscan, London.
- Lehto, J.; Oasmaa, A.; Solantausta, Y.; Kytö, M.; Chiaramonti, D. (2014). 'Review of fuel oil quality and combustion of fast pyrolysis bio-oils from lignocellulosic biomass'. *Applied Energy*, 116, p178-190.
- Leijenhörst, E. J.; Wolters, W.; van de Beld, L.; Prins, W. (2016). 'Inorganic element transfer from biomass to fast pyrolysis oil: review and experiments'. *Fuel Processing Technology*, 149, p96–111.
- Levy, Y.; Sherbaum, V.; Arfi P. (2004). 'Basic Thermodynamics of Floxcom, the Low-Nox Gas Turbines Adiabatic Combustor'. *Applied Thermal Engineering*. 24, p1593-1605.
- Li, P.; Mi, J., Dally, B. B.; Wang, F.; Wang, L.; Liu, Z.; Chen, S.; Zheng, C. (2011). 'Progress and recent trend in MILD combustion'. *Science China Technological Sciences*, 54(2), p255-269.
- Liaw, S.-S.; Zhou, S.; Wu, H.; Garcia-Perez, M. (2012). 'Effect of pyrolysis temperature on the yield and properties of bio-oils obtained from the auger pyrolysis of Douglas Fir wood'. *Journal of Analytical and Applied Pyrolysis*, 93, p52-62, 2012.
- Lievens, C.; Yperman, J.; Vangronsveld, J.; Carleer, R. (2008). 'Study of the potential valorisation of heavy metal contaminated biomass via phytoremediation by fast pyrolysis: Part I. Influence of temperature, biomass species and solid heat carrier on the behaviour of heavy metals'. *Fuel*, 87 (10-11), p1894-1905.
- Liu, Z.; Wang, L. A.; Xiao, H.; Guo, X.; Urbanovich, O.; Nagorskaya, L.; Li, X. (2020). 'A review on control factors of pyrolysis technology for plants containing heavy metals'. *Ecotoxicology and Environmental Safety*, 191, p110181.
- Lua, A. C.; Yang, T.; Guo, J. (2004). 'Effects of pyrolysis conditions on the properties of activated carbons prepared from pistachio-nut shells'. *Journal of Analytical and Applied Pyrolysis*, 72, p279–87.
- Lückerath, R.; Meier, W.; Aigner, M. (2008). 'FLOX® combustion at high pressure with different fuel compositions'. *Journal of Engineering for Gas Turbines and Power*, 130(1), p011505.
- Mahinpey, N.; Murugan, P.; Mani, T.; Raina, R. (2009). 'Analysis of bio-oil, biogas, and biochar from pressurized pyrolysis of wheat straw using a tubular reactor'. *Energy and Fuel*, 23, p2736-2742.
- Marschner, H. (2011). 'Marschner's mineral nutrition of higher plants'. Academic Press.
- McLachlan, D. S.; Cai, K.; Sauti, G. (2001). 'AC and DC conductivity-based microstructural
- Micháleková-Richveisová, B.; Frišták, V.; Pipiška, M.; Duriška, L.; Moreno-Jimenez, E.; Soja, G. (2017). 'Iron-impregnated biochars as effective phosphate sorption materials' *Environmental Science and Pollution Research*, 24, p463–75.
- Milani, A.; Wüning, J.G. (2007). 'Flameless oxidation technology, advanced combustion and aero thermal technologies'. *Environmental Protection and Pollution Reductions*, 6, p343-352.
- Mok, W. S. L.; Antal, M. J. (1983). 'Effects of pressure on biomass pyrolysis. I. Cellulose pyrolysis products'. *Thermochimica Acta*, 68, p155-164.
- Mubarik, S.; Saeed, A.; Athar, M.M.; Iqbal, M. (2016). 'Characterization and mechanism of the adsorptive removal of 2,4,6-trichlorophenol by biochar prepared from sugarcane baggase'. *Journal of Industrial and Engineering Chemistry*, 33, p115.

Naseem, A.; Tabasum, S.; Zia, K.M.; Zuber, M.; Ali, M.; Noreen, A. (2016). 'Lignin-derivatives based polymers, blends and composites: a review'. *International Journal of Biological Macromolecules*, 93, p296-313.

Phyllis2, Energy research Centre of the Netherlands, database for biomass and waste; <https://www.ecn.nl/phyllis2> (accessed June 20, 2021).

Pilon-Smits, E. A.; Quinn, C. F.; Tapken, W.; Malagoli, M.; Schiavon, M. (2009). 'Physiological functions of beneficial elements'. *Current Opinion in Plant Biology*, 12, p267-274.

Pindoria, P. V.; Megaritis, A.; Messenbock, R. C.; Dugwell, D. R.; Kandiyoti, R. (1998). 'Comparison of the pyrolysis and gasification of biomass: effect of reacting gas atmosphere and pressure on Eucalyptus wood'. *Fuel*, 77, 1247-1251.

Pittman Jr, C. U.; Mohan, D.; Eseyin, A.; Li, Q.; Ingram, L.; Hassan, E. B. M.; Mitchell, B.; Guo, H.; Steele, P. H. (2012). 'Characterization of bio-oils produced from fast pyrolysis of corn stalks in an auger reactor'. *Energy and Fuels*, 26(6), p3816-3825.

Puy, N., Murillo, R., Navarro, M. V., López, J. M., Rieradevall, J., Fowler, G., Aranguren, I.; García, T.; Bartrolí, J.; Mastral, A. M. (2011). 'Valorisation of forestry waste by pyrolysis in an auger reactor'. *Waste management*, 31(6), p1339-1349.

Qjan, K., Kumar, A., Zhang, H., Bellmer, D., Huhnke, R. (2015). 'Recent advances in utilization of biochar'. *Renewable and Sustainable Energy Reviews*, 42, p1055-1064.

Raveendran, K.; Ganesh, A.; Khilar, K. C. (1995). 'Influence of mineral matter on biomass pyrolysis characteristics'. *Fuel*, 74 (12), p1812-1822.

Reddy, V. M.; Katoch, A., Roberts; W. L.; Kumar S. (2015). 'Experimental and numerical analysis for high intensity swirl based ultra-low emission flameless combustor operating with liquid fuels'. *Proceedings of the Combustion Institute*, 35(3), p3581-3589.

Rhim, Y.R.; Zhang, D.; Fairbrother, D.H.; Wepasnick, K. A.; Livi, K. J.; Bodnar, R. J.; Nagle, D. C. (2010). 'Changes in electrical and microstructural properties of microcrystalline cellulose as function of carbonization temperature', *Carbon*, 48, p1012-24.

Riccus, O.; Smith, R.; Güthe, F.; Flohr, P. (2005). 'The GT24/26 Combustion Technology and high Hydrocarbon ("C2+") Fuels'. *ASME Turbo Expo 2005: Power for Land, Sea, and Air; American Society of Mechanical Engineers*, p595-602.

Sabia, P.; Sorrentino, G.; Bozza, P.; Ceriello, G.; Ragucci, R.; De Joannon, M. (2019). 'Fuel and Thermal Load Flexibility of a MILD Burner'. *Proceedings of the Combustion Institute*, 37 (4), p4547-4554.

Saxena, S.; Bedoya I. D. (2013). 'Fundamental phenomena affecting low temperature combustion and HCCI engines, high load limits and strategies for extending these limits'. *Progress in Energy and Combustion Science*, 39(5), p457-488.

Scheller H. V.; Ulvskov P. (2010). 'Hemicelluloses'. *Annual Review of Plant Biology*, 61 (1), p263-289

Shen, Y. (2015). 'Chars as carbonaceous adsorbents/catalysts for tar elimination during biomass pyrolysis or gasification'. *Renewable and Sustainable Energy Reviews*, 43, p281-295.

Sorrentino, G.; Sabia, P.; Bozza, P.; Ragucci, R.; de Joannon, M. (2019). 'Low-NOx Conversion of Pure Ammonia in a Cyclonic Burner under Locally Diluted and Preheated Conditions'. *Applied Energy*, 254, p1-7.

Spokas, K. A.; Koskinen, W. C.; Baker, J. M.; Reicosky, D. C. (2009). 'Impacts of woodchip biochar additions on greenhouse gas production and sorption/degradation of two herbicides in a Minnesota soil', *Chemosphere*, 77, p574.

Staals, M.; Thijssen, E.; Vangronsveld, J.; Carleer, R.; Schreurs, S.; Yperman, J. (2010). 'Flash pyrolysis of heavy metal contaminated biomass from phytoremediation: influence of temperature, entrained flow and wood/leaves blended pyrolysis on the behaviour of heavy metals'. *Journal of Analytical and Applied Pyrolysis*, 87 (1), p1-7.



Sun, Y.; Gao, B.; Yao, Y.; Fang, J.; Zhang, M.; Zhou, Y.; Chen, H.; Yang, L. (2014). 'Effects of feedstock type, production method, and pyrolysis temperature on biochar and hydrochar properties', *Chemical Engineering Journal*, 240, p574–8.

Tan, X., Liu, Y., Zeng, G., Wang, X., Hu, X., Gu, Y., Z. (2015). 'Application of biochar for the removal of pollutants from aqueous solutions'. *Chemosphere*, 125, p70-85.

Vassilev, S. V.; Baxter, D.; Andersen, L. K.; Vassileva, C. G. (2010). 'An overview of the chemical composition of biomass'. *Fuel*, 89 (5), p913-933.

Vassilev, S. V.; Baxter, D.; Andersen, L. K.; Vassileva, C. G.; Morgan, T. J. (2012). 'An overview of the organic and inorganic phase composition of biomass'. *Fuel*, 94, p1-33.

Weber, K.; Quicker, P. (2018). 'Properties of biochar'. *Fuel*, 217, p240-261.

Wünning, J.A.; Wünning, J.G. (1977). 'Flameless oxidation to reduce thermal no-formation'. *Progress in Energy and Combustion Science*, 23(1), p81-94.

Xie, M.; Chen, W.; Xu, Z.; Zheng, S.; Zhu, D. (2014). 'Adsorption of sulfonamides to demineralized pine wood biochars prepared under different thermochemical conditions'. *Environmental Pollution*, 186, p187–94.

Yargicoglu, E. N.; Sadasivam, B. Y.; Reddy, K. R.; Spokas, K. (2015). 'Physical and chemical characterization of waste wood derived biochars', *Waste Management*, 36, p256–68.

Zhang, R.; Lei, K.; Bu, Q. Y.; Cao, J.; Liu, D. (2018). 'Effects of alkali and alkaline earth metal species on the combustion characteristics of single particles from pine sawdust and bituminous coal', *Bioresource Technology*, 268, p278–85.

Zhang, Y.; Kajitani, S.; Ashizawa, M.; Miura, K. (2006) 'Peculiarities of rapid pyrolysis of biomass covering medium-and high-temperature ranges', *Energy & Fuel*, 20(6), p2705-2712.

Zhu, X.; Liu, Y.; Zhou, C.; Luo, G.; Zhang, S.; Chen, J. (2014). 'A novel porous carbon derived from hydrothermal carbon for efficient adsorption of tetracycline'. *Carbon*, 77, p627.

## 5 BIOMASS TECHNOLOGY MATRIX

In the previous sections, every step of the CERESiS value chain for biofuel and bio-oil production has been described in detail. A variety of different contaminated biomass samples is going to be treated in a series of process steps involving conversion, decontamination, synthesis and upgrading. Process outcome and performance is influenced by several parameters, depending on the technology, respectively. All these aspects can be summarized in a biomass technology matrix (BTM), which is displayed in Figure 5-1 and Figure 5-3. Newly generated results within the project will be considered and implemented.

The first part of the BTM (Figure 5-1) shows the different plant species that will be considered and the responsibilities of WP2 partners (pretreatment and analysis). Entering the technological pillar, additional pretreatment will be performed depending on the conversion technology, SCWG and fast pyrolysis. Key parameters for each process are listed in Figure 5-1.

Part II (Figure 5-2) describes the process chain and relevant parameters of TP1. The SCWG product gas is cleaned and decontaminated and subsequently converted in a series of catalytic process steps, resulting in FT-biofuel. Additionally, the SCWG liquid streams will be electrochemically treated for decontamination.

A summary of process steps and key aspects of TP2 is given in part III (Figure 5-3). All products of fast pyrolysis, bio-oil as well as gas and bio-char, will be investigated. A membrane separation is implemented to remove contaminants from the bio-oil.

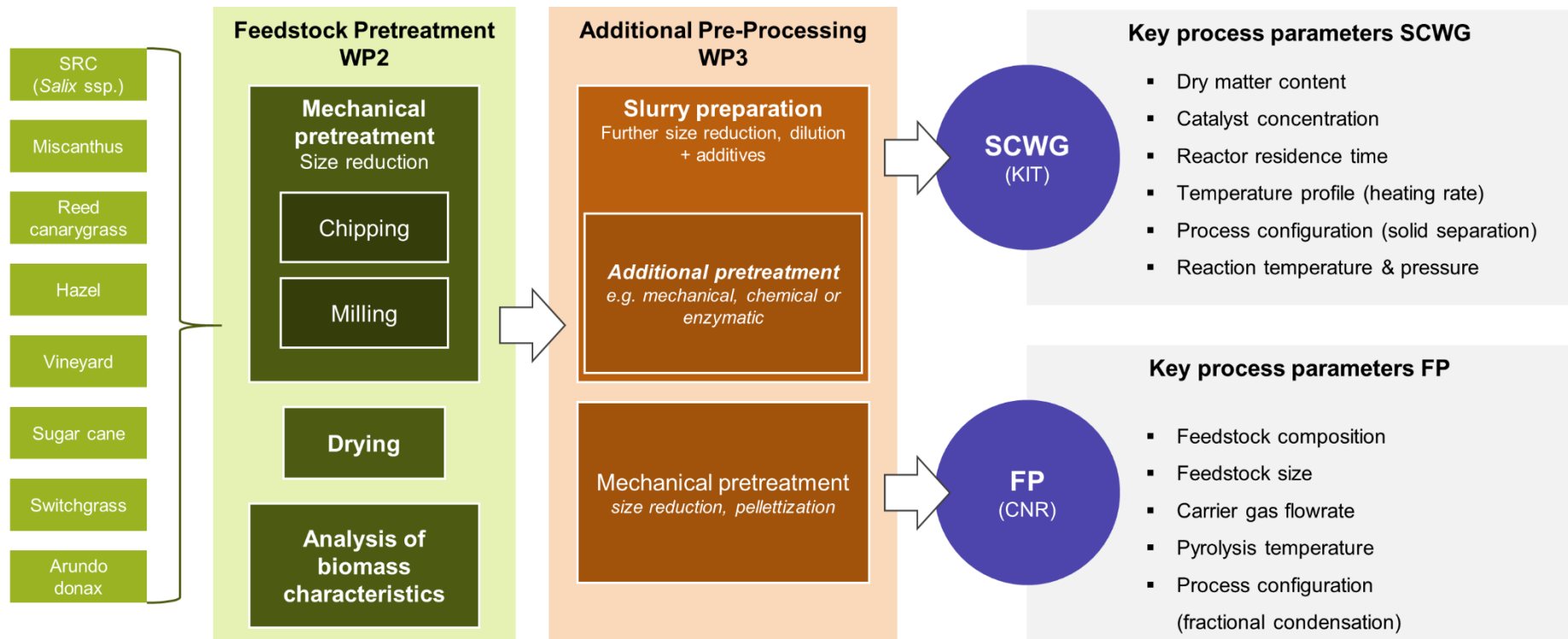


Figure 5-1: Biomass Technology Matrix – Part I: Biomass supply and conversion.

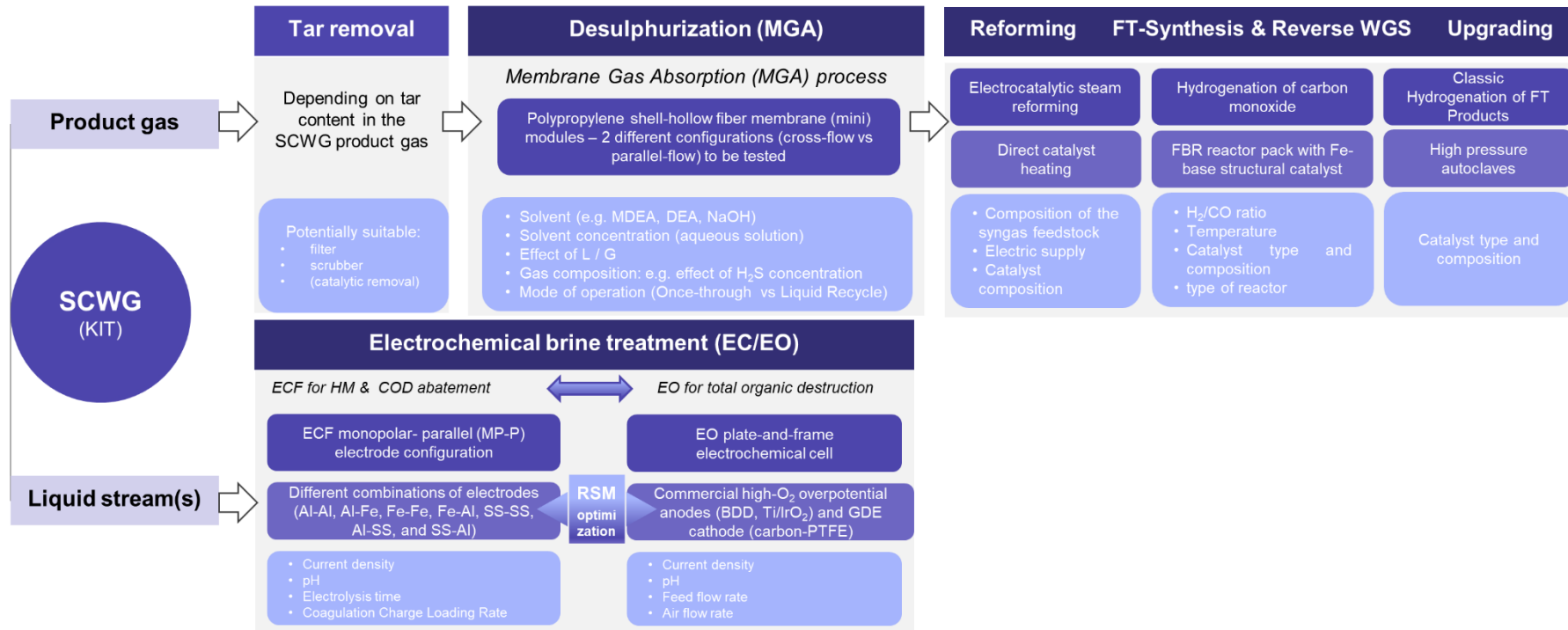


Figure 5-2: Biomass Technology Matrix – Part II: TP1 Decontamination and biofuel production.

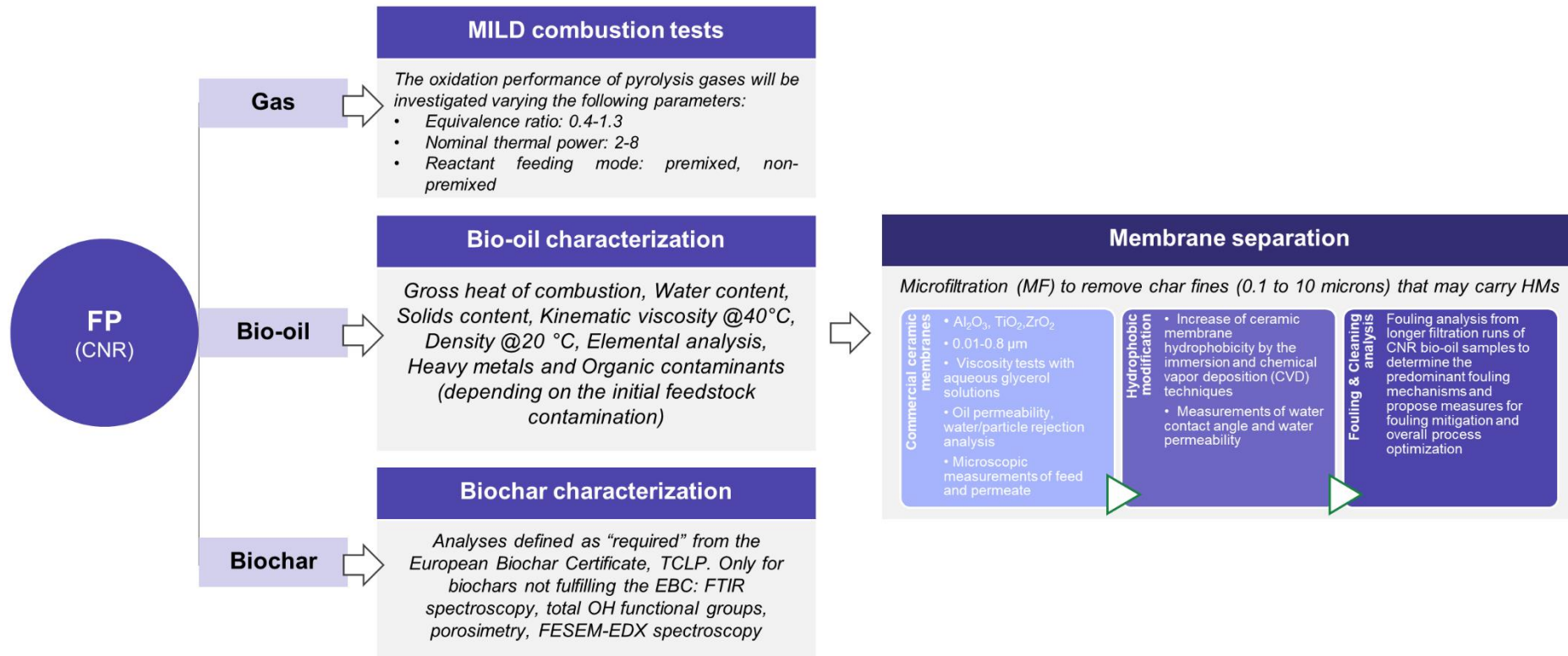


Figure 5-3: Biomass Technology Matrix – Part III: TP2 Bio-oil production and decontamination.

## 6 RISK ASSESSMENT AND MITIGATION MEASURES

In this section, technological risks that can potentially occur throughout the course of CERESiS will be described. This compilation represents an extended version of the risks previously listed in the Grant Agreement. Furthermore, suitable mitigation measures will be proposed. Risks are summarized for both technology pathways and ranked according to the risk levels described in the Grant Agreement. The probability and impact of risks are estimated in a scale where 1 is the lower level and 10 is the highest level. The risk ranking is based on risk level (risk level = probability x impact) and divides into the categories depicted in Figure 6-1.

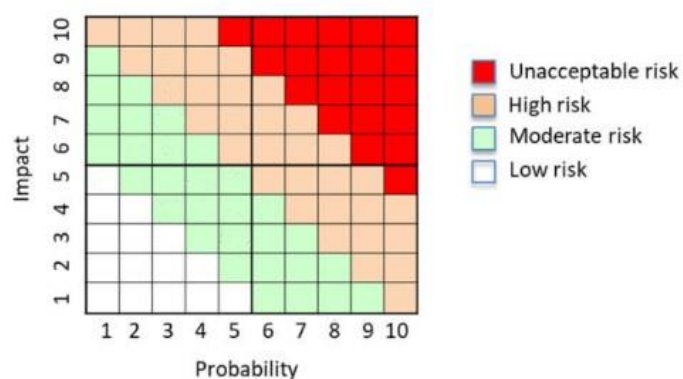


Figure 6-1: Risk ranking: classification of risk level.

### 6.1 SCWG-based technology pathway

#### Supercritical water gasification

##### Risk 1.1: Unstable operation in the presence of heavy metals

With current knowledge, the behavior of HM during SCWG can only be assumed to be comparable to other salt-forming elements. Deposition of solids and subsequent blockage of the reaction system can therefore be possible.

##### Mitigation: Modification of the system for salt separation

There are different possibilities to remove salts and solids (see Section 3.1.3), depending on the concentration of and the properties of the salts.

##### Risk 1.2: Feedstock-related issues

The type of biomass can influence the gasification performance (see Section 3.1.1). Therefore, one objective of the experimental investigations will be to evaluate the applicability of the different plants for SCWG. Another aspect are technical difficulties (blockages) due to the nature of the biomass (e.g. fibers or an initially low moisture content).

##### Mitigation: Improve feed pretreatment, modification & tuning of operational parameters of the SCWG reactor system

Gasification efficiency can be improved by optimizing the various operating parameters (see Section 3.1.1). A modification of the configuration of the SCWG reaction system is also possible. With selection of an adequate pretreatment (see Section 3.1.2), even fibrous, lignocellulosic biomass can eventually be successfully gasified. Eventually, if some specific biomass species cannot be successfully treated by SCWG (e.g. dry material), they will be proposed for treatment with FP.

**Risk 1.3: Detection of contaminants in SCWG effluent streams in case of low concentrations in the biomass**

In case of biomass samples with a low contamination level, detection can become difficult or even not possible.

Mitigation: Consult different/external analytical laboratories

If balance is still not possible due to very low concentration, a statement that the specific stream is not contaminated and thus can be further used or disposed, will be given.

## Decontamination

**Risk 1.4: Unacceptably high capture of CO<sub>2</sub> during deH<sub>2</sub>S of the SCWG gas product**

Mitigation: Investigation of solvent regeneration conditions (temperature, pressure) for controlled release of CO<sub>2</sub> w/o release of H<sub>2</sub>S. Need for definition of minimum CO<sub>2</sub> content (if any) by the downstream (reforming-RWGS-FT) process.

**Risk 1.5: High tar content in the SCWG gas product thereby endangering the MGA process (i.e. plugging/destruction of membrane module)**

Mitigation: Use of additional filters/buffers upstream the MGS process to ensure elimination of tars presence. Provision for periodic replacement of modules if necessary (consideration in process economics).

**Risk 1.6: Reduced performance of the two electrochemical technologies due to high TSS**

Due to the high suspended solids and colloids in the SCWG liquid effluents (e.g. brine), the current efficiencies of EO and ECF processes, may worsen.

Mitigation: Pre-treatment of SCWG liquid effluents for solid separation

CERTH will investigate the effectiveness of ECF to cope with high TSS and turbidity liquids, prior to the EO. In case process efficiency and energy consumption are negatively affected, prior cartridge filtration of the liquids will be considered.

**Risk 1.7: The electrochemical decontamination is achieved at high electricity consumption**

Based on the treatment targets set, the required current densities may result to increased electricity consumption, thus rendering the hybrid process not economic sustainable.

Mitigation: Process optimization by investigating multiple critical parameters

Other than the DC current applied, ECF and EO are affected by several parameters, including the electrical conductivity, the initial pH, the feed flow rate, the air flow rate (EO), the temperature, etc. The optimum values of these parameters will be determined towards minimizing the electrical energy expenditure, the sacrificial anode consumption and maximizing the best performance of coagulation and bubble generation. The success of the hybrid ECF/EO technology will depend on its ability to satisfy commercial criteria such as minimizing operational and maintenance costs.

## Biofuel Synthesis

### Risk 1.8: Unwanted side reactions

Since iron catalysts have activity for the WGS reaction, part of the carbon monoxide is lost as raw material and instead of forming hydrocarbons, CO<sub>2</sub> is formed. Also, FT on iron catalysts can produce small amounts of naphthenes and aromatics reducing the quality of the products obtained.

#### Mitigation: Carefully monitoring of feedstock

Carefully monitor the H<sub>2</sub>/CO ratio that is fed to the reactor to decrease the activity of competitive reactions and the production of unwanted compounds. In general, a higher ratio of H<sub>2</sub>/CO forms more H<sub>2</sub>O, otherwise CO<sub>2</sub> is formed. Plus, high H<sub>2</sub>/CO ratio make it reasonable for synthetic diesel production over Fe-base catalyst because that promotes low hydrogenolysis and low shift activity.

### Risk 1.9: Operation conditions

The major disadvantage of packed bed catalysts is high pressure drop and difficult heat transfer that can generate greater selectivity towards methanization, less towards hydrocarbons.

#### Mitigation: Structural catalyst

The high void fractions of structural catalysts, combined with the laminar flow prevailing in the channels, enable substantial reduction of pressure drop with respect to conventional packed beds of catalyst pellets. Furthermore, conductive heat exchange in structures catalysts can be even more effective than convective heat transfer in packed beds.

## Summary and risk ranking (TP1)

In Table 6-1, the aforementioned risks of TP1 are summarized and evaluated according to the risk level described in the Grant agreement.

**Table 6-1: Risk ranking TP1**

No.	Risk description	Probability	Impact	Risk ranking
1.1	SCWG - Unstable operation in the presence of heavy metals	4	5	20
1.2	SCWG - Feedstock-related issues	5	5	20
1.3	SCWG - Detection of contaminants in effluent streams in case of low concentrations in the biomass	6	4	24



1.4	MGA - Unacceptably high capture of CO <sub>2</sub> during deH <sub>2</sub> S of the SCWG gas product	5	5	25
1.5	MGA - High tar content in the SCWG gas product thereby endangering the process	3	4	12
1.6	EO/EC - Reduced performance of the two electrochemical technologies due to high TSS	5	5	25
1.7	EO/EC -The electrochemical decontamination is achieved at high electricity consumption	3	4	12
1.8	FT - Unwanted side reactions	4	6	24
1.9	FT - Operation conditions	3	6	18

## 6.2 FP-based technology pathway

### Fast Pyrolysis

#### **Risk 2.1: Delay in plant delivery due to COVID-19 emergency**

Mitigation: Preliminary tests will be conducted with a bench-scale reactor already available at CNR

#### **Risk 2.2: Bio-oil specifications will not meet the requirements of the MF unit**

Mitigation:

- Feedstock pre-treatments will be evaluated to reduce the solid particles and the HM content in the bio-oil.
- The condensation unit will be adapted to control the water content in the bio-oil.

### Mild Combustion

#### **Risk 2.3: The LHV of gaseous fraction of pyrolysis process may compromise the oxidation process stability**

Mitigation:

- Evaluation of possible heat losses reduction by proper reactor insulation.
- Evaluation of possible co-combustion strategies by adding fuel «enhancers» (CH<sub>4</sub>, C<sub>3</sub>H<sub>8</sub> etc.).
- Premixed and non-premixed strategies to improve combustion stability.

### Microfiltration

#### **Risk 2.4: Membrane fouling is detrimental to the process performance**

The FP bio-oil microfiltration can result to pore blockage, pore constriction and/or cake layer formation, thus, negatively affecting the oil permeability (and to a lesser extent the solid (char) particles rejection).

**Mitigation: Extensive fouling studies and cleaning protocols**

A detailed investigation of the different factors affecting the fouling process will be carried out by CERTH including the intrinsic properties of the ceramic membrane materials (before and after their hydrophobic modification), the crossflow velocity and the concentration of char particles present in the feed stream. Understanding the underlying mechanisms for char particle removal from bio-oil will allow more efficient membrane separation processes to be designed and the membrane cleaning protocol to be applied (based on literature and CERTH's experience).

## Summary and risk ranking (TP2)

In Table 6-2, the aforementioned risks of TP2 are summarized and evaluated according to the risk level described in the Grant agreement.

**Table 6-2: Risk ranking TP2**

No.	Risk description	Probability	Impact	Risk ranking
2.1	FP - Delay in plant delivery due to COVID-19 emergency	2	4	8
2.2	FP - Bio-oil specifications will not meet the requirements of the MF unit	4	6	24
2.3	MC - The LHV of gaseous fraction of pyrolysis process may compromise the oxidation process stability	4	6	24
2.4	MF - Membrane fouling is detrimental to the process performance	7	5	35

## 7 CONCLUSION

Following an overview on biomass characteristics and expected CERESiS samples, this report describes the workflow between the phytoremediation pillar (WP2) and the technological pillar (WP3). Based on currently available information, a Biomass Decision Tree was developed as guidance for samples prioritization and distribution between the SCWG and FP technology pathway. Furthermore, the whole process chain of both TPs has been described, key operating parameters have been defined and potential risks have been assessed. For TP1, this includes the following:

- **Supercritical water gasification (SCWG)**  
The experimental investigation on SCWG of contaminated biomass will be performed in the KIT laboratory plant. Process optimization will focus on temperature (profiles), residence time, catalyst addition and modification of the process configuration for efficient removal of solids. Additionally, an appropriate technology for tar removal will be implemented, if the tar content in the product gas proves to be significant. An important aspect will be a suitable pretreatment of the feedstock, since dry and fibrous materials can be a challenge in the SCWG process. The fate of contaminants during SCWG will be investigated, with the possibility that detection may be difficult in dilute process streams.
- **Decontamination – product gas (membrane gas absorption)**  
The experimental investigation on MGA based gas desulfurization (de-H<sub>2</sub>S) will be performed in CERTH's bench scale test unit which was modified accordingly for this purpose. Two different types of commercial 3M *Liqui-Cel* membrane modules will be employed. The first experimental test protocol/matrix was determined, including tests at various process conditions (i.e. gas and liquid flow rates, gas compositions, solvent type/concentration, etc). Process performance indicators, i.e. removal efficiency, acid gas loading, treating gas capacity and overall mass transfer coefficient, were identified as parameters for experimental assessment and optimization.
- **Decontamination – liquid stream(s) (electrocoagulation-flotation/electrochemical oxidation)**  
The decontamination of the SCWG liquid stream(s) will be investigated with the aid of two bench-scale ECF and EO setups. Specifically, a special ECF setup has been designed by CERTH, which will be coupled with a bench scale EO unit, aiming at the effective removal of HM and dissolved organics. The choice of the appropriate electrode materials and electrode configuration in the hybrid process will be determined by the removal efficiency and treatment cost in response to modern zero liquid discharge standards. The design of the experiments and the optimization of both ECF and EO processes, will be carried out using the Response Surface Methodology according to the selected independent variables that predominantly affect their performance, i.e., current density, pH, feed flow rate, electrolysis time.
- **Biofuel synthesis – Reforming/WGS & Fischer-Tropsch-Synthesis**  
All reforming and FT synthesis experiments will be performed at the Biomass Technology Laboratory (Université de Sherbrooke). First, the reforming step will be aligned on previous expertise from the team in electrocatalytic dry reforming. The idea is to use renewable electricity to reduce the carbon footprint of the process (which would have otherwise included part of the syngas). Then, the FT synthesis will be performed using a structured catalyst that we are also producing at the BTL. The possibility to add induction heating to the process will also be considered, again in a perspective to reduce the carbon intensity of the downstream fuel.

Regarding TP2, the subsequent technologies are included:

- **Fast pyrolysis (FP)**

The experimental investigation of the FP of contaminated biomass will be performed in the CNR screw reactor that was designed based on the needs of the CERESiS project and is currently under construction.

Process KPIs have been identified for the construction of the experimental matrix: optimization will focus on pyrolysis temperature, carrier gas flowrate, feedstock composition, modification of the process configuration for efficient separation of the aqueous fraction of the bio-oils. Additionally feedstock size will be optimized to avoid operational problems and improve the particle mixing inside the reactor. The fate of contaminants during FP will be investigated, as well as the properties of the char for the assessment of its possible uses.
- **MILD combustion**

The oxidation performance of pyrolysis gases will be investigated in a Lab Unit Cyclonic burner (LUCY) available at CNR. The mixture equivalence ratio, the thermal power and the fuel feeding mode have been identified as key influential parameters and the experimental design has been defined in order to optimize the burner working conditions both in terms of oxidation process stability and pollutant emissions.
- **Bio-oil decontamination (microfiltration)**

The experimental investigation on FP bio-oil decontamination by the undesirable HM-laden char particles (less than 10 micron in size) will be performed in CERTH's MF laboratory-scale pilot unit testing different composite ceramic membranes made of chemical-grade  $\alpha$ -aluminum oxide ( $\text{Al}_2\text{O}_3$ ) onto which a ceramic film is deposited (made of  $\text{Al}_2\text{O}_3$ ,  $\text{TiO}_2$  or  $\text{ZrO}_2$ ) - the actual membrane layer - of nominal pore sizes (e.g. 0.01 to 0.8  $\mu\text{m}$ ). Considering the importance of the membrane hydrophobicity on the effective blockage of the water phase from the bio-oil, efforts will be made to modify the hydrophobic property of the best performing membrane (in terms of higher particle separation and lower fouling tendency) by applying a silane grafting method, recently developed by CERTH, through immersion and CVD. The main challenges in this investigation will be a) to understand, quantify and reduce membrane fouling and b) to deal with highly viscous liquid streams. Special attention will be given to fouling analysis from longer runs of bio-oil through the membranes to determine the predominant fouling mechanisms. This will help propose measures for fouling mitigation and overall process optimization.

This report describes theoretical background and planned activities of the CERESiS technological pillar. The biomass technology matrix presented displays the individual steps of both process chains and summarizes key aspects, according to current state of knowledge. In the course of the project, the parameters will be re-evaluated and adapted if new findings emerge.

## LIST OF FIGURES

FIGURE 1-1: OVERVIEW OF THE CERESiS TECHNOLOGICAL PILLAR (WP3): SUPERCRITICAL WATER GASIFICATION (TP1) AND FAST PYROLYSIS (TP2) BASED TECHNOLOGY PATHWAY.....	7
FIGURE 2-1: BIOMASS SAMPLE OVERVIEW: POSSIBLE COMBINATIONS OF WP2 PARTNER, PLANT SPECIES, HARVEST SITE AND PERIOD AND CONTAMINATION CATEGORY AND LEVEL. MC: MISCANTHUS, RCG: REED CANARY GRASS, SRC: SHORT ROTATION COPPICE, VIN: VINEYARD, HZ: HAZEL, AM: ANDROPOGON MINARUM, PP: PENNISETUM PURPUREUM, SO: SACCHARUM OFFICINALIS, SR: SACCHARUM ROBUSTUS, AD*: ARUNDO DONAX, PV*: PANICUM VIRGATUM, B: BRESCIA. ....	10
FIGURE 2-2: CONCEPTUAL WORKFLOW BETWEEN WP2 UND WP3.....	12
FIGURE 2-3: BIOMASS DECISION TREE: PRIORITIZATION AND DISTRIBUTION OF BIOMASS SAMPLES BETWEEN TP1 AND TP2.....	12
FIGURE 3-1: SCHEMATIC DESCRIPTION OF THE SCWG LABORATORY PLANT AT KIT.....	15
FIGURE 3-2: SCHEMATIC DESCRIPTION OF THE FEED AND REACTION SYSTEM OF THE SCWG PILOT PLANT VERENA AT KIT. AFTER (BOUKIS AND STOLL, 2021). ....	25
FIGURE 3-3: SCHEMATIC DEPICTION OF THE BENCH-SCALE MEMBRANE REACTOR/PRECIPIATOR EXPERIMENTAL UNIT SETUP. ....	27
FIGURE 3-4: SCHEMATIC REPRESENTATION OF THE LIQUI-CEL 0.5X1 MINI MODULE. ....	28
FIGURE 3-5: SCHEMATIC REPRESENTATION OF THE LIQUI-CEL 1.7X5.5 MINI MODULE. ....	29
FIGURE 3-6: MASS TRANSFER REGIONS AND TRANSPORT RESISTANCES IN A MEMBRANE CONTACTOR.....	32
FIGURE 3-7: SCHEMATIC ILLUSTRATION OF THE ECF SETUP.....	36
FIGURE 3-8: A) BENCH-SCALE ELECTROCHEMICAL OXIDATION UNIT, AND B) MICRO FLOW CELL CONFIGURATION. ....	37
FIGURE 3-9: SIMPLIFIED FLOW DIAGRAM FOR FISHER-TROPSCH REACTOR AND PERIPHERAL COMPONENTS: 1. GAS CYLINDERS; 2. PRESSURE REGULATORS; 3. MASS FLOW CONTROLLERS; 4. VALVES; 5. CHECK VALVE; 6. A FRONT PRESSURE GAUGE; 7. RELIEF VALVE; 8. BYPASS VALVE; 9. TUBE AND SHELL CATALYTIC REACTOR; 10. TEMPERATURE SENSORS; 11. SEPARATION COLUMN (HOT TRAP); 12. SEPARATION COLUMN (COLD TRAP); 12. A BACK PRESSURE GAUGE; 13. BACKPRESSURE REGULATOR; 14. GAS FLOW COUNTER; 15. OIL TANK; 16. HEAT EXCHANGER; 17. PUMP. ....	46
FIGURE 4-1: SCHEMATIC REPRESENTATION OF THE EVOLUTION OF THE PYROLYSIS PRODUCTS AS THE SEVERITY OF HEAT TREATMENT INCREASES (GIUDICIANNI ET AL., 2021). ....	64
FIGURE 4-2: SEPARATION EFFICIENCY OF GAS/SOLID SEPARATION SYSTEMS AS FUNCTION OF THE SOLID PARTICLE SIZE. ....	71
FIGURE 4-3: SCHEMATIC DIAGRAM OF THE FP PLANT.....	73
FIGURE 4-4: EXECUTIVE DRAWINGS OF THE PYROLYSIS REACTOR. ....	73
FIGURE 4-5: EXECUTIVE DRAWINGS OF THE PYROLYSIS PLANT. ....	74
FIGURE 4-6: EXPERIMENTAL FACILITY AND GAS FEEDING CONFIGURATION. ....	76
FIGURE 4-7: (A) SCHEMATIC DIAGRAM OF THE EXPERIMENTAL SET-UP, (B) FRONT VIEW OF THE MF PILOT SCALE SYSTEM, (C) MEMBRANE MODULE AND (D) FEED PUMP AND FEED/RECIRCULATION TANK.....	79

FIGURE 4-8: CHANGE OF THE KINEMATIC VISCOSITY OF FIVE BIO-OIL SAMPLES AND A GLYCEROL AQUEOUS SOLUTION OF 83.4 WT.% WITH TEMPERATURE.....	82
FIGURE 5-1: BIOMASS TECHNOLOGY MATRIX – PART I: BIOMASS SUPPLY AND CONVERSION. ....	97
FIGURE 5-2: BIOMASS TECHNOLOGY MATRIX – PART II: TP1 DECONTAMINATION AND BIOFUEL PRODUCTION. ....	98
FIGURE 5-3: BIOMASS TECHNOLOGY MATRIX – PART III: TP2 BIO-OIL PRODUCTION AND DECONTAMINATION. ....	99
FIGURE 6-1: RISK RANKING: CLASSIFICATION OF RISK LEVEL. ....	100
FIGURE A-1: BIOMASS DECISION TREE: PRIORITIZATION AND DISTRIBUTION OF BIOMASS SAMPLES BETWEEN TP1 AND TP2.....	111

## LIST OF TABLES

TABLE 2-1: BASIC FEEDSTOCK REQUIREMENTS OF SCWG AND FAST PYROLYSIS.....	11
TABLE 3-1: ESTIMATED CONCENTRATION RANGE OF SCWG PRODUCT GAS SPECIES. ....	19
TABLE 3-2: RANGE OF OPERATIONAL CONDITIONS AT KIT’S SCWG LABORATORY PLANT “LENA”.....	19
TABLE 3-3: OVERVIEW ON PRETREATMENT METHODS FOR LIGNOCELLULOSIC BIOMASS.....	20
TABLE 3-4: BEHAVIOUR OF N, K, P, MG, CA, S AND SI DURING A SCWG PROCESS.....	23
TABLE 3-5: MAIN CHARACTERISTICS OF THE TWO SELECTED MEMBRANE MODULES .....	29
TABLE 3-6: SELECTED SET OF EXPERIMENTAL CONDITIONS THAT WILL BE TESTED (INITIAL ESTIMATIONS) .....	30
TABLE 3-7: COMPOSITION OF LIQUID EFFLUENTS DURING A SCWG PROCESS. ....	34
TABLE 3-8: ESTIMATED EXPERIMENTAL RANGE AND LEVELS OF INDEPENDENT VARIABLES FOR THE ECF AND EO TESTING .....	38
TABLE 4-1: OPERATING CONDITIONS AND CHARACTERISTICS OF THE BIOMASS PYROLYSIS PROCESS IN SCREW REACTORS. ....	70
TABLE 4-2: TYPICAL CONCENTRATION RANGES OF PERMANENT GASES UNDER FP CONDITIONS. (DI BLASI ET AL., 2009) .....	74
TABLE 4-3: EXPERIMENTAL CONDITIONS OF THE COMBUSTION EXPERIMENTS IN THE MILD BURNER. ....	78
TABLE 4-4: TECHNICAL DATA OF THE CERAMIC MEMBRANES SELECTED FOR THE MF OF THE PRODUCED BIO-OIL.....	79
TABLE 4-5: PHYSICAL PROPERTIES OF WOOD FAST PYROLYSIS BIO-OILS (LETHO ET AL., 2014). ....	81
TABLE 4-6: VISCOSITY OF AN AQUEOUS SOLUTION OF GLYCEROL AT 83.4 WT.% AND OF 4 DIFFERENT BIO-OILS. ....	82
TABLE 4-7: PRIMARY ADVANTAGES AND DISADVANTAGES OF VARIOUS CHAR APPLICATIONS (ZHANG ET AL., 2019). ....	89
TABLE 6-1: RISK RANKING TP1.....	102
TABLE 6-2: RISK RANKING TP2.....	104
TABLE A-1: COMPOSITION OF SCWG FEEDSTOCK PRIOR TO CATALYST ADDITION (K <sup>+</sup> ). ....	112

## **ANNEX 1      BIOMASS DISTRIBUTION**



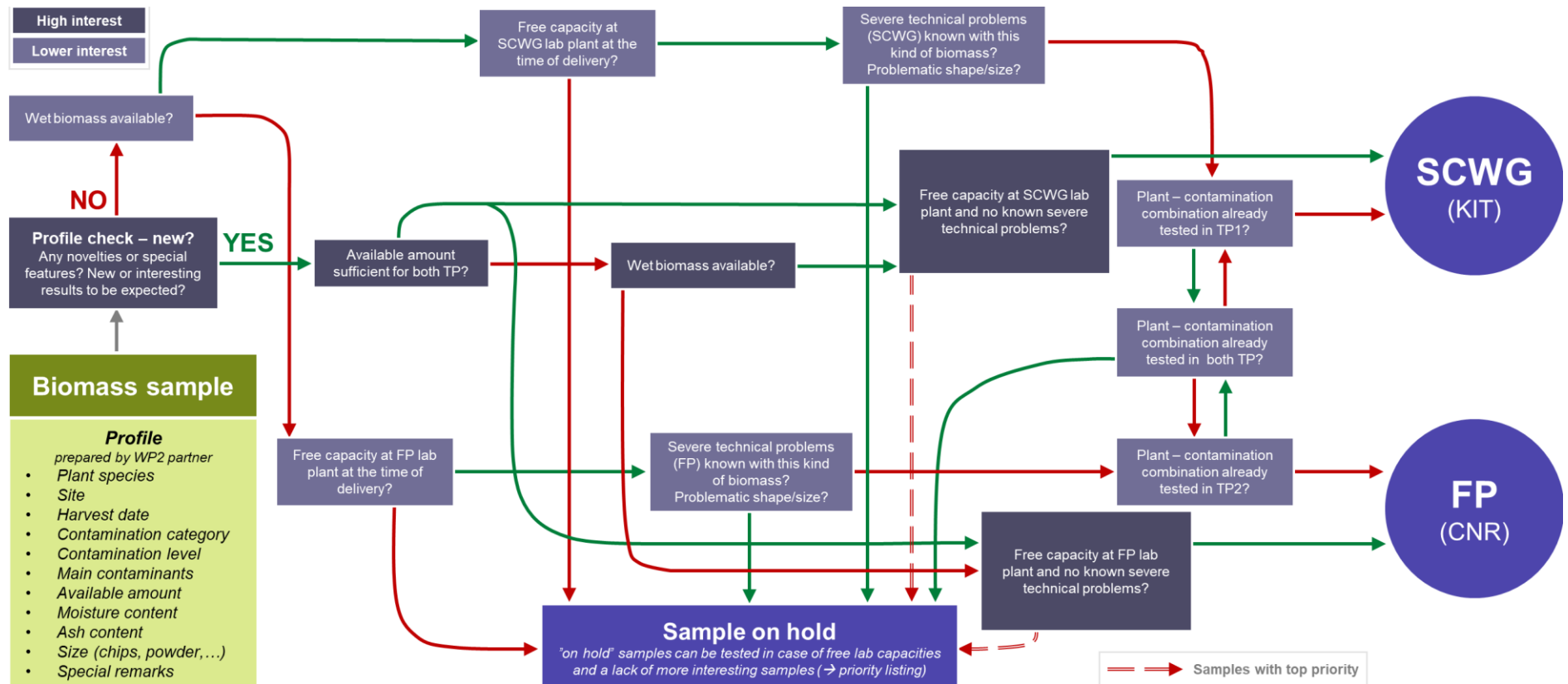


Figure A-0-1: Biomass Decision Tree: Prioritization and distribution of biomass samples between TP1 and TP2.

## ANNEX 2 SCWG FEEDSTOCK COMPOSITION

In Table 3-7, the composition of the SCWG reactor effluent (R) and brine (S) has been described for previous experimental work carried out in the KIT laboratory plant with sewage sludge and brewer's spent grain. Table A-2 shows the average elemental composition of the feedstock used for these experiments. Again, it is stressed that the distribution of the elements among the liquid streams depends strongly on the process configuration and cannot be classified in general.

**Table A-1: Composition of SCWG feedstock prior to catalyst addition (K<sup>+</sup>).**

Element	Sewage sludge	Brewer's spent grain
[mg/g]		
TOC ( C )	421,9	495,0
H	61,8	66,7
N	57,5	43,3
P	25,75	5,87
S	8,06	6,10
Ca	15,09	3,53
K	5,96	0,40
Mg	4,77	2,97
Na	1,00	n.a.
Si	26,70	8,03
Al	8,41	n.a.
Fe	10,60	0,18
Zn	0,56	0,14
[µg/g]		
As	7,3	n.a.
Cu	911,8	n.a.
Pb	56,0	n.a.
Cr	44,4	n.a.
Mo	8,0	n.a.
Ni	15,4	n.a.
Cl	1405,3	n.a.
Hg	0,4	n.a.